Using the jawed yet toothless *Trp63* mouse mutant to understand the morphogenetic relationship between developing lower teeth and mandibles

A Thesis Submitted to the College of Graduate Studies and Research in Partial Fulfilment of the Requirements for the

Degree of Master of Science

in the

Department of Anatomy and Cell Biology,
University of Saskatchewan, Saskatoon, Saskatchewan, Canada

Muhammad Talha Raj

Permission To Use

In presenting this thesis in partial fulfillment of the requirements for a Postgraduate degree from the University of Saskatchewan, I agree that the Libraries of this University may make it freely available for inspection. I further agree that permission for copying of this thesis/dissertation in any manner, in whole or in part, for scholarly purposes may be granted by the professor or professors who supervised my thesis work or, in their absence, by the Head of the Department or the Dean of the College in which my thesis work was done. It is understood that any copying or publication or use of this thesis or parts thereof for financial gain shall not be allowed without my written permission. It is also understood that due recognition shall be given to me and to the University of Saskatchewan in any scholarly use which may be made of any material in my thesis/dissertation.

DISCLAIMER

Reference in this thesis/dissertation to any specific commercial products, process, or service by trade name, trademark, manufacturer, or otherwise, does not constitute or imply its endorsement, recommendation, or favoring by the University of Saskatchewan. The views and opinions of the author expressed herein do not state or reflect those of the University of Saskatchewan, and shall not be used for advertising or product endorsement purposes.

Requests for permission to copy or to make other uses of materials in this thesis/dissertation in whole or part should be addressed to:

Head of the Department of Anatomy & Cell Biology, 107 Wiggins Rd.
Saskatoon, SK S7N 5E5.

University of Saskatchewan, Saskatoon, Saskatchewan

Canada

OR

Dean of the College of Graduate Studies and Research, 105 Administration Place
Saskatoon, SK S7N 5A2

University of Saskatchewan, Saskatoon, Saskatchewan

Canada

Abstract

Across vertebrates, the coordinated evolution and synchronous development of teeth and the mandible must require specific timing and positioning of gene expression. While debate persists about whether teeth have evolved before or after mandible, currently, the consensus is that these systems evolved at separate times and thus have discreet origins. This raises an important question of whether tooth and mandibular tissues have over the course of their evolution become developmentally co-dependent or, as separate evolutionary origins would imply, remain developmentally autonomous of each other.

The molecular signaling that patterns the genesis of upper versus lower jaw skeletons, as well as specifies tooth type (i.e., molar vs. incisor) is relatively well understood. To date, the distinct genetic processes that drive tooth development distinct from jaw skeletal development has been little-studied, in no small part due to the technical complexity of this task. The main hypothesis of thesis is that a collection of genes acting within a gene regulatory network (GRN) drives odontogenesis with neither input from, nor influence on, jaw morphogenesis.

The Transformation Related Protein (TRP63) is a master transcription factor that is vital to odontogenesis because TRP63 maintains the competence and proliferation of the epithelial layer of the tooth organ. Thus the "toothless" TRP63 homozygote mouse mutant (*Brdm2* mutant) fails to develop teeth even though it develops a virtually unperturbed mandible. This combination of lower jaw morphogenesis in the absence of odontogenesis presents a rare model to study the genetic changes that occur when teeth but not jaws fail to form. A previous microarray gene expression analysis (Boughner laboratory, unpublished data) of mandibular prominences (MdPs) derived from embryonic day (E) 10-13 revealed that, compared to heterozygote (*Trp63*$^{+/-}$) MdPs, in *Brdm2* mutant MdPs, transcript

levels of cerebellin 1 (*Cbln1)*; keratin 2-8 (*Krt2-8)*; phospholipid transfer protein (*Pltp)* and fermitin 1 (*Fermt1)* were altered in at least some of the four embryonic stages. Specifically *Cbln1* and *Krt2-8* were up-regulated while *Pltp* and *Fermt1* were down-regulated. None of these four genes have previously been linked to odontogenesis yet all are potential candidates for a "tooth-specific" GRN.

Using RT-qPCR analysis, I aimed to test the validity of the microarray work and confirmed its veracity by showing that, generally, *Cbln1* and *Krt2-8* mRNA were up-regulated, while *Fermt1* (but not *Trp63* or *Pltp*) mRNA was significantly down-regulated in the MdPs of *Brdm2* mutant mice relative to *Trp63*$^{+/-}$ mice. Conversely, western blotting protein expression analysis showed little-to-no change among *Brdm2* MdPs relative to either wild type (Trp63 $^{+/+}$) or *Trp63*$^{+/-}$ embryos, making it difficult to tease out the precise relationship between CBLN1, FERMT1, KRT2-8, and PLTP and TRP63. These results show a lack of strong correlation between mRNA and protein expression. Because the mRNA analyses showed disturbances in the expression level in a few of these five genes within the MdPs during the earliest stages of tooth development, these genes remain candidates for an odonto-specific GRN.

In complement to the genetic work, to characterize the tandem developmental morphology of tooth and jaw skeleton tissues, my work included developing a new tissue staining protocol. Using Protargol, a silver-based compound, to enhance in uncut mouse embryos contrast among tiny, soft oral tissues and visualize their organization in 3D and microscopic detail across several embryonic stages. This novel protocol offers a simple, easy-to-follow, and relatively inexpensive way to effectively stain whole embryos aged E10-15 for X-ray based micro-computed tomography (μ-CT) imaging using synchrotron and desktop scanning systems. Because the scan data are digital, this new method also allows more precise, accurate and rapid empirical studies of the sizes, shapes and positions

of teeth as they form within the jaw to clarify how these tissues are integrated as they develop.

The work presented in this thesis investigated tooth development exclusive of mandible development from complementary molecular and morphological points of view. Driven by the lack of understanding of the genetic mechanisms that orchestrate tooth with jaw skeletal development, this study has for the first time isolated a set of genes that are potential candidates for tooth formation only. These results set the stage for next steps in testing the developmental-genetics that enable teeth and jaws to “fit” together as they develop.

Acknowledgements

I would like to thank my supervisor, Dr. Julia Boughner, for accepting me as her student. It has been a long journey. Your patience and guidance have been invaluable. Thank you very much.

I am also grateful for the advice, encouragement, and expertise offered from my committee members, Dr. David Cooper and Dr. William Kulyk, throughout my studies.

The College of Medicine, the Department of Anatomy and Cell Biology, and University of Saskatchewan through the CIHR-THRUST fellowship and NSERC that have supported and allowed me to do this research.

To our animal care expert, Carmen, for her amazing ability to take care of my project's animal needs throughout the program.

Finally, to my parents, sister and brother: thanks for pushing me all along this journey. Your encouragement and unwavering support will always be appreciated.

Table of Contents

List of Tables

List of Figures

List of Abbreviations

ΔN-p63	p63 isoform missing N-terminal transactivating domain
µ-CT	micro-computed tomography
µ-MRI	micro-magnetic resonance imaging
µ-US	micro-ultrasound
AER	apical ectodermal ridge
BAs	branchial arches
BMP	bone morphogenetic protein
BP	base pair
Brdm2	homozygote mutant of *Trp63*
CBLN1	cerebellin-1
cDNA	complimentary DNA
CNS	central nervous system
CT	cycle threshold
CXCL14	chemokine (C-X-C Motif) ligand 14
DEPC	diethyl pyrocarbonate
Dlx	distal-less homeobox
DMSO	dimethyl sulfoxide
dNTPs	deoxynucleotriphosphates
E	embryonic day
ECE-1	endothelin converting enzyme 1
EDTA	ethylenediaminetetraacetic acid
EEC	ectrodactyly-ectodermal dysplasia-cleft lip/palate syndrome
FERMT1	fermitin-1 or kindlin-1
FGF	fibroblast growth factor
FGFR	fibroblast growth factor receptor
FNP	frontonasal prominence
GAPDH	glyceraldehyde3-phosphate dehydrogenase
GBX 2	gastrulation brain homeobox 2
GLIS	glio-similar protein
GRID	glutamate receptor delta 2
GRN	gene regulatory network
HAND	Heart And Neural Crest Derivatives Expressed
HDL	high-density lipoprotein
HRP	horseradish peroxidase
IKI	iodine-potassium staining agent
kDa	kilodalton
KRT2-8	keratin 8
LDL	low-density lipoprotein
LEF1	lymphoid enhancer binding factor 1
MdP	mandibular prominence
MRI	magnetic resonance imaging

mRNA	messenger ribonucleic acid
MSX1	msh homeobox 1
MxP	maxillary prominence
NCBI	National Center for Biotechnology Information
NIH	National Institute of Health
OPT	Optical Projection Tomography
PAX9	paired box 9
PBS	phosphate buffered saline
PCR	polymerase chain reaction
PEST	proline, glutamic acid, serine, and threonine rich amino acid sequence
PITX1	paired-like homeodomain 1
PLTP	phospholipid transfer protein
PTA	phosphotungstic acid
PVDF	polyvinylidene fluoride
REST	relative expression software tool
RIPA	radioimmunoprecipitation assay buffer
RPM	rounds per minute
RQI	RNA quality indicator
RT	room temperature
RT-qPCR	Reverse transcription quantitative polymerase chain reaction
SAM	sterile alpha motif
SATB2	Special AT-Rich Sequence-Binding Protein 2
SDS	sodium dodecyl sulphate
SHH	sonic hedgehog
TA-p63	transactivating p63.
TAQ	*Thermus aquaticus* polymerase
TBP	TATA binding protein
TCF	T-cell factor
TNF	tumor necrosis factor
TRP63	transformation related protein-63
$Trp63^{+/+}$	wild type
$Trp63^{+/-}$	heterozygote
TTBS	tris tween buffered saline
YWHAZ	14-3-3 Protein Zeta/Delta
WNT	wingless type

1 Introduction

1.1 The evolutionary origins of teeth versus jaws.

Teeth are one of the most important organs to have evolved in vertebrates because, coupled with an anchoring point (jaws), teeth allowed animals to hunt, fight and eat a broader range of foods; thus adapting to new and different environments and surviving during times of environmental stress. The evolutionary origin of dental tissue has been debated amongst scientists working to unravel the development and evolution of dentitions. For many years, two opposing theories were proposed and have been repeatedly tested to model the evolutionary-developmental origins of tooth-like structures. These are the Outside-In theory, and the Inside-Out theory.

The Outside-In theory proposes that teeth in early vertebrates derived from an invasion from external body surfaces into the oral cavity by a layer of skin competent to form odontodes, tooth-like structures (Huysseune et al., 2009). In this scenario, odontodes originally developed from surface skin denticles, spiked tooth-like structures found on the skin of many fish species (Liem and Walker, 2001). In essence, this theory suggests that teeth are modified skin denticles (Sire et al., 1997; Sire, 2001; Sire and Akimenko, 2004). Conversely, the Inside-Out theory postulates that teeth first appeared in jawless vertebrates in the posterior pharyngeal cavity, which contained mostly endodermal cells (Smith, 2003). Through as yet undefined molecular signaling, the anterior oral cavity became competent to develop teeth (Smith and Coates, 1998; Ahlberg and Systematics Association., 2001; Fraser et al., 2009). Thus, in this model, the dentition and skin denticles developed independently from separate embryonic origins (endoderm and ectoderm, respectively) (Teaford et al., 2000).

Both theories are supported by fossil, embryological and anatomical evidence, which partly explains the longstanding contention about which theory is correct. Very recently, new fossil and molecular data have required a reassessment of the Outside-In theory. The revised version of this theory now suggests that teeth formed from odontode-competent ectoderm invading the oro-pharyngeal cavity through the mouth and gill slits (Donoghue and Rucklin, 2014). If tooth-forming ectoderm was displaced into the oro-pharyngeal cavity, in close proximity to where mandible ultimately develop and without much signaling direction from them, then a molecular pathway may have evolved specific to the normal formation of the teeth to the exclusion of the jaw.

Studies on the early *jawless* vertebrate *Loganellia scotica* showed odontode formation within the oro-pharyngeal region (Rucklin et al., 2011), revealing that developmental-genetics and morphogenesis of tooth-like structures existed *prior to* the first signs of jaw-like tissue (Donoghue and Rucklin, 2014). However, there is an equally strong and opposite contention that teeth evolved through the invasion of odontogenetic-competent external dermis to the internal epithelium *after* the origin of a jaw skeleton (Murdock et al., 2013). In this context, the upper jaw skeleton refers to the maxilla and the pre-maxilla and the lower jaw skeleton refers to the mandible, which in mammals is composed of the dentary bone. Although the true understanding of what evolved first, teeth or upper jaw/mandible, remains a debate; there is at this time general agreement that teeth evolved from odontode-competent ectoderm invading the oro-pharyngeal cavity through the mouth and gill slits (Blais et al., 2011). Furthermore, recent work from Fraser and co-workers (2009) suggested that the first vertebrate dentition appeared in areas of the oral cavity expressing hox and ectodysplasin pathway genes. Conversely, hox-negative regions ultimately resulted in differentiation and formation of jaw structures (Fraser et al., 2009). Collectively, this body of previously published work suggests that mandible/upper jaw and tooth tissue were commanded by independent gene regulatory networks (GRN). Yet, the identification and number of genes within each

respective GRN, and even the existence of a network specific to odontogenesis, is still very speculative. The main aim of this thesis is to begin to resolve this particular conundrum.

1.2 The developmental stages of tooth morphogenesis in mammals.

The development of craniofacial structures is a highly complex process involving a vast network of cross-communicating genes (Brunskill et al., 2014). Neuroectoderm cells within rhomobomeres (r1-4) in the developing posterior midbrain and anterior hindbrain transform into cranial neural crest (CNC) cells. This unique population of cells then give rise to the first branchial arch (BA) and the mid-facial prominences including the frontonasal prominence (FNP) (Noden, 1978; Couly et al., 1993; Osumi-Yamashita et al., 1994; Kontges and Lumsden, 1996; Chai et al., 2000). Later in development, the FNP gives rise to the mid face and upper face. Ultimately, CNC cells localize in areas that develop into the upper jaw prominence (prospective upper jaw, MxP) and mandibular prominence (prospective lower jaw, MdP) (Jeong et al., 2008). The MxP and MdP pave the way for the upper and lower jaw skeleton respectively, as well as the lateral skull and middle ear (Kontges and Lumsden, 1996). Note that, in this thesis, "mandible and upper jaw" refer only to the bones within these anatomical structures. The MxP and MdP refer to the early embryonic structures that give rise to several different tissues, including the upper jaw and mandible and their respective dentition. Previous experimental studies have successfully tracked the paths that neural crest cells follow as they migrate such that, in the developing tooth organ, ectomesenchyme is derived from CNC cells (Chai et al., 2000). This CNC-derived ectomesenchyme forms part of the condensed dental mesenchyme that encapsulates the early tooth structure at about E13 and, later, that contributes to the dental papilla mesenchyme, preodontoblast, odontoblast/dentin matrix, pulp, cementum and periodontal ligament (Chai et al., 2000). Thus the various stages of tooth formation heavily depend on the normal function and signaling patterns of CNC cells; however, these cells are not the only

requirement for proper odontogenesis as, non-CNC cells contribute significantly to the production of dental papilla (Chai et al., 2000). In regards to jaw skeleton formation, Meckel's cartilage is a unique bar of cartilage found in the first branchial arch that develops in close proximity to the mandible. Meckel's cartilage starts as an aggregated cell mass containing CNC-derived cells that extends both anteriorly and posteriorly and ultimately forms support for mandible formation (Chai et al., 1994; 1998). To further develop Meckel's cartilage, CNC-derived cells mix with non-CNC-derived cells. Although tooth and upper jaw/mandible formation is directed by CNC cells (Oka et al., 2007), how differential gene expression is programmed and gives rise to these two anatomically different structures still remains something of a mystery.

Teeth develop according to very similar processes in all mammals (even among all vertebrates) studied thus far. Mouse is the classic model system for characterizing the developmental-genetics and morphogenesis of mammalian teeth; albeit only for incisors and molars since mice canine and premolar development is inhibited (Peterkova et al., 2005). In mice, molar teeth develop via a multi-step process that starts on embryonic day (E) 11.5 and finishes much after birth. Visually, odontogenesis begins with a localized thickening of the oral epithelial cell layer (Figure 1). Next, at about E12, this epithelial thickening forms a placode, which begins to invaginate into the underlying mesenchyme – derived from CNC cells (Chai et al., 2000) . This process subsequently forms a "bud", one of the early classic morphological stages (E13.5) through which the tooth organ passes (Tucker and Sharpe, 2004). Condensing dental mesenchyme penetrates into the bud structure, and the "cap" stage of tooth morphogenesis begins around E14.5. At this time point, the cusp pattern of the tooth begins to form. Several days after, at E18.5, the organ enters the "bell" or differentiation stage, when cell layers such as odontoblasts and ameloblasts begin to form and secrete dentin and enamel, respectively, in what are now beginning to look recognizably like teeth. Depending on the species, tooth development continues for months – or in the case of humans, for example, years –

after birth with the eruption of the teeth into the oral cavity. Figure 1, below, summarizes the stages of molar odontogenesis in mice.

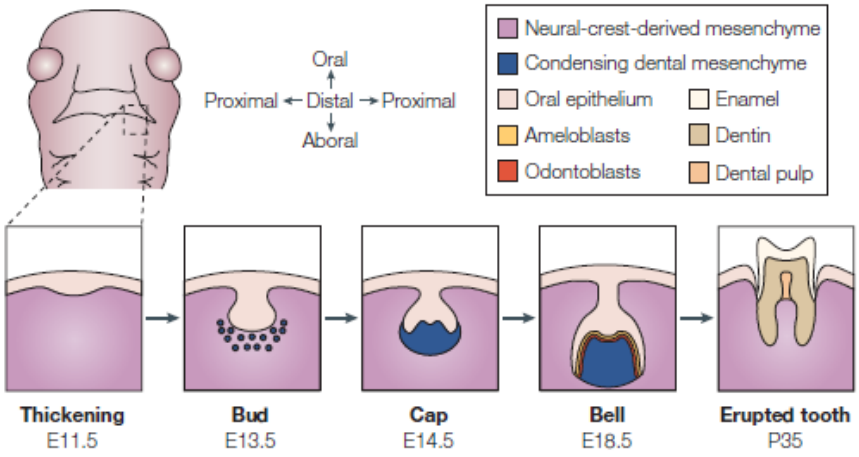

Figure 1. Schematic of the various stages of molar development in mice, beginning at E11.5 with the epithelial thickening, further development and differentiation *in utero*, and eruption after birth. (Adapted from Tucker and Sharpe, 2004).

Odontogenesis is a complex process that involves intricate signaling among all the layers and parts of the tooth organ. To date, over 300 genes have been identified to play a role in normal tooth development (Thesleff, 2006). Some of these genes include transformation related protein 63 (*Trp63*) (Mills et al., 1999); msh homeobox 1 (*Msx1)* (Satokata and Maas, 1994); *Drosophila* distal-less homologs homeobox 1 and 2 *(Dlx)* (Thomas et al., 1997); members of the bone morphogenetic protein (*BMP*) (Bei et al., 2000; Tasli et al., 2014); and fibroblast growth factor (*FGF*) families (ten Berge et al., 2008; Liu et al., 2013); and GLIS family zinc finger (*Gli*) proteins 1-3 (Hardcastle et al., 1998). The specific roles that these genes play in tooth and jaw development have been the subject of many studies and will be discussed later in this thesis with respect to the new research presented here. To demonstrate the complexity of gene function in coordinated tooth development, I

will now discuss the known and distinct genetic needs of incisor versus molar formation.

1.3 Molecular differences between molar and incisor development in mice.

As just noted, any specific tooth-only formation requirements have yet to be discovered; however, there exists a number of studies revealing that incisor and molar development generally require separate genetic pathways. If two structurally similar organs – incisors and molars – are governed by distinct genetic pathways, than it is plausible to propose that mandible and teeth have separate genetic pathways for their respective development. Mice have one incisor separated from three molars by a toothless space known as a diastema. The molecular differences between incisor and molar development are worth discussing briefly in order to appreciate the genetic complexity underlying these two anatomically similar structures that are different in their localization within the oral cavity.

Prior to any signs of tooth formation, *Fgf8* and *Bmp4* are expressed in adjacent and non-overlapping regions within the oral epithelium. This localized expression pattern establishes the boundaries of molar and incisor development, respectively (Caton and Tucker, 2009). Zhang and colleagues (2005) reported the phenotypic changes associated with a deletion of *Fgf8*, which included the complete loss of molars but formation of normal incisors. Within the diastema are expressed several inhibitory factors, such as wingless-type 7b (WNT-7B) (Sarkar et al., 2000); sprouty 2 and 4 (Klein et al., 2006); and ectodin (Kassai et al., 2005), that inhibit the formation of all molar and incisor teeth. Within tissues that form normal incisors, β-catenin-TCF1-LEF1 complex must be present within the mesenchyme (Fujimori et al., 2010) to permit the expression of *Bmp4*, which further induces *Msx1* expression. Meanwhile, suppressing *Barx1* expression prevents molar formation in incisor-specific epithelia (Tucker et al., 1998b). *Barx1* is one of many molar-specific genes

that, if mis-expressed in the developing incisor region, will direct the development of molars where incisors should be (Tucker et al., 1998b). In the same study, Tucker and colleagues (1998b) showed that mesenchymal FGF8 expression positively induced *Barx1* expression, hence driving molar formation. It is important to note that although *Msx1* is initially restricted to incisor developing regions, at the bud stage *Msx1* is expressed in the mesenchyme surrounding all tooth germs and is needed for the proper formation of subsequent cap and bell stages (Tucker et al., 1998a). Global deletion of *Msx-1* therefore, results in the arrest of odontogenesis at bud stage for all teeth (Satokata and Maas, 1994). Further, the *Dlx1* and *Dlx2* genes known to participate in mandible and upper jaw skeleton formation are also required for molar development: a mutation in both genes prevents upper jaw molar development, yet surprisingly, incisor formation is undisturbed (Thomas et al., 1997).

After the bud stage, molar and incisor development both generally involve distinct genetic pathways, comprising *Pitx1* (Mitsiadis and Drouin, 2008)*, Dlx 1 and 2* (Thomas et al., 1997) in the former and Special AT-Rich Sequence-Binding Protein 2 (*Satb2)* (Britanova et al., 2006)*,* and *Hand 1* and *2* (Barbosa et al., 2007) in the latter. If this complexity underlies the genetic differences between a molar and an incisor, then it would not be unreasonable to postulate that teeth and mandible development would entail even more complex and *discrete* molecular mechanisms.

1.4 Current knowledge of the genetic requirements of jaw skeleton morphogenesis

Of course, with its vital role in anchoring teeth and masticating, the jaw skeleton has also been studied extensively in the past three decades, particularly towards understanding the molecular patterning that specifies the development of upper jaw versus lower jaw skeletons. Like the lower dentition, the mandible develops from within the MdP (Theiler, 1989). The same is not entirely true of the

upper dentition, which derives from not only the MxP but also from the nasal/frontonasal prominences (Theiler, 1989). Returning to the MdP, the common embryonic origin of the lower dentition and mandible suggests that their development involves a common set of genes (Figure 3). The hypothesis that a common set of genes dictates both lower dentition and mandible formation has led to several studies that have identified a collection of genes that play important roles in both tooth and mandible morphogenesis (Peters et al., 1998; Sarkar et al., 2000; Harada et al., 2002; Tasli et al., 2014). While these genes may be active in both mandible and dental tissues, often serving similar types of functions, it is still not clear whether these two different tissue types signal to each other in order to orchestrate their development in space and over time.

Among these genes that play a dual role in tooth and mandible formation is the family of *Dlx* genes, expressed in the developing appendages of at least six phyla (Panganiban and Rubenstein, 2002). In mice, *Dlx* genes give rise to six different protein products (DLX 1-6). DLX 1, 2, 5, and 6 are specifically restricted to the MdP, whereas only DLX 1, and 2 are found in MxP (Depew et al., 2002). Astoundingly, the simultaneous inactivation of only *Dlx5* and *Dlx6* converts the lower jaw to an upper jaw (Beverdam et al., 2002; Depew et al., 2002; Depew et al., 2005). Likely in part because *Dlx* expression patterns differ markedly between MdP and MxP, they express different downstream genes. DLX5 and DLX6 collectively promote the expression of heart and neural crest derivatives expressed (*Hand) 1* and *2*; paired-like homeodomain 1 *(Pitx1)*; and gastrulation brain homeobox 2 (*Gbx2)* in the MdP (Jeong et al., 2008). Further, DLX5 and DLX6 suppress the MxP-specific expression of *Pou3f3* and *Foxl2* (Jeong et al., 2008), ostensibly preventing the transformation of lower jaw to upper jaw.

Another example of a gene acting in a mandible-specific formation pathway is the endothelin converting enzyme-1 (ECE-1), known classically to play functional and developmental roles in cardiac (Yanagisawa et al., 1998; Yanagisawa et al.,

2000) and renal systems (Wada et al., 1999). A mutation in *Ece-1* causes severe craniofacial defects, including incomplete mandible formation (Yanagisawa et al., 1998). Interestingly, in *Ece-1* mutants, molar and incisor development occur normally (Yanagisawa et al., 1998), suggesting a level of autonomy between the mandible and its respective dentition. Thus while much work remains to be done, scientists today have a good understanding of how jaw skeleton formation occurs, including the vast array of genes involved, some of which were highlighted above. This past work also begs the question: if there exists a jaw-specific genetic pathway (or two pathways, for upper vs. lower jaw skeletons), then could teeth also develop via an exclusive genetic pathway? That tooth-like structures have been recognized in jawless vertebrates suggests that such a "tooth-only" pathway was present and independent of, and likely prior to, any initiation of mandible-forming pathways (Fraser et al., 2009). This further begs some "big picture" questions that are central to this research project. Specifically, these questions are: how do teeth develop and evolve in tandem with the jaw skeleton? Do the tooth organs receive instructions from the jaw tissues? Or do tooth and jaw tissues cross-talk to coordinate changes in size, shape and position? Surprisingly, in current understanding of tooth and jaw skeleton development, little is known about the genetic products *exclusively* driving odontogenesis. It is probable that genes that specifically direct tooth morphogenesis may have a minute role in development and/or maintenance of the mandible. This could simply be due to the close proximity between the developing dental-upper jaw tissues, thus enabling sharing of genes expressed in one tissue or the other. Also, as discussed above, several genes that have a dual role in both dental and mandible formation have been identified (Figure 3). It is important to highlight however, that identification of genes within this thesis would primarily function in the process of odontogenesis and have minimal to no role in genesis of mandible. Therefore, I propose that the complex and yet unknown GRN within which these genes function is *specifically* found in regions of the mesenchymal-ectodermal space that is dedicated to tooth formation. This study then, is an attempt to unravel a few candidate genes within a putative odonto-specific GRN.

How then can one explore the molecular differences involved in tooth versus jaw morphogenesis and skeletogenesis? It would be ideal to generate a mutant animal model that develops the upper and lower jaw skeleton normally but not teeth, thereby genetically and physically separating the jaws from their dentitions. Subsequent genetic testing could then be used to assess how the molecular profile of the mandible or upper jaw is altered by the absence of the dentition. Comparison of the mutant to a wild type model would provide useful insights about genes with perturbed expression, thereby partially explaining the toothless phenotype.

The *Brdm2* mouse mutant offers just such a model to tease apart the development of the mandible from that of the dentition. The *Trp63* mouse mutant, generated by Mills and colleagues (1999), has been an important tool in understanding the roles of *Trp63* in the development of all epithelial-derived structures including limbs, hair follicles, skin and teeth (Laurikkala et al., 2006; Koster et al., 2007; Wolff et al., 2009). Mills et al. (1999) generated the *Brdm2* mouse mutant by inserting targeting vector (pTV12E) to truncate the messenger RNA at exon 10 (Figure 2). Interestingly, amongst researchers who use the *Brdm2* mouse mutant generated by Mills and colleagues (1999), there exists a debate about the presence of transcriptional and subsequent translational products of the mutated *Trp63* gene. In their original report, Mills et al. (1999) proposed that if the mutated gene was translated, the resulting protein product would contain an intact DNA-binding domain but would be missing the highly conserved carboxyl region of the TRP63 protein. Using northern blotting, a less precise technique now replaced with more sensitive assays, the authors noted the absence of *Trp63* transcripts in the *Brdm2* mutant embryos. The *Trp63* gene has two variants – *TA-p63* and *ΔN-p63* – each giving rise to three different isoforms: alpha (α), beta (β), and gamma (γ) (Mills et al., 1999). TA-p63 contains the N-terminal transactivation (TA) domain whereas the ΔN-p63 lacks this domain and is therefore truncated (Yang et al., 1998). A few years later, Laurikkala and co-workers (2006), revealed using western blotting that

in the homozygote skin there is a complete absence of the α, β, and γ isoforms belonging to the ΔN-p63 variant. Wolff et al. (2009) however, challenged this idea and confirmed via extensive reverse transcription quantitative polymerase chain reaction (RT-qPCR), western blotting, and luciferase assay that at least the γ isoforms is present within the homozygote and has biological activity. Related to the aim of probing for a signaling pathway specific to odontogenesis that also presumably acts in the *Trp63* gene regulatory network, this thesis will examine the transcriptional and translational products of the *Trp63* gene in the homozygote in an attempt to resolve this debate.

Since the mutant was generated, there have been many attempts to define the molecular mechanisms that are perturbed to cause the severe *Brdm2* mutant phenotypes. For instance, the apical ectodermal ridge (AER) in mice forms at the tip of the limb precursors (Theiler, 1989). Current research suggests that proper signaling in the AER requires FGF8, WNT, and BMP amongst others (ten Berge et al., 2008; Benazet and Zeller, 2009; Zeller et al., 2009; Zeller, 2010). On mutation of *Trp63*, FGF8 signaling is reduced and the AER fails to stratify (Restelli et al., 2014). TRP63 is also known to participate in hair follicle formation, and the ΔN-P63 variant functions in the developing placodes of hair follicles (Romano et al., 2010). In at least hair follicles, ΔN-P63 works within the Wnt/β-Catenin signaling pathway (Huelsken et al., 2001; Choi et al., 2013) to drive hair follicle stem cell survival and proliferation. How does *Trp63* contribute to the development of the MdP, specifically the tooth primordia in E10-13 embryos? Work by Laurikkala and colleagues (2006) has shown the strong presence of *ΔN-p63* in developing molars at the bud stage and beyond. Their work also indicated the strong presence of *Fgfr2b*, *Jag1* and *Bmp7*, all downstream targets of *ΔN-p63,* localized within or adjacent to the developing tooth organ (Laurikkala et al., 2006). Are these downstream targets identified by Laurikkala and colleagues (2006) directing only the formation of teeth and not mandible? This question will be discussed in the next section.

The *Trp63* gene continues to be the subject of myriad developmental studies, primarily due to the central role of *Trp63* in limb embryogenesis and cancer/tumor biology. TRP63 has recently been found to target over a 1000 genes in keratinocytes alone, confirming its role as an essential master transcription factor (Pozzi et al., 2009).

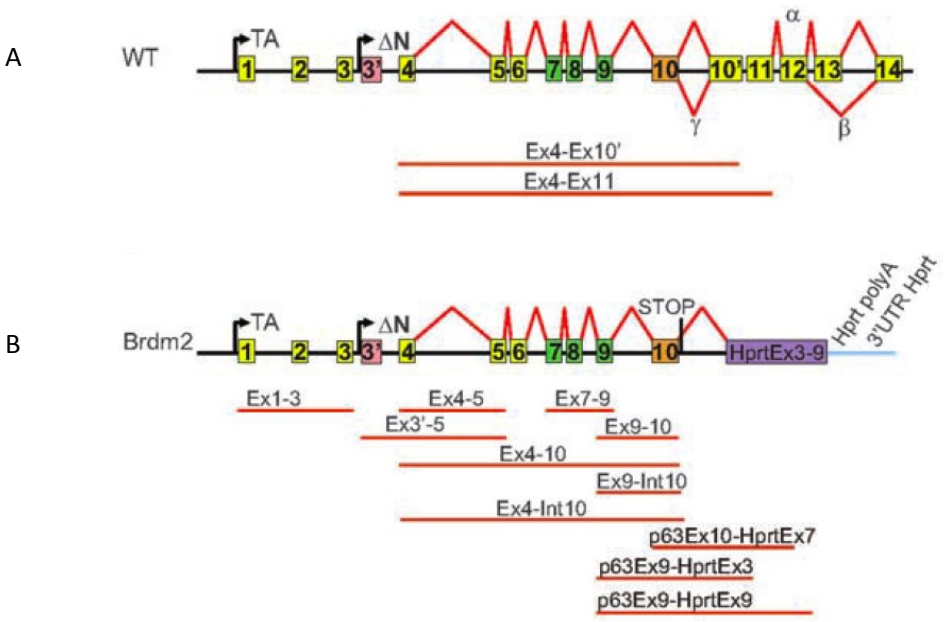

Figure 2. A) Gene locus representing the *Trp63* gene within chromosome 16. Differential exon (numbered boxes) splicing yields two major variants: *TAp63* and *ΔN-p63* each subdividing into α, β and γ isoforms. B) The mutated allele generated by inserting pTV12E vector after exon 10. (Adapted from Wolff et al., 2009).

Mills and colleagues (1999) also noted in the Brdm2 mutants, severe morphological defects including transparent skin, cleft palate, and severely truncated limbs. Histological sectioning revealed that the AER, required for the proximal-distal outgrowth of limbs, was completely absent by E11.5 in homozygote embryos. The *Brdm2* mutant was toothless, yet possessed a mandible, but because

this was not a focal point for the authors, this phenotype was not explored further. Rather, recent evidence from a related project on which I worked has shown that the mandible forms virtually unperturbed in homozygote mice relative to wild type or heterozygote littermates (Paradis et al., 2013). Malformations in the homozygote mouse were restricted to epithelial-derived structures: dissection of abdominal, thoracic, and brain tissues showed no abnormalities (Mills et al., 1999). Homozygote mice showed normal central nervous system development (Holembowski et al., 2011). Mills and colleagues (1999) also reported that, due to the underdeveloped skin in the mutants, 30x more water loss was seen in homozygotes compared to heterozygote and wild type newborns. The mutation therefore was lethal shortly after birth. Interestingly, children with a mutation of *Trp63* display similar birth defects as seen in mice, including ectrodactyly-ectodermal dysplasia- cleft lip/palate syndrome (EEC), adhesion of eyelids, and Rapp–Hodgkin's syndrome (Celli et al., 1999; McGrath et al., 2001; van Bokhoven et al., 2001; Duijf et al., 2002; Kantaputra et al., 2003; Vanbokhoven et al., 2011).

Referring back to the mouse mutant generated by Mills et al. (1999), how can the presence of a normal mandible and yet, a complete lack of teeth be explained using our current knowledge of early embryonic development? One approach to this problem would require referring back to the origins of these two tissues types during early embryogenesis. As was mentioned earlier, both tooth and mandible are derived from CNC cells. Could it be that a mutation of *Trp63* directly hampers the ability of the some CNC cells to direct odontogenesis and yet, have no real effect on CNC cells that promote the genesis of at least the lower jaw skeleton? Although this theory is speculative, I believe it could partially explain how this interesting mouse mutant forms a normal mandible despite the absence of the dentition. Another point to consider is that tooth tissue formation at E10 and beyond, must require normal molecular cross-talk between the epithelial and underlying mesenchyme (Jheon et al., 2013). Conversely, mandible requires appropriate signaling within the mesenchyme in which they form and mature, and have virtually no need of a

functional epithelium for normal development as demonstrated by our labs recently published article on the morphology of the mandible in the *Brdm2* mutant (Paradis et al., 2013). Thus in the *Brdm2* mutant, tooth formation which demands epithelial-mesenchymal interaction is disrupted, whereas mandible formation in need of only the mesenchyme develops normally.

1.5 Well-known participants in odontogenesis also play important roles in bone formation.

Classical studies attempting to understand the genetic basis of tooth development have generally revolved around the following genes: *Bmp7* (Tasli et al., 2014); *Fgf10* (Harada et al., 2002); *Fgf*-receptor 2 (Rufini et al., 2011); *Fgf8* (Yang et al., 1999); *Msx1* (Chen et al., 1996); sonic hedgehog (*Shh*) (Sarkar et al., 2000); paired box 9 (*Pax9)* (Peters et al., 1998); and tumor necrosis factor (*Tnf*) (Ohazama and Sharpe, 2004) (Figure 3 below). The mentioned genes can be classified into a group of "essential factors" that largely regulate organogenesis across a variety of animal models including: *Drosophila melanogaster* (fruit fly), *Danio rerio* (zebrafish), and *Mus musculus* (mouse). Hence, because of their multiple roles during embryonic development, several studies have also discovered that these "essential factors" participate in odontogenesis. The aforementioned genes are just a few that are regulated, either positively or negatively, by the master transcription factor, TRP63. The problem here is that many of these "classic" genes are involved not only in tooth but also bone morphogenesis in the jaw; hence, the roles of these genes do not appear to be exclusive to tooth-only regulatory networks or at the very least make it nigh-impossible to test for dental versus mandible signaling pathways. For instance, BMP7 interacts with BMP2 to induce osteogenesis and odontogenesis in human tooth germ stem cells (Tasli et al., 2014). Furthermore, combined inactivation of *Bmp2*, *Bmp4*, and *Bmp7* specifically in the cranial neural crest region of the developing mouse embryo results in truncated bone and cartilage development (Bonilla-Claudio et al., 2012). *Msx1* is a homeobox gene expressed at the epithelial-mesenchymal cell border required for normal development of teeth (Satokata and Maas, 1994), limbs (Bensoussan-Trigano et al., 2011), the atrio-ventricular cushion (Chen et al., 2008), and Rathke's pouch (Lu et al., 2000). Prior to understanding the role played by homeobox genes in tooth morphogenesis, it was known that *Msx1* expression is required for the development of the craniofacial skeleton (Alappat et al., 2003). *Msx1*-deficient mice have cleft plate, deficient alveolar bone (the bone that

houses the teeth) and, most importantly, arrested tooth development (at bud stage) (Satokata and Maas, 1994). Other evidence revealed that a mutation in mice for *Msx1* directly hampers mandible outgrowth via apoptosis in cortical bone that ultimately decreases bone mineralization (Nassif et al., 2014). Humans with mutated *Msx1* have cleft palate and tooth agenesis (Nassif et al., 2014). Thus, *Msx1* is understood to play crucial roles in both bone and tooth development, in mice and humans. Another key contributor to normal tooth formation is the Tumor necrosis factor, or *TNF* (Ohazama and Sharpe, 2004). Recently, this gene was discovered to play a role in inducing bone resorption via osteoclastogenesis (Zhao et al., 2012). In addition, the SHH protein, well known for its role in odontogenesis in mice has been shown via *in vitro* studies to possess transcriptional control of osteocalcin mRNA via BMP-2 dependent pathway (Yuasa et al., 2002). It is apparent that most of the genes and their protein products that have well-established roles in tooth morphogenesis are also known to function in bone development, remodeling and resorption (Figure 3, below). This is at the heart of the problem. That although our understanding of the complex genetic requirements of dentition and mandible development has tremendously improved within the past two decades, our comprehension of the specific genetic needs of normal tooth formation is extremely poor. To date, only *Trp63* has been shown to participate in a currently unknown yet *probable* tooth-only genetic pathway. One of the main goals of this thesis is to further identify potential targets of *Trp63* that are involved in this odonto-specific pathway. I believe this work is a small but important step that will help fill the vacuum in our current understanding of molecular requirements of tooth vs. mandible formation and ultimately towards resolving fundamental questions about how vertebrates develop and evolve.

I hypothesize that there are signaling pathways, and therefore genes, that are solely responsible for either tooth or mandible development but not both. This hypothesis comes from acknowledging the evolutionary differences in timing of teeth versus jaw development (Rucklin et al., 2011), and the observation that teeth

can develop in cancerous teratomas, i.e., without the presence of either the upper jaw skeleton or mandible (Ingale et al., 2013). Nonetheless, normal tooth formation can only occur via a well-established physical connection between the dental epithelium and the underlying mesenchyme, thereby allowing the necessary molecular cross-talk (Zhang et al., 2005). Appreciating this complexity and the relatively short period within which tooth morphogenesis occurs alongside a history of mutant animal models with disrupted dental *and* gnathic development, can the genetic pathways specifically directing odontogenesis be unraveled.

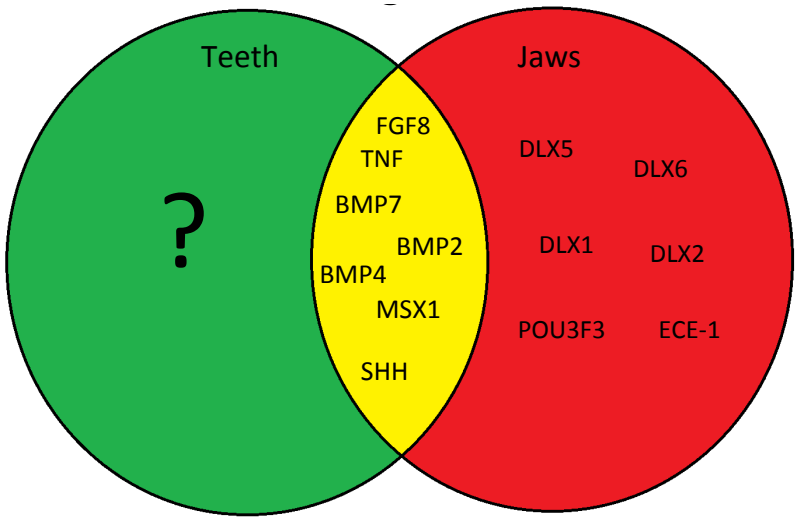

Figure 3. Summary of the current knowledge of a subset of genes and their protein products needed for teeth and jaw development. As of yet, no targets have been identified to specifically regulate only tooth morphogenesis exclusive of jaw morphogenesis (green).

So far, this thesis has summarized the necessary background information of what is currently known in tooth versus mandible development and the gaps within the current literature pertaining to the specific requirements for tooth morphogenesis. I have briefly highlighted the current knowledge that is available on genes regulating specifically jaw skeleton development. Furthermore, I have briefly reviewed the molecular explanation for two similarly structured organs: molars and

incisors, particularly the different genes that are responsible for the genesis of one or the other. Yet, few studies have focused specifically on the networks that allow independent but complementary development of dentitions versus jaw skeletons. It is important here to understand how the *Brdm2* mutant mice can help us identify a collection of genes that exclusively participate in the formation of teeth, and hopefully the mechanism with which these genes interact with each other and the TRP63 protein to initiate, develop and maintain the initiation and subsequent stages of odontogenesis.

1.6 Towards understanding molecular networks specifically involved in tooth morphogenesis exclusive of jaw development, using the *Trp63* mouse mutant.

A few years ago, Boughner (2010, personal communication) investigated the transcriptional changes between E10-13, in the MdP extracted from homozygote and heterozygote embryos. Since *Trp63* is a transcriptional controller of many genes, a mutation within its gene locus would obviously have great consequences. The objective of the microarray analysis was to determine the changes in gene expression caused by the null-mutation of *Trp63*, specifically within the MdP across the beginning stages of odontogenesis (E10-13). Recall, that these are the beginning stages of tooth development in mice and that any genetic disturbance in these early stages would likely result in no teeth at all or a deformed/perturbed dentition. Nonetheless, the microarray showed a few targets of *Trp63* that were up-regulated or down-regulated in expression and had established relationships to tooth development. Some examples include the keratins 14/15 (Mills et al., 1999) and membrane bound claudin 6 (Lopardo et al., 2008). However, the intent of the microarray was to identify candidate targets of *Trp63* that were altered within the *Brdm2* mutant MdP, including genes with no previously recognized relationship to tooth development. The microarray test was the first study that we know of to start to unravel the genetic needs of normal tooth formation distinct from mandible

formation. A set of genes: cerebellin 1 (*Cbln1*), fermitin 1 (*Fermt1*), phospholipid transfer protein (*Pltp*), and keratin 2-8 (*Krt2-8*) highlighted in the microarray (Table 1, below), had no previous known relationship to tooth or upper/lower jaw skeletal morphogenesis yet showed consistent change (decrease, or increase) at most or all four stages of development studied (E10-E13).

As stated earlier, the *Brdm2* mutant fails to develop all epithelial-derived structures including teeth yet, forms a normal mandible. Conversely, the mutant often develops a deformed upper jaw as noted by the presence of facial clefting (Thomason et al., 2008; Thomason et al., 2010). The microarray analysis showed changes in expression of a collection of genes that have no known relationship to tooth development. As such, it is worthwhile to discuss briefly the known physiological roles and cell/tissue specific expression patterns of these genes.

Table 1. Transcript levels change in the homozygote relative to normal-looking heterozygote in E10-13 MdP.

FC≥2, p≤0.05	Expression change in p63-/- (compared to p63+/-)	
GD	**Decreased**	**Increased**
10	**Fermt1, Krt1-14 P63** Pltp Cxcl14 Kremen2, Osr2, Ifitm3	**Krt2-8, Krt1-18** Stx3, Slc2A3 Espn, Prss8
11	**Fermt1, Krt1-14, P63** Pltp, Krt-15	**Krt2-8, Krt1-18** Cbln1, Sst, StfA1 Ckb, S100A8
12	**Fermt1, Krt1-14 P63,** Col17A1, Krt-15	**Krt2-8, Krt1-18** Cbln1, Slc2A3
13	**Fermt1, Krt1-14 P63,** Col17A1, Krt15 ItgB4, Trim29, Krt2-8	**Krt2-8, Krt1-18** Cbln1, Cldn6

Cbln1 is a 15 kiloDalton (kDa) protein that is primarily restricted to expression in the brain (Kavety et al., 1994). CBLN1, has been known for some time

to interact with glutamate receptor delta-2 (GRID2), to induce new synapses *in vitro* and in adult mouse cerebellum (Matsuda et al., 2010). CBLN1 is also vital for Purkinje cells within the cerebellum for synaptic integrity and plasticity (Hirai et al., 2005). In addition, CBLN1 inhibits the formation of inhibitory synapses within the mouse cerebellar Purkinje cells (Ito-Ishida et al., 2014). Convincing evidence suggests that multiple homologues of CBLN1 have been detected outside of the cerebellum; CBLN 1-4 are present in human adrenal glands (Rucinski et al., 2009). In rats, CBLN1 is localized within the membrane and cytoplasm of adrenocortical cells and higher expression is seen within the cortex compared to the medulla of the gland (Rucinski et al., 2009). During embryogenesis, CBLN1 expression is detected as early as E10-13 in the mouse brain, and its expression is up-regulated thereafter (Miura et al., 2006). It is clear than that despite work characterizing the roles of CBLN1, it has yet to be identified as a potential participant in the development of teeth or the upper or lower jaw skeletons.

Fermt1, also known as kindlin-1, is one of the genes whose mRNA expression was decreased in the homozygotes, per the microarray. FERMT1 protein is one amongst 4 homologue variants known, and is comparatively the largest in molecular mass, at 77 kDa (Abcam, Cambridge, U.S.A.). FERMT1 has been the subject of quite a number of studies, particularly with a focus on its function in keratinocytes. FERMT1 has been shown to have strong expression in epidermal keratinocytes, principally on the side closest to the basement membrane (Herz et al., 2006). Herz and colleagues (2006) have also revealed that due to a deficiency of FERMT1 in skin, proliferation of keratinocytes is stunted, and apoptosis signaling is active. *In vitro*, a deficiency in *Fermt1* in keratinocytes lead to similar results as seen in skin: reduced cell proliferation, and decreased adhesion to basement membrane. It has been shown that FERMT1 activity is dependent on β1 integrin activation, and a down-regulation of FERMT1 in skin leads to decreased levels of β1 integrins (Lai-Cheong et al., 2010). A mutation in *Fermt1* causes kindler syndrome, a rare autosomal recessive disorder in humans characterized by skin blistering, photosensitivity, skin

atrophy, and an increased chance of skin melanoma (Has et al., 2011). Most important for us is that *Fermt1* has no known roles in odontogenesis or upper or lower jaw morphogenesis and from previous studies, what can be concluded is that FERMT1 is necessary for keratinocyte survival and homeostasis and perhaps has structural role in anchoring the epithelial to the underlying mesenchyme. Consistent down-regulation of *Fermt1* in the MdP across E10-13 in mutant was noted, warranting further investigation of this gene's participation in evolution and development of teeth and mandible.

Phospholipid transfer protein also known as PLTP, was another gene that was shown to be reduced in its mRNA expression, albeit only at E10-11. As the name suggests, this protein has primarily been studied in involvement in metabolism of high-density lipoprotein (HDL) and low-density lipoprotein (LDL). PLTP is a 54kDa protein (Huuskonen et al., 1998) that in humans is strongly expressed in the ovary, thymus and placenta (Albers et al., 1995). In mice, PLTP mRNA transcription is activated by many signals one of which is a high fat, high cholesterol diet (Jiang and Bruce, 1995). *Pltp* transcription is also triggered in alveolar pre-type II epithelial cells exposed to hypoxia (Jiang et al., 1998), suggesting that it has cell-specific roles. In any case, an overwhelming majority of the research of PLTP function focuses on its relationship with HDL and LDL metabolism. Without delving too deep into the actual mechanisms with which this protein functions, it is sufficient to recognize that PLTP can help enlarge HDL particles (Lusa et al., 1996). Further, alpha-tocopherol, the most common form of Vitamin E, is permitted to transfer between various cellular compartments with the help of PLTP (Kostner et al., 1995; Desrumaux et al., 1999). Mice with mutated PLTP therefore, exhibit disruption of cholesterol transfer into HDL (Jiang et al., 1999). Recent work by Vuletic and co-workers (2003), has demonstrated strong presence of PLTP in neurons, astrocytes, microglia, and oligodendroglia in the human brain. Interestingly these researchers also demonstrated that a marked increase of PLTP levels were observed in brain tissue affected by Alzheimer's. Therefore, PLTP protein is not only involved in lipid

processing in cells, but also activated in response to biochemical stress and disease. However, the relationship of PLTP with TRP63, has not been studied. Also, from published work, it seems that PLTP has little to no role in any developmental processes. However, according to the microarray, the mRNA levels of this gene were altered amongst the homozygote MdP at E10-11, the very beginning stages of odontogenesis. Further examination of the mRNA and protein levels of this gene is therefore necessary.

Knowing that *Trp63* acts as a "molecular switch" allowing the expression of many genes and that the *Brdm2* mutant fails to develop all epithelial-derived tissues particularly teeth, I hypothesize that there is a yet unknown molecular mechanism dependent on *Trp63* that is in control of odontogenesis and is disturbed within the *Brdm2* mutant. In the *Brdm2* mutant, this theoretical GRN is compromised, and can be detected via RT-qPCR and western blotting. The genes under investigation: *Cbln1*, *Pltp*, and *Fermt1*, I propose, have little to no role in normal morphogenesis of Meckel's cartilage or the dentary bone, the two elements that make up the lower jaw skeleton/mandible. If both the protein as well as the mRNA levels of the genes to be studied are altered then this will validate the microarray results and strengthen the hypothesis that these genes act in a tooth-specific regulatory network that has little or no effect on the lower jaw.

1.7 Translating molecules to morphology by combining genetic insights with 3D imaging.

It is important to note that although the complex GRN's involved in tooth and jaw development can help us explain at a molecular level the morphogenesis of these two structures, it is equally important to characterize the gross morphology orchestrated by these GRNs such that teeth grow within jaws in the proper place at the proper time to naturally fit "side-by-side" within the mandible and the upper jaw skeleton (i.e., in the premaxilla and maxilla bones). Since teeth and jaw

skeletons develop in close proximity to one another, they may influence each other's development but, either way, whatever developmental-genetic mechanisms coordinate the spatial organization of teeth and jaws are still largely unknown.

One of the main reasons for this knowledge gap is that, conventionally, researchers have used 2D histological techniques to study the sizes, shapes and positions of 3D structures. For example, Radlanski and co-workers (2003) reconstructed in 3D the MdP from sectioned (i.e., 2D) human embryos and fetuses, to understand the growth processes that develop a mature mandible. Some studies have used relatively new forms of microscopy, with minimal use of harsh chemicals that destroy tissue to study the development of teeth in 2D (Pan et al., 2014). Lungova and colleagues (2011) used 2D histology sections of tooth-bone tissue that were virtually stacked using special software to reconstruct and visualize developmental morphology in 3D. Chlastakova and colleagues (2011) also used histological sections to reconstruct the 3D organization of third molars with respect to the jaws. A commonality amongst the aforementioned techniques is the physical destruction of the sample compounded by the error introduced by the virtual reconstruction process. In order to best understand the physical relationship between the growing jaw skeletons and teeth, preservation of all tissues in their actual 3D organization is optimal. Newer, non-destructive imaging modalities such as micro-Magnetic Resonance Imaging (μ-MRI), micro-Computed Tomography (μ-CT), Optical Projection Tomography (OPT) and micro-Ultrasound (μ-US) can be used to study internal tissues without the need for dissection. These various scanning techniques carry their own limitations including cost and availability, yet offer unique advantages for seeing and measuring in 3D the structures within tiny, intact specimens such as mouse embryos.

Micro-MRI imaging has advanced over the past few years such that current models offer resolutions as high as 25-100 μm. This imaging modality is particularly safe for live animal imaging as μ-MRI exploits paramagnetic properties of naturally

occurring hydrogen, or of contrast media containing gadolinium (Zhou and Lu, 2013) or manganese (Pan et al., 2011). These contrast agents are used extensively in clinical settings because they are safe to ingest or inject in small quantities. Contrast agents help enhance how various tissues - such as musculature and connective - react to the magnetic fields. Detailed soft tissue imaging is often possible even without contrast dyes such as iodine and other toxic compounds. This non-radioactive imaging modality also overcomes the problem of radiation dose, a major issue in μ-CT of live animals. Despite all these benefits, μ-MRI has some serious drawbacks for my particular research aims. Firstly, μ-MRI machines are expensive and rare compared to desktop μ-CT machines, thus limiting access. Secondly, the maximum resolution of 25 μm would simply be unable to visualize newly-forming tooth organs in any great detail. Lastly, scan times can be arduously long (6-24 hours) if detailed high resolution imaging is needed (Turnbull and Mori, 2007), making this imaging modality cumbersome and simply unusable.

Micro-US detects high frequency sound waves that penetrate tissues to generate 2D or 3D images. Like μ-MRI, ultrasonic waves are generally considered to be harmless in comparison to X-rays. Portability and cost-effectiveness in μ-US machines make them an ideal choice for quick general scanning at the clinic. Current resolution of 30 μm is possible (Foster et al., 2009), however there are experiments that report a resolution as high as 10-20 μm (Rissanen et al., 2008), which would allow for the visualization of all stages of tooth formation. However, sound wave penetration is limited to approximately 3 cm below the skin (Foster et al., 2000), which can be a problem for morphological studies using adult mice or rat specimens. Secondly, there exist only a few companies that produce μ-US systems; VisualSonics (Toronto, Canada) and Exact Imaging (Toronto, Canada), making this imaging modality relatively rare.

Micro-CT has been used for many years since its first use by Elliot and colleagues (1982), imaging the internal anatomy of a tropical snail. Since then,

desktop μ-CT technology has drastically improved and become an indispensable scanning tool in the physical and biological sciences. For instance, μ-CT scanning is used today to study specimens as large as whole fish and mice embryos (Metscher, 2009a) to tiny miniscule tissue structures within bone (Britz et al., 2010). Further, the use of synchrotron-based μ-CT has recently grown among researchers in biological and physical sciences. Synchrotrons, although rare, offer a few uniquely powerful and advantageous features including a monochromatic X-ray source, the capacity to scan using different modes of CT (i.e., absorption, phase contrast), a larger photon flux to shorten scanning time, and inter-changeable camera systems that enabling extremely high resolution imaging (Lewis, 1997).

One of the goals of my project was to compare synchrotron and desktop μ-CT scanning in order to try to visualize in high-level detail the real-life 3D morphology and structure of teeth as they actually are positioned in the jaws by scanning whole embryonic heads. This aim included piloting a tissue contrast agent called Protargol, which is a silver-based stain previously used only to visualize nerves in the mouth but not specifically teeth or tooth organs. Protargol was first used when Bodian (1936) developed a protocol to stain with Protargol and copper nerve fibers embedded in paraffin. This method for studying nerve tissues was simplified and shortened to two hours by others (Davenport et al., 1939; Foley, 1943). Until my study, Protargol had not been tested as a contrast agent for whole (i.e., unsectioned) tissues such as intact embryos. Other tissue contrast agents such as: PTA (Metscher, 2009b), Iodine-Potassium agent (IKI) (de Crespigny et al., 2008), and osmium tetraoxide (Johnson et al., 2006; Ribi et al., 2008) have been successfully used for μ-CT imaging whole embryos (e.g., mouse, chick). Most of these staining agents however are toxic in very small quantities and thus riskier to work with, and involve more complex, multi-step protocols to get the stain successfully absorbed into the tissue. Thus a simpler, less toxic tissue contrast protocol that would quickly capture at high resolution and in digital format the morphology of tooth organs within the

developing jaw would be a significant and useful new tool for the greater scientific community.

Between synchrotron and desktop μ-CT scanning, I predict perhaps obviously that the former would be superior to the latter in visualizing in 3D as the earliest developmental morphology of teeth and jaws in clear microscopic detail. This prediction stems specifically from the ability to tune the synchrotron radiation, or beam, to the specific energy that excites silver particles only to generate maximum contrast in any silver-impregnated tissues. As silver has a K-edge of 25.5 KeV, this lower energy is certainly achievable using the Canadian Light Source synchrotron. Furthermore, the camera system setup allowing resolutions of 8 μm or higher would be adequate to visualize the various structures of the tooth in histology-like detail. Based on past reports using conventional desktop μ-CT, I predicted that while this scanning system would visualize tooth organs it would not be able to show the specific structures within the tooth organ (i.e., histological detail).

To conclude, the *Brdm2* mutant mouse model is uniquely useful in deciphering the molecular pathways that permit the normal formation of the mandible *in absentia* of its dentition. The corresponding expectation is that the expression of genes perturbed in this mutant will thus relate only to tooth, and not mandible, development. The next chapter of this thesis reports the results of my work testing the veracity of the microarray assay using RT-qPCR. Using western blotting, I probed protein levels of the respective mRNAs to further confirm the expression differences reported via the microarray in *Brdm2* mutant embryos. Chapter 3 reports the outcomes of the novel method developed to image in 3D the morphology of embryonic teeth and jaw skeletons. This information will help us characterize the autonomous versus dependent developmental-genetic interactions between tooth and jaw tissues, as well as the “close-knit” physical arrangement between dental and gnathic tissues, at least in a mouse model system.

1.8 Experimental Objectives and Hypotheses

Aim 1

To validate using RT-qPCR experiments the results of the microarray analysis by focusing on *Trp63* as well as a subset of genes with no previously established relationship to tooth or mandible development.

Hypothesis and *Prediction 1*

- I hypothesize that RT-qPCR and microarray results will be congruent, i.e., I predict that both will show in the homozygote MdPs increased expression of *Cbln1* and *Krt2-8* and decreased expression of *Trp63*, *Fermt1* and *Pltp*.

Aim 2

To test using western blotting if protein levels mirror mRNA levels reported by the microarray analysis for the same genes specified (excluding KRT2-8 and chemokine (C-X-C Motif) ligand 14 (CXCL14)).

Hypothesis and *Prediction 2*

- I hypothesize that, congruent with the microarray and RT-qPCR results, western blotting will show increased expression of CBLN1 and decreased expression of TRP63, FERMT1 and PLTP.

Aim 3

To visualize tooth organogenesis *in situ* in 3D using Protargol to deeply penetrate uncut, whole soft tissue in mouse embryos.

Hypothesis and *Prediction 3*

- I hypothesize that visualizing tooth organogenesis in 3D in whole embryos is possible using Protargol as a tissue stain alongside a beam energy near the silver K-edge using high-resolution μ-CT imaging at the synchrotron.

2 Molecular perturbations in the MdP of *Trp63* mutated mice

2.1 Introduction

The aim of the work presented in this chapter is to help identify and characterize new functions for genes and their protein products in the formation of teeth but not the mandible. This chapter focuses on testing the mRNA and protein levels amongst wild type, heterozygote, and homozygote MdP of mouse embryos aged E10-13 for *Cbln1*, *Pltp*, *Fermt1* and *Trp63*, whilst assessing only the transcript levels of *Cxcl14* and *Krt2-8* for reasons explained shortly. As revealed by microarray analysis, the expression of these genes was either up-regulated or down-regulated in the homozygote compared to the phenotypically normal heterozygote. Hence, the primary goal of the present study was to validate the microarray results by testing whether the expression of these same genes and their protein products was similarly up- or down-regulated in the homozygotes as shown by RT-qPCR (for mRNA) and western blotting (for protein). I studied the expression of *Trp63* mRNA and protein not only as another type of experimental control but also because of ongoing debate amongst researchers about whether proteins from the various isoforms of *Trp63* are synthesized in the homozygote despite the mutation of both *Trp63* alleles.

I hypothesize first, that the genes identified by the microarray: *Cbln1*, *Pltp*, *Fermt1*, *Krt2-8*, *Cxcl14* and *Trp63* are notably different in their mRNA and protein levels in the homozygote MdP compared to heterozygote. Second, since the *Brdm2* mutant mouse develops virtually normal mandible but no teeth, I would not expect that the genes involved in mandible development would be perturbed at the transcript and protein level in *Brdm2* mutant. If the transcript and protein expression for the studied genes collectively reveal the genetic changes within the homozygote, than this would point to an as yet unexamined GRN network that is specifically dictating tooth morphogenesis exclusive of mandible development.

2.2 Materials and Methods

All the following studies used prenatal mice derived from the B6.129S7-*Trp63*^{tm2Brd}/J strain (Jackson Laboratory, Sacramento, U.S.A). Heterozygote mice were bred and pregnant dams were taken care of by a professional animal technician in the Animal Care Facility in the Health Sciences Building at the University of Saskatchewan. Between 10 and 13 days post-coitum, pregnant females were sacrificed by cervical dislocation in accordance with University of Saskatchewan animal use protocol #20110008, and Biosafety protocol #R-ANA-15. Immediately after sacrifice, all embryos were extracted from the uterus. Next, MdP and tail tissue were dissected out and placed in L-15 media (Life Technologies, Carlsbad, U.S.A.) for subsequent DNA, RNA, or protein work.

The microarray was performed by Dr. Julia Boughner (2010) on MdP's using the two genotypes (Heterozygote and Homozygote) aged E10-13, when odontogenesis begins in mice. Hence, as done for the microarray work, RT-qPCR experiments (below) were performed using embryos aged between E10-13.

2.2.1 DNA extraction and genotyping

Tail clips or whole heads were snap-frozen dry at -20 °C until DNA extraction and subsequent polymerase chain reaction (PCR) work was done. DNA was extracted using Phire Tissue Direct PCR master mix (Thermo Scientific, Waltham, U.S.A.). DNA release buffer (0.5 µl) and dilution buffer (20 µl) were added to each tissue sample, and incubated at room temperature (RT) for 5 min. Thereafter, samples were heated at 98 °C for 2 min., and then the supernatant collected and stored at -20 °C until thawed for PCR and electrophoresis work. For quality control, purified DNA was occasionally tested for quantity and quality using NanoVue plus spectrophotometer (GE Life Sciences, Pittsburg, U.S.A.).

Brdm2 toothless mutants were easily distinguishable from phenotypically normal wild type and heterozygote embryos (Figure 4).

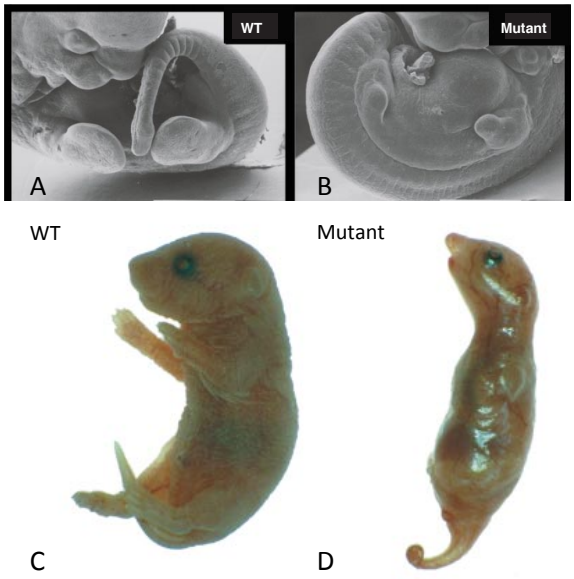

Figure 4. Morphological differences between wild type (*Trp63*$^{+/+}$) and mutant (*Brdm2*) embryonic and adult mice. A) Healthy limb bud outgrowth in a normal embryo with functional *Trp63* alleles. B) Underdeveloped/atrophied limb buds in an embryo with *Trp63* mutated at both alleles. C) Newborn mouse with functional *Trp63* gene in contrast to D), a newborn mouse with both *Trp63* alleles mutated. (Adapted from Mills et al., 1999).

Because homozygote mice displayed from at least E9.5 striking morphological deformities including absence of limbs, thin and underdeveloped epithelial skin, and generally smaller body size it was not necessary to genotype these embryos. Nonetheless, the homozygote tail clips were collected and used as positive controls for the PCR work. Conversely, distinguishing the morphologically similar heterozygote and wild type mice did require doing PCR using primers complementary to the *Trp63* insertion mutation. Presence of *Trp63* insertion mutation was detected with the following primers:

Forward (oIMR1029) 5’ - GTG TTG GCA AGG ATT CTG AGA CC - 3’;
Reverse (oIMR1030) 5’ - GGA AGA CAA TAG CAG GCA TGC TG - 3’.

If present, this amplified insertion mutation yields a sequence that is 410 base pairs (bp) in length.

Genomic sequence coding for T-cell receptor, an internal positive control, was also amplified, with a product length of 210 bp, using the following primers:

Forward (oIMR8744) 5’ - CAA ATG TTG CTT GTC TGG TG – 3’
Reverse (oIMR8745) 5’ - GTC AGT CGA GTG CAC AGT TT - 3’.

Primers were designed and validated by Jackson Laboratories and purchased from Sigma. Refer to the following link for more primer and PCR protocol information: http://jaxmice.jax.org/protocolsdb/f?p=116:2:753578398088607::NO:2:P2_MASTER_PROTOCOL_ID,P2_JRS_CODE:5248,003568.

All PCR reaction ingredients listed below were stored at -20^{o}C, and thawed on ice before preparing the master reaction mixture. Note, TAQ polymerase was added at the end of Step 1. Each PCR reaction mixture consisted of the following:

Ingredient	Volume (µL)
Forward Primer	0.375
Reverse Primer	0.375
10x Buffer - $MgCl_2$ (Invitrogen)	1.5
dNTP 10µM (Invitrogen)	3.0
50x $MgCl_2$ (Invitrogen)	0.75
Ultra pure H_20 (Gibco)	7.85
DNA	0.5-1.0
TAQ polymerase (Invitrogen)	0.150
Total volume	**14.5-15**

Thermocycler (Bio-Rad, Hercules, U.S.A.) was programmed with the following protocol:

1. 94°C for 5min
2. 94°C for 30sec
3. 55°C for 30sec
4. 72°C for 30sec
5. Back to step 2 and repeat 32x
6. 72°C for 5min
7. 4°C hold

After heating the thermocycler to the temperature noted in Step 1, the program was paused for only as long as it took to add 0.150 µl of TAQ polymerase to each reaction mixture – that is, each sample tube – still on ice. Afterwards, all tubes were placed into the thermocycler and the program was resumed and allowed to run to completion.

Upon completion of the PCR, tubes were removed from the thermocycler and placed on ice (or overnight in the 4^{o}C fridge). Next, 4 µl of 5x Blue Juice (Life technologies, Carlsbad, U.S.A.) was added to each PCR product (i.e., sample tube) and loaded into a 1.5% agarose gel (Invitrogen Ultra-Pure Agarose, Life technologies, Carlsbad, U.S.A.) that was made in 1x TAE (2M tris acetate, .05M EDTA, pH 8.3. Life technologies, Carlsbad, U.S.A.) with 0.4x Gel Green added (Biotium, Hayward, U.S.A.). The electrophoresis gel was then run for approximately 1h at 100 Volts. The gel was imaged using a UVP BioDoc-It imaging system (UVP, Upland, U.S.A.) (Figure 5).

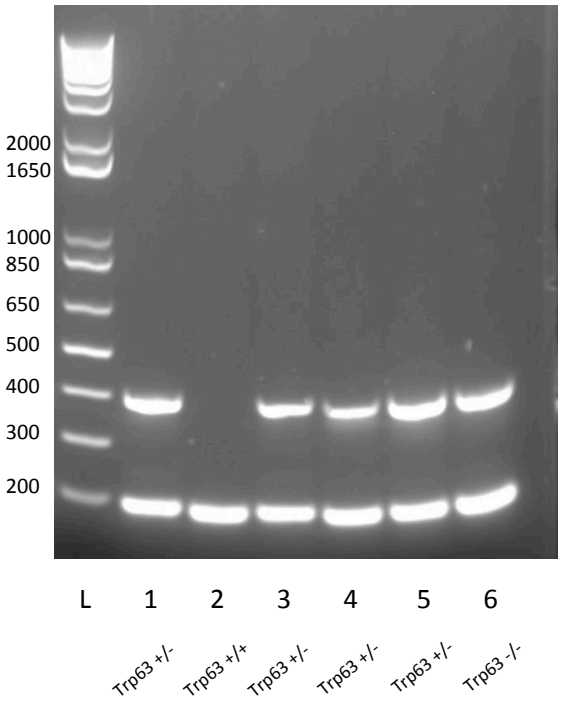

Figure 5. A UV-lit agarose gel showing the amplified internal control band (200bp) and mutated allele in heterozygote (*Trp63+/-*) or *Trp63-/-* homozygote (*Brdm2*) via amplification of a 400bp band. The absence of a 400bp band indicates that both alleles are normal and the embryo is therefore wild type (WT; $Trp63^{+/+}$), as shown in Lane 2. L = DNA ladder (Invitrogen Ultra-Pure Agarose, Life technologies, Carlsbad, U.S.A.).

2.2.2 Extraction of total RNA from E10-13 mandibular processes

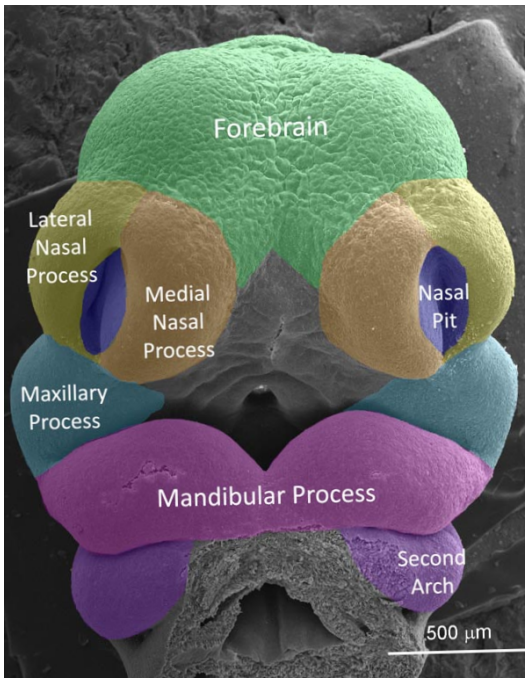

Figure 6. Embryonic mouse head aged day 10 showing the various facial processes, including the whole mandibular process (lavender) that was micro-surgically excised for RNA and protein extraction (see sections 2.2.3 and 2.2.5). The *entire mandibular process* was excised for all the various stages, E10-13, for wild types, heterozygotes and homozygotes. Source: https://www.facebase.org/sites/default/files/SEM_images/anatomy.html

On Day 1 of the procedure, total RNA was extracted from entire MdP of wild type, heterozygote, and homozygote embryos aged E10-13. RNA was extracted using an RNeasy Mini Kit (Qiagen, Valencia, U.S.A). For maximum RNA purity, tissues were spun down for 5 min at 4°C, the L-15 was extracted and replaced with 1 ml of cold TRIzol (Life Technologies, Carlsbad, U.S.A). Tissues were then completely homogenized using a 23-gauge needle (with 1 ml syringe, Becton Dickinson, Franklin Lakes, U.S.A.). Next, 300 µl of chloroform was added to each tube, which was then vortexed for 15 seconds. This was followed by RT incubation

for 4 min., then a centrifuge spin for 20 min. at 12,000 (12K) RPM at RT. Only the clear supernatant was extracted and an equal amount of DEPC treated 70% ethanol (EtOH) was added to the supernatant, and immediately stored at -80°C until Day 2 of extraction procedure.

Day 2 of the RNA extraction procedure began by transferring each sample of the stored, thawed supernatant/ethanol solution to an RNeasy spin column, followed by a 1 min. spin at 12K RPM at RT. Spin columns were washed with 380 µl of RW1 buffer and centrifuged for 2 min. at 12K RPM followed by 80 µl of RNase-free DNase treatment (7:1 of RDD buffer:RNase-free DNase) incubation for 30 min. at 37°C. Subsequent steps involved: one 350 µl RW1 and two 500 µl RPE washes, with a spin at 12K RPM for 2 min. between each wash. The last RPE wash was followed by a 5 min. spin to ensure that all of the wash buffer was removed. Lastly, 30 µl of RNase-Free water was transferred to each spin column and incubated at 10 min. at RT followed by a 3 min. spin at 12K RPM. Eluted RNA was immediately stored at -80°C, until needed for further analysis.

Three biological replicates for each genotype (wild type, heterozygote, homozygote) and embryonic stage (E10-13) were collected for RT-qPCR assay, for a total of 36 samples.

Table 2. Summary of sample set of mandibles collected for RT-qPCR assay. For each stage and genotype, 3 mandibles were excised from embryos of different litters.

	Genotype and **number of mandibles collected**
Embryonic stage	
E10	Wild type – 3 Heterozygote - 3 Homozygote -3 Total = 9
E11	Wild type – 3 Heterozygote - 3 Homozygote -3 Total = 9
E12	Wild type – 3 Heterozygote - 3 Homozygote -3 Total = 9
E13	Wild type - 3 Heterozygote - 3 Homozygote – 3 Total = 9

2.2.3 RNA integrity and quantity assessment

An Experion Automated Electrophoresis Station (Bio-Rad, Hercules, U.S.A.) was used to quantify and quality-check extracted RNA. The electrophoresis station uses minute quantities of extracted RNA pipetted into a 12-well microfluidic chip to

measure RNA concentration (ng/µl) and integrity via an RNA quality indicator value (RQI). An RQI value of 10 indicates high quality RNA, while an RQI value of 1 indicates degraded RNA. Manufacturer instructions were used for sample and chip preparation. In short, the chip was primed with gelstain (as provided in the kit), and loaded with appropriate buffers (i.e., gel and loading buffers, ladder and samples) prior to the electrophoresis run. The RQI value and concentration values of each sample were noted. Samples with an RQI above 7 were used for downstream RT-qPCR. Results from a sample run are shown in Figure 7, below.

Figure 7, shows RNA quantity and quality as assessed with the Experion Electrophoresis System. Detailed information for extracted RNA, such as concentration, integrity via RQI value (Table 3), and ratio of 28S:18S rRNA is also given (not shown). Also shown in the Figure 7 is the electrophoresis profile indicating presence of 28S, 18S, and 5S rRNA in every sample.

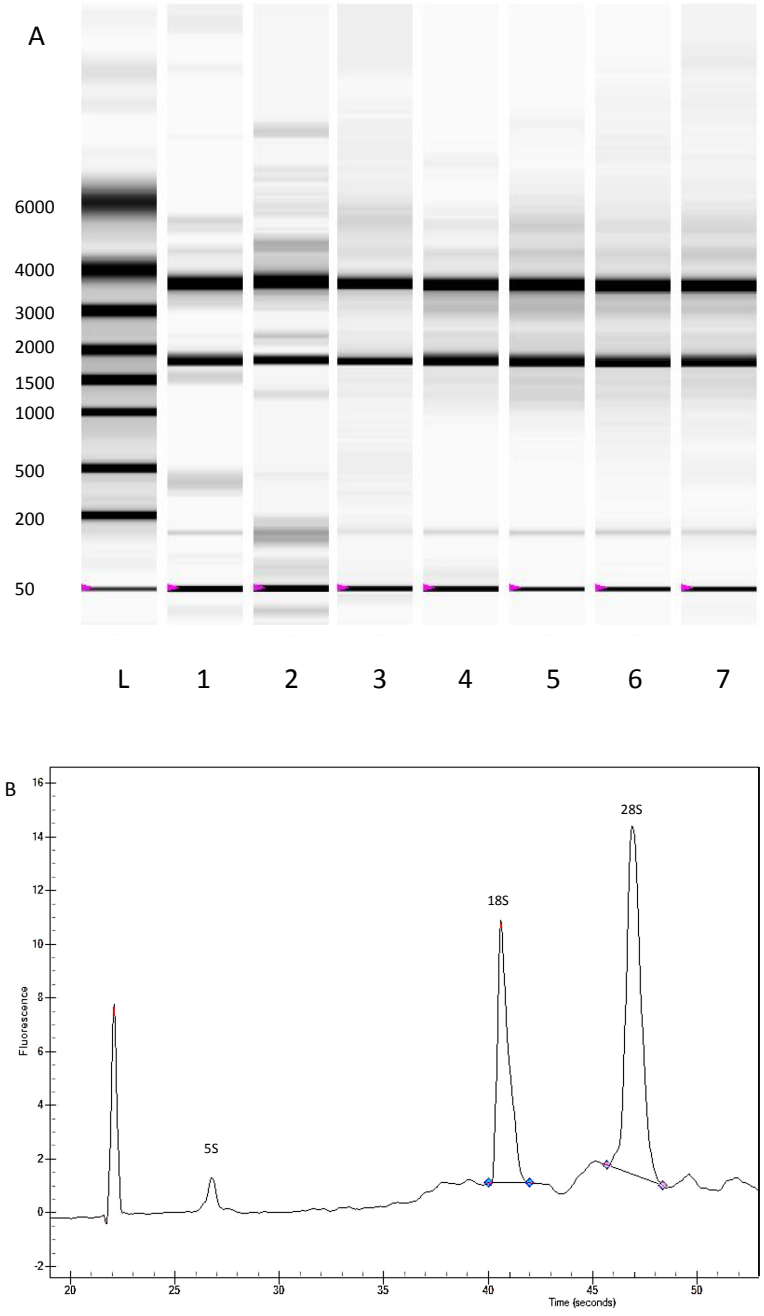

Figure 7. Profiles of 7 different RNA samples analyzed with the Experion Electrophoresis System. A) Virtual image of RNA separated via microfluidic electrophoresis shows the ladder for RNA extracted from a single MdP. Black bands show presence, density and concentration of 18S and 28S rRNA. B) Histogram from a lane, depicting peaks in fluorescence corresponding to 5S, 18S and 28S rRNA.

Table 3 indicating RQI value and concentration of extracted RNA in lane 1-7.

Lane	RQI value	Concentration (ng/uL)
1	10	11.51
2	10	10.48
3	9.4	17.90
4	9.7	19.88
5	9.6	50.51
6	9.3	37.22
7	9.5	24.91

Frozen fully-extracted RNA samples from above were overnight-shipped on dry ice to Plateforme Génomique, Université de Montréal, Quebec for RT-qPCR assay.

2.2.4 Reverse Transcriptase Quantitative Polymerase Chain Reaction

At Plateforme Génomique (Montreal, Canada), purified RNA was reverse transcribed with random primers using the High Capacity cDNA Reverse Transcription Kit (Life Technologies, Carlsbad, U.S.A.). Table 4, below summarizes the reagents used for the protocol, as prescribed by the manufacturer.

Table 4. Details of reagents used for reverse transcription of mRNA to cDNA.

Reagent	**Volume per reaction (uL)**
10X reverse transcription buffer	2.0
25X dNTP Mix (100 mM)	0.8
10X reverse transcription Random Primers	2.0
MultiScribe Reverse Transcriptase	1.0
Nuclease-free H_20	4.2
Extracted RNA	10
Total	**20**

Reaction mixture above (Table 4) was incubated for 10 min. at RT and then for 2h at 37°C. Immediately afterwards, cDNA template product was diluted 1:5 and stored in -20°C for downstream qPCR.

Primers for qPCR were designed with the UPL Assay Design service (Roche, Indianapolis, USA). A standard curve was performed to calculate primer efficiency. Quantitative PCR was performed using the master mix summarized in Table 5.

Table 5. Specific reagents and volumes used in amplification of cDNA. The Viia7 qPCR instrument (Life Technologies, Carlsbad, U.S.A.) was used to detect amplified cDNA via fluorescence intensity measurements, and was programmed as shown below.

Reagents	**Volume (µl) per reaction**
cDNA template	1.5
2x TaqMan Advanced Fast Universal PCR Master Mix	5.0
50 µM primer mix (forward and reverse)	0.05
1 µM UPL probe	1.0
MilliQ water	2.45

Table 6. Depicting the thermocycler program used for amplification of cDNA in qPCR assay using Viia7 qPCR instrument (Life Technologies, Carlsbad, U.S.A.).

95°C for 20sec	
95°C for 1sec	Repeat for 40 cycles
60°C for 20sec	

All reactions performed on the 36 samples collected (Table 2) were run in three technical replicates. Mean cycle threshold (CT) values were used for data analysis. The three housekeeping genes tested were glyceraldehyde 3-phosphate dehydrogenase (GAPDH), TATA binding protein (TBP), 14-3-3 protein zeta/delta (YWHAZ).

Table 7. Primer information outlining forward and reverse sequences, NCBI reference numbers, and primer efficiencies of the genes assayed using RT-qPCR.

Gene	**Fwd. Primer Sequence**	**Rev. Primer Sequence**	**Reference Sequence**	**Primer Efficiency %**
Fermt1	Cgccaatatgaagcagtgg	gtcaaactcgattgccacct	NM_198029.2	101
Pltp	Gacacttgttggggacaagg	gtggggagttaatcactgtcg	NM_011125.2	101
Cbln1	Cacactcccgtttccaaaat	ttcctcgattactgcgactg	NM_019626.3	101
Trp63	ctgatgattttggcattagcc	ctaaacactggtgtgaggagaca	NM_001127259.1 (exon 14 isoforms 1,2,4,5,6)	96
Cxcl14	Gacagacggcaggagcac	tttcaagcacgcctctctc	NM_019568.2	97
Krt8	Agttcgcctccttcattgac	ccacttggtctccagcatct	NM_031170.2	91
Gapdh	Tgtccgtcgtggatctgac	cctgcttcaccaccttcttg	NM_008084.2	91
Tbp	Cggtcgcgtcattttctc	gggttatcttcacacaccatga	NM_013684.3	92
Ywhaz	cttcctgcagccagaagc	gggtttcctccaatcactagc	NM_011740.3	101

Analysis of RT-qPCR data was performed with Rest Expression Software Tool (REST, Qiagen, Valencia, U.S.A.). Primer efficiencies were accounted for using REST,

and mRNA expression was studied in heterozygote and homozygote samples. All data were normalized to the most stable gene, TBP, with 2000 randomizations.

2.2.5 Protein extraction from mandibular tissue and immuno-blotting

All the following procedures were done with samples kept on ice for protein preservation and sample integrity. Pregnant mice were sacrificed and collected for embryos staged between E12-13. Upon excision, whole MdPs were collected in 20 µl of RIPA buffer (5 mM Tris, 150 mM NaCl pH 7.4, 1% Triton X-100, 0.1% sodium deoxycholate, 5 mM EDTA) and immediately stored in -80°C. Remaining tail clips were frozen in -20°C for genotyping, performed as described above. Sample preparation for RT-qPCR work did not require the need of pooling multiple MdPs into one to generate a concentrated sample for subsequent mRNA testing. Conversely, the protein yield of a single MdPs was simply not enough to even perform one run with western blotting therefore, pooling of tissue for protein work was necessary. For E13, three genotypically identical MdPs were pooled into a total volume of 60 µl of RIPA buffer to yield one sample (n=1). For E12, four genotypically identical MdPs were pooled in 40 µl of RIPA to yield one sample (n=1). E10-11 mandibles were excluded from protein study due to extremely small protein yield per MdPs. This would require pooling more than 5 separate MdPs in a small volume of RIPA buffer, which required sacrificing many mice beyond what could comfortably be justified, further prolonging the length of my MSc Program of Study. Pooled tissues were digested using a 1.5 ml plastic pestle, followed by the addition of 100x protease inhibitor (G-Biosciences, St. Louis, U.S.A.) to a final concentration of 1x. A centrifuge spin at 12K RPM at 4°C was performed and supernatant collected. Approximately 8 µl of supernatant was used to assess protein concentration with 660nm protein assay (Thermo Scientific Pierce, Waltham, U.S.A.) on a 96-well plate reader (Molecular devices, Sunnyvale, U.S.A.).

At least three biological replicates (n=3) for each genotype (wild type, heterozygotes, homozygotes) and embryonic stage (E12-13) were collected for western blotting assay.

Immuno-blotting was used to test FERMT1 (77 kDa Abcam (ab68041), Cambridge, U.K.), PLTP (55 kDa Abcam (ab18990), Cambridge, U.K.), TRP63 (63 kDa Santa Cruz Biotechnology (sc-8609, discontinued), Dallas, U.S.A.), GAPDH (37 kDa loading control, Santa Cruz Biotechnology (sc-25778), Dallas, U.S.A.) and CBLN1 (15kDa Abnova (PAB13159), Taipei, Taiwan). Antibody for TRP63 was specific to the α, β and γ isoforms belonging only to the ΔN-P63 variant. Several positive control lysates extracted from tissue and cell lines were also used: HeLa cells staurosporine treated (Abcam, Cambridge, U.K.), mouse brain tissue lysate (prepared in lab), and HEK293 cells (Santa Cruz Biotechnology, Dallas, U.S.A.). Precision Plus Protein™ Kaleidoscope™ molecular marker (Bio-Rad, Hercules, U.S.A.) was used according to manufacturer recommended instructions. An 8% running gel was prepared for FERMT1 and PLTP, 6% for TRP63, and 12% for CBLN1

Table 8. Reagents and volumes used for the 6% running gel (left), and stacking gel (right). Asterisk indicates values that vary depending on gel percentage.

Reagents (for 6% running gel)	**Volume**	**Reagents (for stacking gel)**	**Volume**
Acrylamide:Bis 29:1 (30%)	2.26 ml *	Acrylamide:Bis 29:1 (30%)	2.5 ml
Tris 2M (pH 8.8)	2.8 ml	Tris 0.5M (pH 6.8)	6.5 ml
MilliQ H20	9.84 ml *	MilliQ H20	50 µl
20% sodium dodecyl sulfate	75 µl	20% sodium dodecyl sulfate	50 µl
10% Ammonium persulfate	75 µl	10% Ammonium persulfate	15 µl
Temed	10 µl	Temed	15 µl

10 µg of digested mandibular tissue lysates and positive controls were separated on a running gel for approximately 1h. Following electrophoresis, the gel was soaked in transfer buffer (25 mM Tris base, 0.2 M glycine, 20% methanol) for 20 min. prior to transferring the protein to a polyvinylidene fluoride (PVDF, Bio-Rad, Hercules, U.S.A.) membrane using Trans-Blot SD Semi-Dry electrophoresis Transfer Cell (Bio-Rad, Hercules, U.S.A.). Sandwich assembly for transfer was done according to manufacturer recommendations. Transfer of FERMT1, PLTP and TRP63 was performed at 18V for about 70 min. Transfer for Cbln1 was performed at 18V for 20 min.

Blocking buffer and 5% milk powder (Cell Signaling, Danvers, U.S.A.) in tris tween buffered saline (TTBS, Tris 19.9mM pH 7.8, NaCl 154mM, 0.001% Tween-20) was incubated with the membrane for 1h at RT. This was followed by incubation with primary antibody using the following dilutions: FERMT1 1:1000, PLTP 1:1000, GAPDH 1:1333, CBLN1 1:500**,** TRP63 1:1000 in either TTBS or 5% milk powder in

TTBS at 4°C overnight. The next day, 3 x 10 min. TTBS washes were performed, followed by secondary antibody incubation. Secondary HRP-conjugated antibody (Invitrogen, Carlsbad, U.S.A.) and Strep-Tactin® tagged HRP for detection of ladder (Bio-Rad, Hercules, U.S.A.), with dilutions of 1:5000 and 1:15000 in TTBS, respectively were applied to the membrane at RT for 2h, followed by three 10 min. washes with TTBS. Chemiluminescence detection solution (68mM p-Coumaric acid in DMSO, 1.25mM luminol in 0.1M Tris (pH 8.5), and 3% hydrogen peroxide mixed at .010:1:.003, respectively) was applied to the membrane for 1 min. Membranes were then exposed to radiography film (Denville Scientific, Holliston, U.S.A.) for varying times. ImageJ (NIH, Bethesda, U.S.A.) and GraphPad prism 5 (La Jolla, U.S.A.) was utilized for band densitometry analysis.

Note that only mRNA was studied for *Krt-8* and *Cxcl-14*. Western blot analysis was not performed on these two genes due to insufficient tissue lysates, time constraints, need for significantly more breeding and thus increased cost.

2.3 Results

2.3.1 RT-qPCR REST analysis

RT-qPCR was performed on RNA extracted from the MdP of embryonic mice aged E10-13. Raw data from the RT-qPCR assay was analyzed with REST expression analysis (Pfaffl et al., 2002) to determine: 1) the integrity of the microarray results and; 2) changes in RNA quantity in the edentulous homozygote vs. the normal-looking heterozygote samples.

2.3.1.1 mRNA quantities differed between homozygote and heterozygote mandibular primordia aged E10-13

Amongst the homozygotes aged E10 (Figure 8), expression of the genes-of-interest (*Fermt1*, *Pltp*, *Cbln1*, *Krt-8*, *Cxcl14,* and *Trp63*) were both increased and

decreased as assessed by RT-qPCR quantification. REST expression analysis of RT-qPCR data revealed *Fermt1* was down-regulated in homozygote embryos by a magnitude of 0.657 relative to heterozygotes. RT-qPCR detected more *Cbln1* and *Krt-8* mRNA by factors of 3.73 and 2.96, respectively, amongst homozygotes relative to heterozygotes. Meanwhile, mRNA products for *Cxcl14*, *Trp63* and *Pltp* were not significantly altered in their quantity in homozygotes relative to heterozygotes.

E10

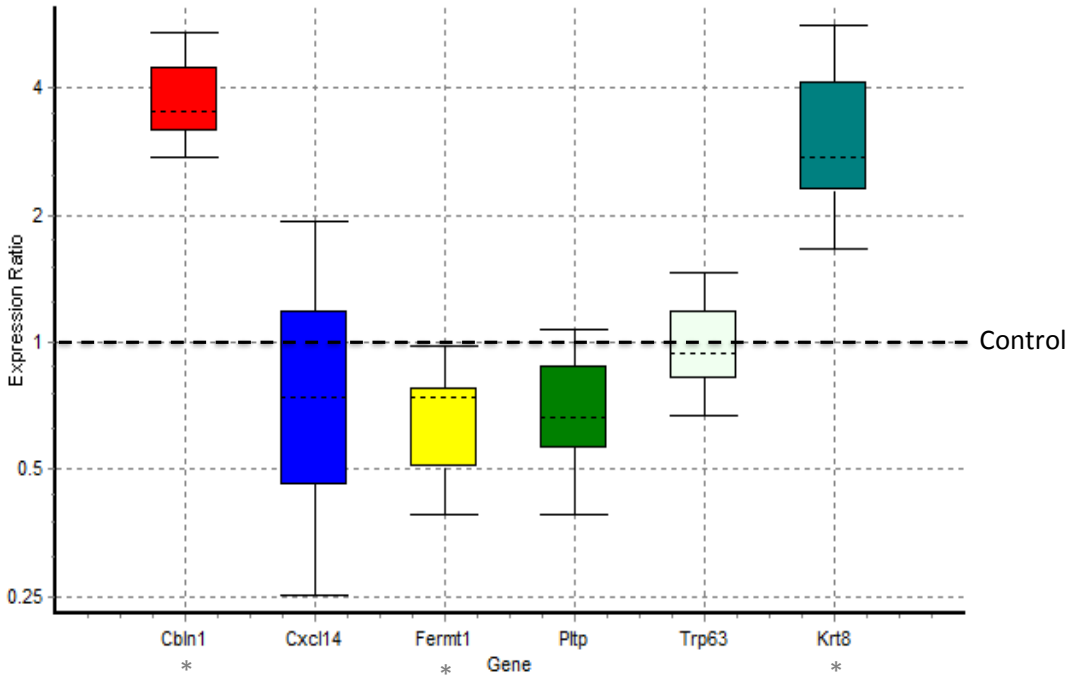

Figure 8. Relative expression software tool (REST) analysis of RT-qPCR performed on RNA derived from E10 homozygotes (experimental) vs. heterozygotes (control). At E10, quantities of *Cbln1* and *Krt-8* mRNA were increased in the homozygote relative to heterozygote by a magnitude of 3.73 and 2.96, respectively. Conversely, quantity of mRNA for *Fermt1* was decreased in the homozygote by a magnitude of 0.657 compared to E10 heterozygotes. *Trp63* mRNA was unchanged in the homozygote relative to heterozygote. N=3 for each genotype, significance of $p \leq 0.05$. Reference mRNA was *Tbp*. Error bars indicate range of maximum and minimum mRNA values. The lower and upper limit of each box accounts for the interquartile range, or the middle 50% of observations. Asterisks indicate mRNA's with significant change in expression. The dashed line within each colored box represent median. Dashed line outlined across the graph, represents levels within the heterozygotes (control).

Likewise, similar patterns of changes in mRNA quantities were seen for E11 embryos (Figure 9). Quantity of *Fermt1* mRNA was lower in homozygotes than in heterozygotes by a factor of 0.11. Interestingly, *Pltp* mRNA decreased in homozygotes compared to heterozygotes by a magnitude of 0.22. Conversely, compared to heterozygotes, homozygotes had 5.84 and 2.15 times the amount of mRNA for *Cbln1* and *Krt-8*, respectively. As seen at E10, normal levels of *Trp63* mRNA in E11 were present in homozygote relative to the heterozygote mandibles.

E11

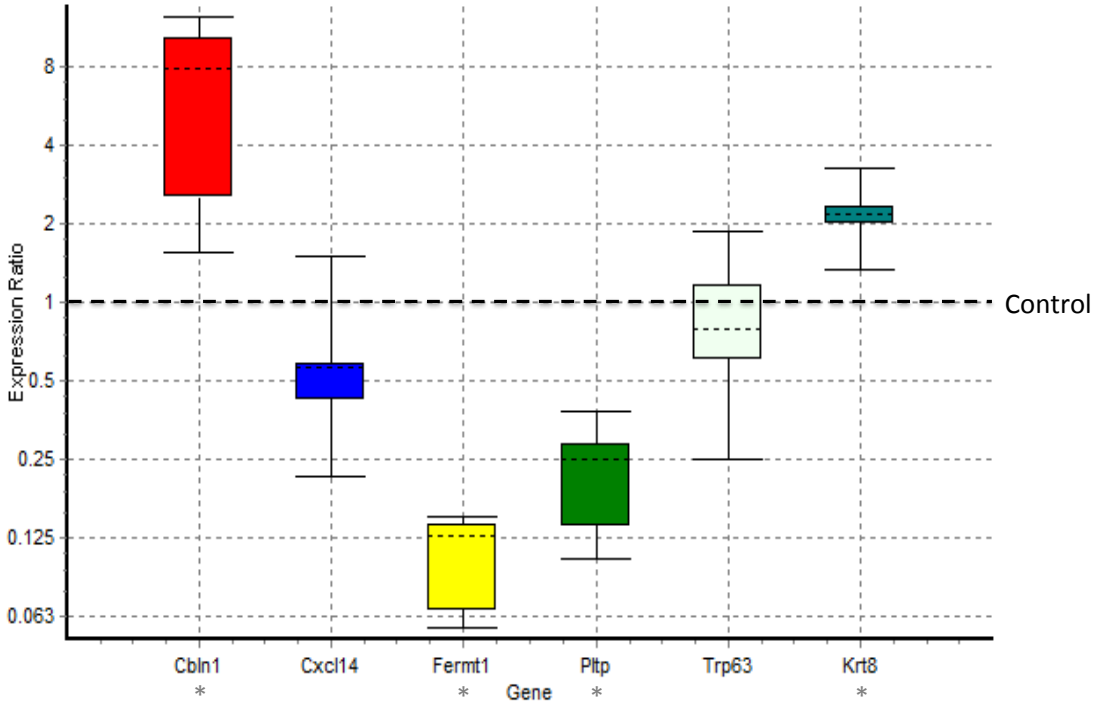

Figure 9. Box and whisker plot of REST expression analysis on output from RT-qCPR assay performed on mandibular derived RNA from E11 mice for homozygotes (experimental) relative to heterozygote (control). In comparison to the heterozygote, homozygotes show an increase in *Cbln1* and *Krt-8* mRNA's on the magnitude of 5.84 and 2.15, respectively. Significant down-expression was also seen in *Fermt1* and *Pltp* mRNAs on the order of 0.11 and .22, respectively, in the homozygote vs. the normal-looking heterozygote. *Trp63* mRNA was unchanged in the homozygote relative to heterozygote. N=3 for each genotype. Significance of $p \leq 0.05$. Reference mRNA was *Tbp*. Error bars indicate range of maximum and minimum values. The lower and upper limit of each box accounts for the interquartile range, or the middle 50% of observations. Asterisks indicate genes that showed significant change in expression. Dashed line within box and whiskers represents median. Dashed line outlined across the graph, represents levels within the heterozygotes (control).

An embryonic day later, at E12 when tooth primordia are nearing bud-stage, the homozygote MdP showed a significant increase in *Cbln1* and *Krt-8* RNA quantity by factors of 5.290 and 7.514, respectively. Unexpectedly, no down-regulation of any mRNA was seen in E12 homozygote relative to heterozygote. *Trp63* levels were unaltered in the homozygote compared to the heterozygote.

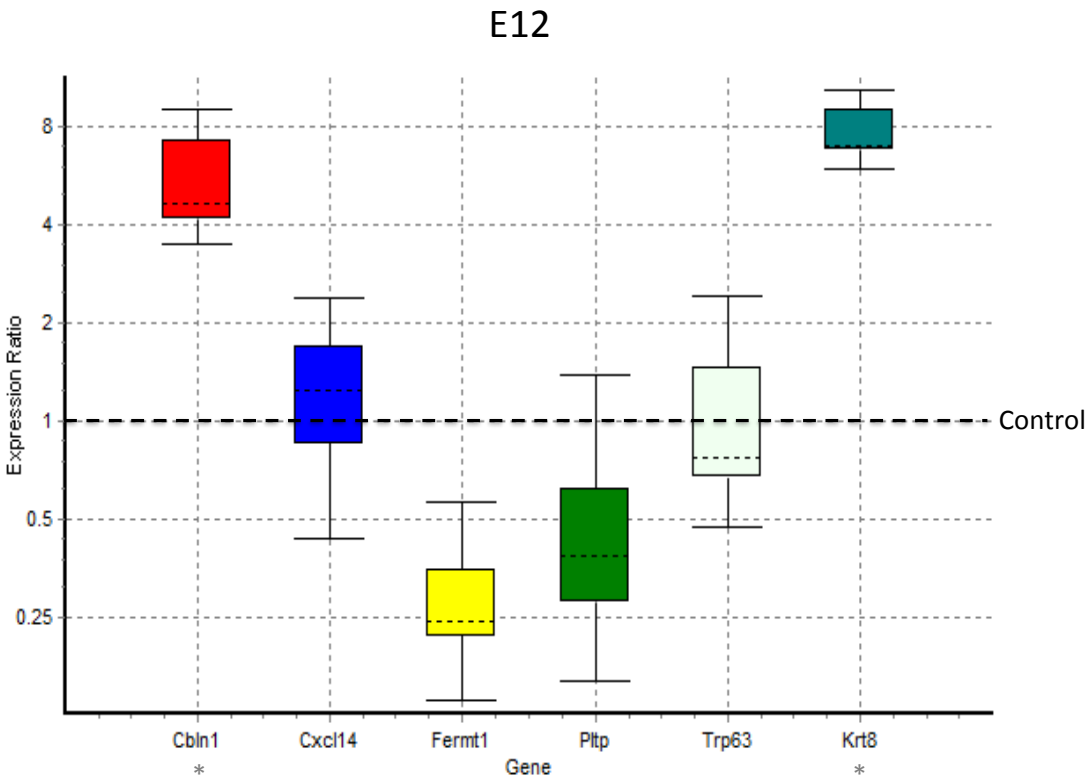

Figure 10. Box and whisker plot showing that, in E12-aged homozygotes, there was 5.290 and 7.514 times more mRNA measured, respectively, for *Cbln1* and *Krt-8* compared to heterozygotes (control, represented by the dashed black line). Significant under-expression in the homozygote was not seen in any mRNAs tested. In other words, mRNA levels for any gene tested did not decrease in the experimental relative to control. N=3 for each genotype, significance of $p \leq 0.05$. Reference gene was *Tbp*. Error bars indicate range of maximum and minimum values. The lower and upper limit of each box accounts for the interquartile range, or the middle 50% of observations. Asterisks indicate genes that showed significant change in expression. Dashed line within box and whiskers represents the median.

Lastly, at E13, expression patterns of *Fermt1*, *Cbln1*, and *Krt-8* mRNAs were altered (Figure 11) in homozygote relative to heterozygote mandibles. Lower-than-normal expression levels, by a factor of 0.1, were seen for *Fermt1* mRNA in homozygotes relative to heterozygotes. Greater-than-normal expression of *Cbln1* and *Krt-8* mRNA were detected in the homozygote vs. the heterozygote by factors of 6.4 and 6.2, respectively.

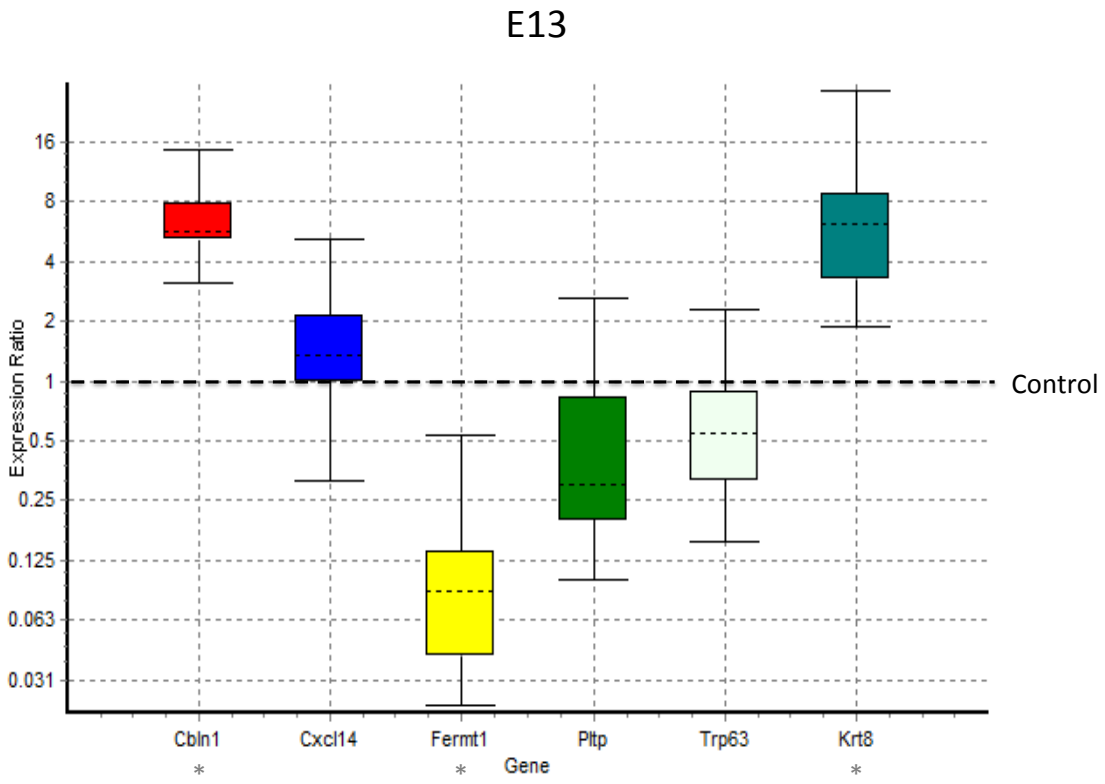

Figure 11. E13 mRNA expression profile generated by REST expression analysis on RT-qPCR data. Box and whiskers represent homozygotes (experimental) and colored and dashed line represents heterozygotes (control). Within homozygotes, *Cbln1* was increased by a factor of 6.4, while *Krt-8* was increased by a factor of 6.2, both relative to heterozygotes. Only *Fermt1* mRNA was significantly down-expressed, and by a factor of 0.1 times the levels in heterozygotes. N=3 for each genotype, significance of $p \leq 0.05$. Reference gene was *Tbp*. Error bars indicate range of maximum and minimum values. The lower and upper limit of each box accounts for the interquartile range, or the middle 50% of observations. Asterisks indicate genes with significant change in expression. Dashed line within box and whiskers represent median.

2.3.2 Western blotting revealed no significant change in protein expression in the homozygote

As described in the Methods (2.2.5), E10-11 mandible primordia were excluded from the protein analysis. E12-13 MdP tissue digests extracted from wild type, heterozygote, and homozygote were used to quantify FERMT1, PLTP, CBLN1, and TRP63 protein products.

At E12, western blot analysis showed no statistically significant ($p>0.05$) change of FERMT1 in homozygote compared to wild type MdPs. For PLTP expression, a similar result was seen whereby, there was no significant change ($p>0.05$) in the homozygote relative to wild type MdPs. Western blot results for FERMT1 (Figure 12) aligned with the RT-qPCR (Figure 10) results, showing that levels of neither mRNA nor protein significantly differed in homozygote relative to wild type or heterozygote embryos at E12. This is also true for *Pltp*, as there appeared to be no significant alteration in mRNA or protein product of this gene in the homozygote relative to wild type or heterozygote at E12.

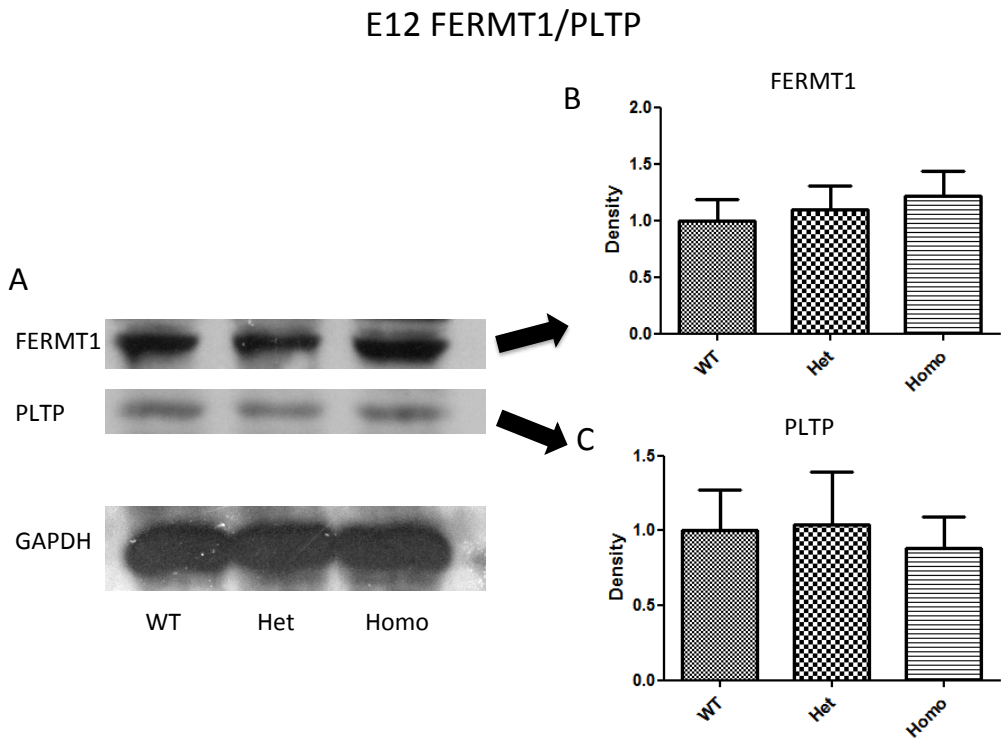

Figure 12. A) Image of Western blot indicating protein levels of FERMT1 (77 kDa), PLTP (55 kDa), and loading control GAPDH (37 kDa) at E12 in wild type, heterozygote, and homozygote mandibular tissue lysates. B) Densitometry analysis revealed no significant ($p>0.05$) decrease in FERMT1 in homozygotes relative to wild type. C) Densitometry analysis of PLTP also showed no significant ($p>0.05$) decrease in the homozygote relative to wild type. N=3 for each genotype. Error bars indicate minimum and maximum range at 95% confidence interval.

For CBLN1, electrophoresis and immuno-blotting on E12 mandibular lysates revealed no significant change in protein level in homozygote relative to wild type MdP (Figure 13). This result disagreed with what was seen at the mRNA level: a significant up-regulation of *Cbln1* by a factor of 5.2 in the homozygote relative to heterozygote (recall no wild-type data for comparison).

E12 CBLN1

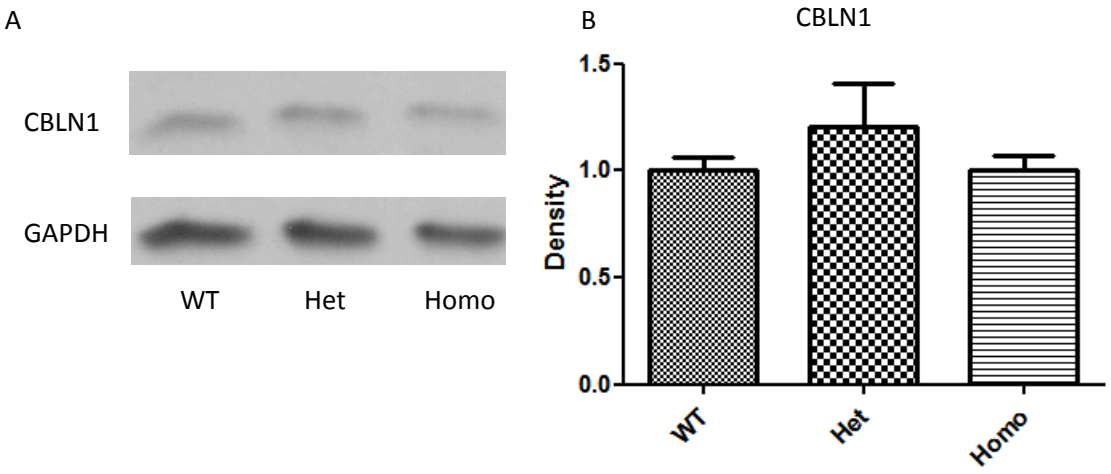

Figure 13. A) Western blot image depicting band density of the CBLN1 (15 kDa) and GAPDH (37 kDa, loading control) in E12 wild type, heterozygote, and homozygote mandibular tissue lysates. B, densitometry analysis indicating insignificant ($p>0.05$) differences in expression amongst homozygote, heterozygote and wild type mandibular tissues. N=3 for each genotype. Error bars indicate minimum and maximum values at 95% confidence interval.

Lastly, E12 lysates were used to study TRP63 protein expression amongst the three genotypes. TRP63 (Figure 14) was unaltered ($p>0.05$) amongst the homozygote relative to wild type lysates. The phenotypically normal heterozygote also showed no significant change in TRP63 protein compared to wild type. A strong presence of *Trp63* was also seen at the mRNA transcript level amongst the homozygotes, affirming that within the double mutated MdP, *Trp63* is being transcribed and translated.

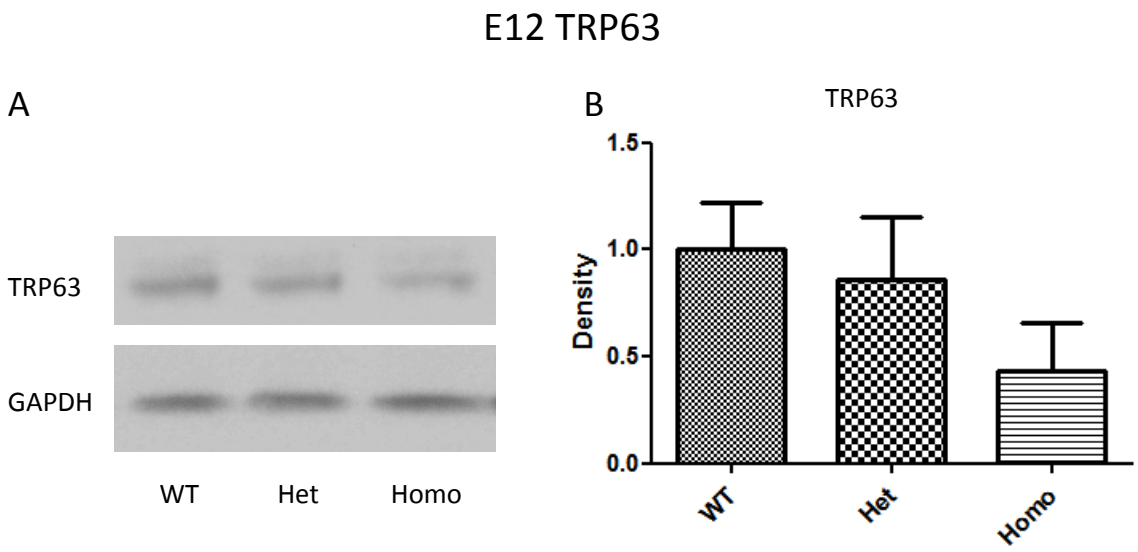

Figure 14. A) Western blot image indicating protein levels of TRP63 (63 kDa) and reference gene GAPDH (37 kDa) in wild type, heterozygote, homozygote E12 mandibular tissue lysates. Densitometry analysis in B) showing what appears to be a noticeable decrease in TRP63 protein in homozygote relative to wild type, but which is statistically insignificant. N=3 for each genotype. Error bars indicate minimum and maximum range at 95% confidence interval. Statistically significance of $p \leq 0.05$.

Moving forward to E13, similar patterns of protein expression were seen as in E12. First, western blot analysis revealed no change in the homozygote mandible for FERMT1 (Figure 15) compared to wild type ($p > 0.05$). Interestingly, heterozygote mandibles also exhibited nearly identical levels of FERMT1 as homozygotes.

Detection of PLTP amongst E13 mandible-derived lysates showed no real change in the homozygotes vs. the wild type (Figure 15), although interestingly the heterozygote showed levels of PLTP that were significantly lower ($p < 0.05$) than both other genotypes.

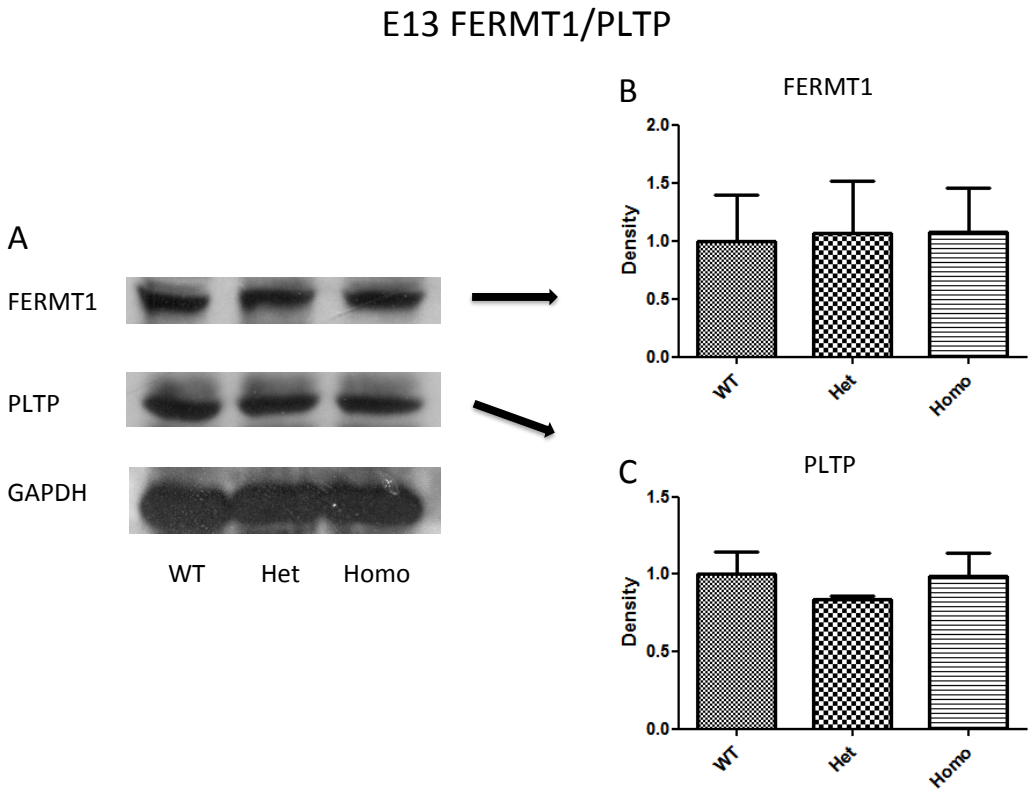

Figure 15. A) Western blot protein profile revealing protein levels of FERMT1 (77 kDa), PLTP (55 kDa) and reference gene GAPDH (37 kDa) in wild type, heterozygote and homozygote E13 mandibular tissue lysates. Densitometry analysis revealing no significant ($p>0.05$) differences in FERMT1 (B) and PLTP (C) within homozygote lysates compared to wild type. N=3 for each genotype. Error bars indicate minimum and maximum range at 95% confidence interval.

CBLN1 was also probed in E13 MdP lysates using western blotting. This protein, like others that were examined, was virtually unaltered ($p>0.05$) in the homozygote vs. heterozygote/wild type MdP (Figure 16).

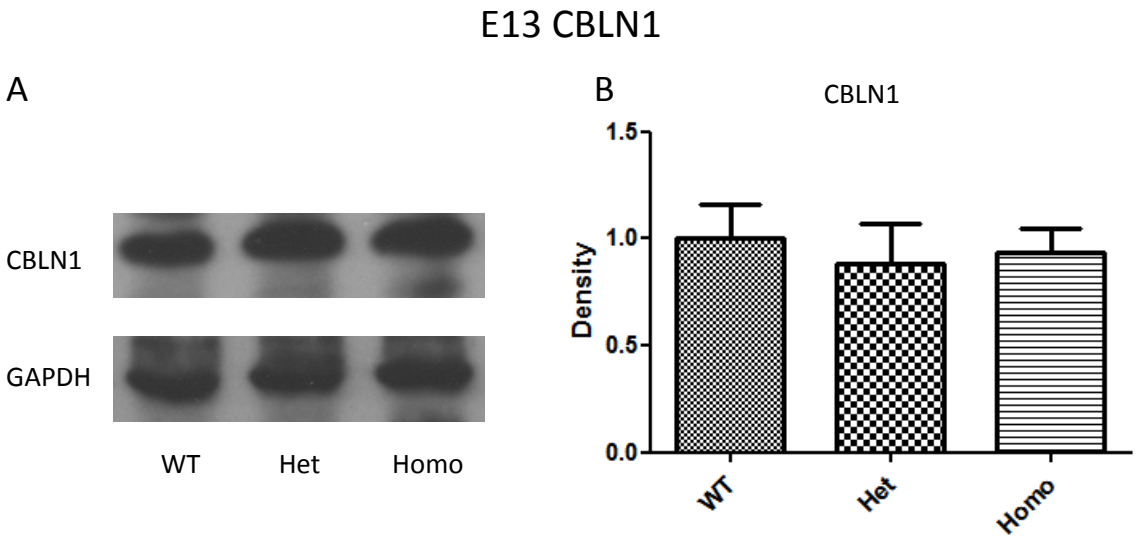

Figure 16. A) CBLN1 (15 kDa) protein profile generated by western blot run on wild type, heterozygote, and homozygote lower jaw tissue lysate derived from E13 embryos. B) Densitometry analysis revealing unchanged levels of CBLN1 amongst homozygote relative to wild type MdP. N=3 for each genotype. Error bars indicate minimum and maximum range at 95% confidence interval.

Lastly, TRP63 protein expression was analyzed via western blotting, within wild type, heterozygote, and homozygote E13 mandible-derived lysates. Surprisingly, in the homozygote, TRP63 (Figure 17) was present at near-normal levels relative to heterozygote MdPs.

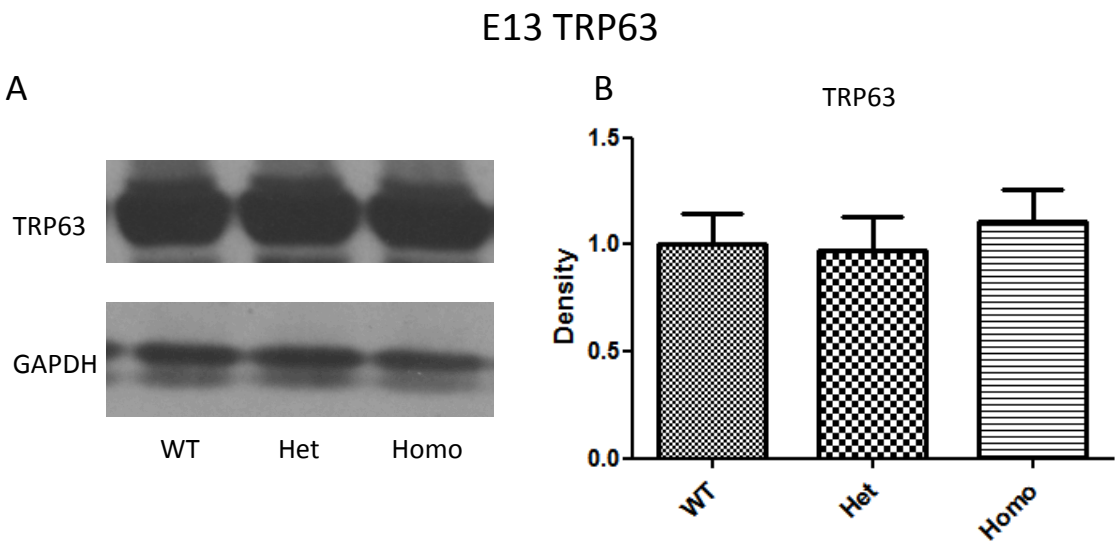

Figure 17. A) Abundance of TRP63 (63 kDa) and GAPDH (37 kDa) in wild type, heterozygote, and homozygote in E13 mandibular tissue lysates. B) Densitometry analysis revealing no significant ($p>0.05$) change in TRP63 amongst homozygote relative to wild type. N=3 for each genotype. Error bars indicate min and max range at 95% confidence interval.

In summary, RT-qPCR revealed genetic perturbations within the toothless mouse mutant. For *Trp63,* mRNA and protein levels were both unchanged in the homozygote relative to heterozygote/wild type MdP. For *Cbln1,* an increase in expression levels were only seen for mRNA but not protein. For *Pltp*, down-expression was seen only at E11 at the mRNA level and protein levels were unchanged. *Fermt1* mRNA down-expression was seen in all stages except E12 meanwhile, protein analysis showed no change. Lastly, *Krt2-8* mRNA levels were increased for all stages (E10-13) and protein expression was not studied. These results are also summarized in Table 9 below.

Table 9. Summary of mRNA and protein expression showing increase (black arrow), decrease (grey arrow), and lack of change (dash) in homozygote relative to wild type/heterozygote mandibular primordial amongst E10-13 embryonic mice.

Gene expression in homozygote (relative to wild type/ heterozygote)					
Embryonic day (E)	***Cbln1***	***Krt2-8***	***Fermt1***	***Pltp***	***Trp63***
10	**mRNA: ↑**	**mRNA: ↑**	**mRNA: ↓**	**mRNA: –**	**mRNA: –**
11	**mRNA: ↑**	**mRNA: ↑**	**mRNA: ↓**	**mRNA: ↓**	**mRNA: –**
12	**mRNA: ↑ protein: –**	**mRNA: ↑**	**mRNA: – protein: –**	**mRNA: – protein: –**	**mRNA: – protein: –**
13	**mRNA: ↑ protein: –**	**mRNA: ↑**	**mRNA: ↓ protein: –**	**mRNA: – protein: –**	**mRNA: – protein: –**

2.4 Discussion

2.4.1 Relative to wild type, in *Brdm2* mutant mice normal levels of CBLN1 protein suggest its expression is regulated by *Trp63*-independent pathways.

This study revealed the dynamics of a few genes with mRNA expression levels that were significantly up-regulated or down-regulated in the *Brdm2* mutant mouse MdP. My mRNA results returned by RT-qPCR indicated the strong over-expression of two transcripts, *Cbln1* and *Krt2-8*, in the toothless mutant relative to dentate heterozygotes. Recall that CBLN1 is thus far known to help with signaling in the brain (Hirai et al., 2005) and endocrine secretion (Rucinski et al., 2009). Interestingly, the role of CBLN1 in development, particularly of tooth and upper jaw skeleton/mandible, has yet to be investigated: my results justify doing further work along this line of inquiry. KRT2-8 plays a key role in cell structural integrity particularly within keratinocytes (Oshima, 2002). Previously, it was unknown if or how TRP63 interacted with *Cbln1* and *Krt2-8* products; however, from my mRNA analysis it is evident that if *Trp63* is non- or dysfunctional (i.e., decreased), then *Cbln1* and *Krt2-8* expression levels are increased, at least at the early stages of tooth formation studied here. These increased levels of *Cbln1* and *Krt2-8* mRNA at stages E10-13 in the absence of any normal *Trp63* allele indicate that, in healthy mice, TRP63 normally down-regulates transcription of *Cbln1* and *Krt2-8*. Conversely, in terms of the protein products, deciphering the relationship between CBLN1 and TRP63 was complicated by normal-like levels of CBLN1 protein at E12-13 in homozygotes relative to wild type or heterozygote embryos. Thus the change in CBLN1 levels was not linear across all four stages. The stable levels of CBLN1 protein at E12-13 amongst the homozygotes suggests that a web of molecular pathways, outside of the TRP63 pathway, tightly regulates CBLN1 expression. Cells within the MdP detect the over-expressed *Cbln1* mRNA but maintain CBLN1 protein at normal levels.

Since incongruity exists between mRNA and protein levels one might wonder if a technical problem is at play, but there is little support for this concern because western blot (and RT-qPCR) experiments were performed with multiple biological and technical replicates that yielded consistent results. Rather, the variable levels of *Cbln1* expression warrant a discussion on the lack of consensus in the scientific community about correlation between mRNA and protein expression. Some published reports suggest a negative correlation (Tian et al., 2004) and others a positive correlation (Shebl et al., 2010). To add to the conflict, Glanemann and co-workers (2003) reported that transcriptome and proteome expression levels have no correlation! They showed that a large increase in mRNA abundance does not correspond to a large increase in enzyme activity; which, by extension, means that over-expressing a particular mRNA does not always mandate similar change in protein production. Jang and co-workers (2006) also showed a similar trend with 11-Beta hydroxysteroid dehydrogenase type 1, further confirming the complex and sophisticated relationship between mRNA and protein levels. While these reports explain the various patterns of mRNA vs. protein expression, I believe it is important to note that discrepancies between the levels of these two gene products must be interpreted specific to the genes studied. To clarify, CBLN1, FERMT1, and PLTP may belong to a minority of genes that exhibit non-correlation between mRNA and protein. While this may be unlikely, too little is known from the literature of mRNA and protein expression levels of these genes to test this theory at this time. What is also unknown currently is the minimum change required in mRNA transcript expression to warrant a significant change in protein expression (You and Yin, 2000). The conversion of DNA to mRNA to protein involves highly regulated post-translation and post-transcription modifications (Alberts, 2002). Other factors such as translation efficiency, mRNA stability and mRNA half-life are all variables that may also influence and thus help explain differences between mRNA and protein expression such as that seen here for *Cbln1* and *Fermt1* (discussed shortly). Further, post-translation modifications such as protein ubiquitination, protein half-life and presence of specific amino acids that target protein degradation such as those rich

in proline, glutamic acid, serine, and threonine (PEST) sequences (Vogel and Marcotte, 2012) also regulate protein abundance. Tightly-controlled expression of even a single protein requires negative and positive feedback loops (Franco and Galloway, 2015). These loops are well-regulated pathways composed of several proteins involved in complex biochemical processes. I propose that CBLN1 protein expression depends on such feedback loops whereby, in the *Brdm2* mutant embryo, cells in the MdP recognize the need for normal CBLN1 expression, independent of the loss of normal *Trp63* activity and the subsequent, abnormal increase in *Cbln1* mRNA. CBLN1 protein levels are thus near normal in the homozygote compared to wild type.

Related to the sustained expression of CBLN1 in the MdP, it is known that the overall development and health of nervous tissue is unaffected by the mutation of both normal *Trp63* alleles (Holembowski et al., 2011). The central nervous system (CNS) in the *Brdm2* mutant develops normal neural cells and does not show any malformations at the cellular level (Hernandez-Acosta et al., 2011). The *Trp63* homologue, *Trp73*, and specifically the *ΔN-p73* variant, play a much more pronounced role in the development of the nervous system: deletion of *Trp73* leads to an underdeveloped CNS (Pozniak et al., 2000; Yang et al., 2000). Anatomically, Fried and co-workers (1982), have shown that nerve fibers are present within the MdP and MxP prior to tooth formation. In addition, differentiation and localization of nerves surrounding tooth bud structures have been detected in mice staged as early as E13 (Mohamed and Atkinson, 1983). Therefore, I propose that CBLN1 protein expression in the *Brdm2* mutant MdP is maintained by healthy nerve cells, independently of the *Trp63* network.

Further, for my experimental work I examined the entire MdP, thus adding another level of complexity by including multiple tissue layers and, within these layers, different cell types: epithelial, mesenchymal, muscular, connective. During development, these different cell types have highly specific gene expression and

biochemical responses to stimuli, as well as diverse mitotic rates (Alberts, 2002; Tam and Loebel, 2007). Further, how a cell responds to genetic stress caused by absent, misfolded, mutated or non-functional proteins (Scacheri et al., 2004; Schroder and Kaufman, 2005; Shebl et al., 2010) also affects the understanding of the link between transcript and protein expression levels. The *Trp63* variant, ΔN-p63, is known to regulate the transcription of more than 60 downstream targets (Birkaya et al., 2007). Therefore, a disturbance in this master transcription factor, as seen in the *Brdm2* mutant mouse, results in biochemical chaos including deviation from cellular homeostasis.

In summary, all of the above-mentioned variables need to be appropriately considered to clarify the nuanced relationship between mRNA and protein expression and construct in the MdP the genes that regulate *Trp63* expression, as well as the downstream targets of *Trp63*. From my data, I conclude that expression of the CBLN1 protein does not entirely depend on the presence of normal TRP63 protein, and that other molecular pathways maintain near-normal CBLN1 expression in the *Brdm2* mutant embryos.

2.4.2 Down expression of *Fermt1* mRNA but not protein emphasizes a non-linear relationship between transcript and protein. *Fermt1* role in tooth formation unclear.

Lower levels of *Fermt1* mRNA were seen via the RT-qPCR assays in the MdP of homozygotes at E10, 11 and 13 – but not at E12 – relative to heterozygotes. Thus the RT-qPCR work confirms the microarray results where *Fermt1* mRNA was also decreased in *Brdm2* mutant relative to $Trp63^{+/-}$ embryos. Conversely, FERMT1 expression at E12-13 did not differ between homozygotes and wild types. Hence, in homozygotes non-conformity between mRNA and protein levels of *Fermt1* existed only at E13 (not E12). Many reasons could explain this puzzle, the first of which is the complex relationship between mRNA and protein expression, and the variables

that regulate the levels of each, as discussed above. Also to be considered is the detection limit of western blotting. Some chemiluminescent substrates claim to detect a difference of 1.25 picograms of protein (Life Technologies, Carlsbad, U.S.A.). That our laboratory-made chemiluminescent solution is less sensitive may partially explain why minute differences in protein expression in the homozygotes relative to wild types/heterozygotes would be undetected. Secondly, because bud stage of tooth development begins at E13, cells within the MdP may detect a shortage of *Fermt1* mRNA at E10-11 and attempt to rescue its protein expression via other, *Trp63*-independent pathways. Due to this redundancy, relatively normal levels of *Fermt1* are thus seen at E12. However, if this rescue is real then it is short-lived and slow in response, as by E13, the MdP has grown larger with further differentiation and corresponding change in gene activity, potentially nullifying this partially successful attempt of rescuing *Fermt1* mRNA expression. In other words, the rescue mechanism is simply inadequate to maintain a normal base level of *Fermt1* mRNA and by E13, when the tooth bud is forming, the development of the overall MdP is such that the cells are unable to "keep up". Of course this is simply a prediction of what is possibly occurring and requires further investigation to establish the true relationship of *Fermt1* to TRP63 during early stages of odontogenesis, as I discuss later.

Tiny differences in the protein levels of the genes tested in the homozygotes relative to wild types could also be explained as follows. First, the volume of tooth tissue is of course quite small at E12-13 compared to later stages. If the proteins tested were expressed specifically in and around the developing teeth, then we would expect to see a large decrease in the levels of these protein in, say, E18 homozygote lower jaws relative to those of same-aged wild type or heterozygote mice. However, in homozygote E12-13 MdPs relative to those of wild type or heterozygote, a subtler difference in protein levels would be expected due to the minute volume of the tooth organ at these early embryonic stages. Thus, tooth organ volume could partially explain why at E12-13 little to no difference in protein level

was seen amongst homozygote mandibular tissues in relation to wild type or heterozygote (Figure 18). Another important point to note is that our western experiments were conducted on digested whole MdPs. The digested lysates therefore included both dental and non-dental epithelium as well as regions of the mesenchyme that do not house the developing teeth. Perhaps differential protein expression in these various tissues and regions is not visible in mutant *Brdm2* embryos using western blotting due to tissue mixing and subsequent sample homogenization that obscures expression differences specific to dental epithelium and mesenchyme.

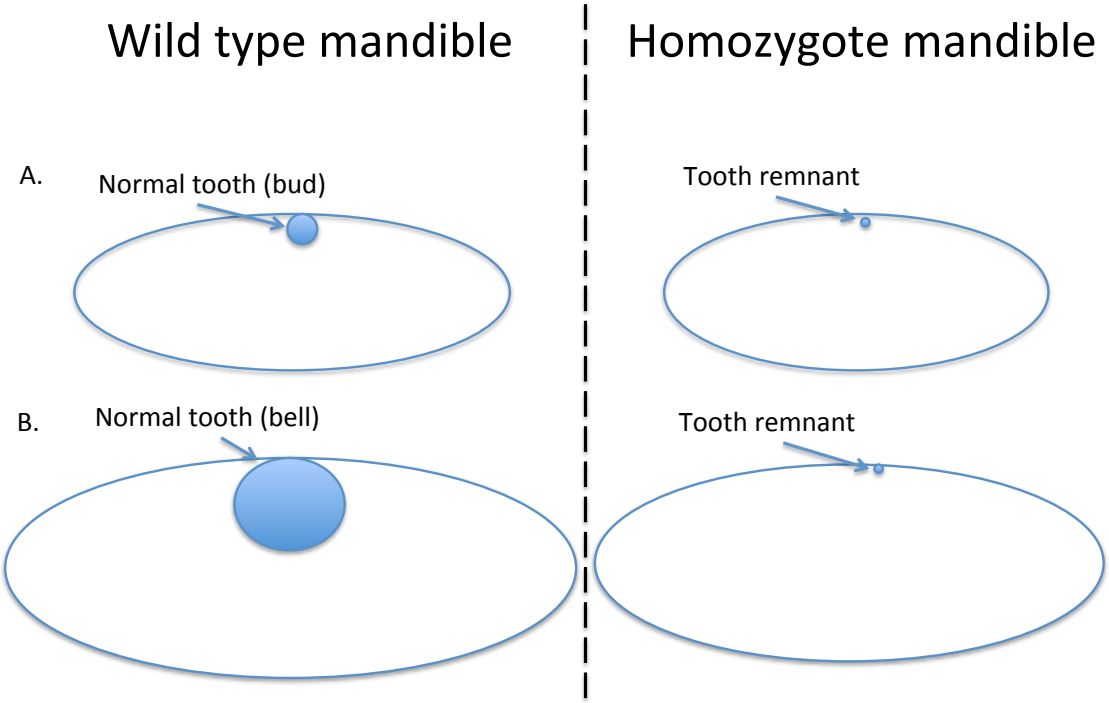

Figure 18. A, At left, a wild type E13 MdP with the blue circle representing a tooth organ at bud stage. On the right is a homozygote MdP with the remnant of a tooth organ shown as the tiny blue dot. Differences between levels of a protein expressed within the normal tooth bud (left) vs. the remnant (right) are likely to be more difficult to detect, with conventional western blotting. B, After a few days of

development, the tooth organ has grown larger (bigger blue dot) in wild type or heterozygote, especially compared to any remnant (if present) in the homozygote. This larger difference in protein levels is much more likely to be detected between wild type/heterozygote and homozygote.

FERMT1 is involved in epithelial cell adhesion via integrin activation (Calderwood et al., 2013). Because FERMT1 binds to integrin, it is partially responsible for maintaining the bond between the epithelium and mesenchyme. This maintenance job then aids the work of laminin and collagen IV genes, which participate in epithelium-mesenchyme adhesion (Konig and Bruckner-Tuderman, 1991). At E13, FERMT1 is primarily localized to epithelial cell lining in the oral cavity, tongue and gut (Ussar et al., 2006). A mutation of *Fermt1* in mice leads to a lethal intestinal epithelial dysfunction causing death within 3 days of birth (Ussar et al., 2008). Unfortunately, Ussar and co-workers (2008) did not report the status of tooth formation in the mutated *Fermt1* mice. Either information gathered from Ussar and colleagues about tooth development in their *Fermt1* mutant, or if necessary, generating a Fermt1 mutant, would be needed to address this question (see 2.4.6).

2.4.3 Undisturbed level of transcript and protein in homozygotes, an indiscernible role of *Pltp* in odontogenesis.

It is well established that PLTP protein participates in LDL and HDL metabolism (Albers et al., 1995). The role of PLTP or the pathways within which this protein works all involve lipids (Massey et al., 1984; Huuskonen et al., 1996; Rao et al., 1997). What is unknown is the potential role of PLTP outside of metabolic signaling mechanisms. In this study, I found that transcript level of *Pltp* in the MdP of *Brdm2* mutant mice was significantly altered only at E11. Protein analysis revealed no significant change in PLTP in E12 or E13 homozygotes. Hence, my data combined with the absence of a previous association of PLTP with epithelial-

mesenchymal signaling, or its physical relationship with TRP63, leads me to conclude that PLTP has little bearing on tooth or jaw morphogenesis in mice, particularly between E10-13. Perhaps later in development, when skin covering the presumptive mandible is stratifying and its various layers forming, PLTP is involved in fat cell deposition for structural support. However, as of yet, this idea is but speculation and future research is needed to specify the role of PLTP, if any, in instructing tooth and jaw morphogenesis.

2.4.4 Previously established negative relationship between TRP63 and *Krt2-8* confirmed with RT-qPCR, implying a probable negative role in odontogenesis.

Krt2-8 mRNA was one of the genes with mRNA levels increased at all four stages in the homozygote relative to the heterozygote MdP according to the RT-qPCR work. Thus, it appears that TRP63 and *Krt2-8* have an inverse relationship, whereby deletion of the former allows the latter to be expressed more. Truong and colleagues have shown (2006), that down-regulation of *ΔN-p63* results in induction of KRT2-8 protein in epidermal tissue. Although my results do not speak to protein levels, the mRNA levels of *Krt2-8* show a similar pattern. Still unclear is where Keratin 2-8 protein is expressed in the MdP or, particularly, in the tooth organ. If ΔN-P63 down-regulates expression of KRT2-8, then what might be the function of this protein in odontogenesis? It is known that ΔN-p63 is specifically expressed within the tooth organ as it develops (Laurikkala et al., 2006). Other previous studies have shown that KRT2-8 is expressed in single layered internal epithelia (Oshima, 2002) and shows a strong presence in carcinomas. This suggests that KRT2-8 is involved in differentiation and epithelial growth. As a member of the *Trp53* family of tumor-suppressors, it follows that if KRT2-8 is involved in cancerous growth, then TRP63 would act to suppress KRT2-8 signaling. This explanation needs further testing, beginning with immuno-localization of KRT2-8 protein within the tooth organ.

2.4.5 Presence of TRP63 in the *Brdm2* mutant suggests the production of a truncated protein and only partial mutation of *Trp63*.

The presence of a translated TRP63 protein in the *Brdm2* mutant is still debated amongst researchers currently using this mouse model for experimentation. Some believe that TRP63 is absent in the mutant mice (Mills et al., 1999; Laurikkala et al., 2006) while others argue that *Trp63* mRNA as well as protein are expressed at normal levels in the homozygote relative to wild type mice (Wolff et al., 2009; Talos et al., 2010). Technically, it is possible to alter two alleles such that there is no effect on the final protein product (Alberts, 2002). Related to this, where the mutation is made within the allele is important: if a mutation is near the beginning of the coding region, then the affect is much more severe. As happens without experimental intervention, random mutations may occur during the lifespan of the cell that have absolutely no effect on the gene or the fully folded protein (Alberts, 2002). One of the two original reports of this mouse mutant (Mills et al., 1999) argued that if the mutated *Trp63* gene were translated into a protein then it would contain an intact DNA-binding domain but lack the highly conserved 3'-carboxy terminal region. Although they did not test for TRP63 protein presence, the authors did report the complete absence of *Trp63* transcript in the homozygote via northern-blot analysis. Strangely, the authors make no mention of the precise sequence, binding site, or specificity of the probes used for the northern-blot work. Although northern blotting was extensively used in the past, today a more sensitive method for mRNA detection, RT-qPCR, is used. Laurikkala et al. (2006) concluded from a western blot experiment that there is a complete lack of ΔN-P63 protein in the homozygote. The source of the protein lysate used for this work was skin; however, there is no mention of which particular layers of skin, and where on the embryo the skin was extracted from. Moreover, Laurikkala et al. (2006) used *in-situ* hybridization to provide strong evidence of expression of *ΔN-p63* mRNA in-and-around tooth germs of normal wild type embryos, yet they fail to show a single image of *ΔN-p63* expression in the homozygote (negative control). Conversely, Wolff

and colleagues (2009) confirmed via: western blotting, an extensive RT-qPCR experiment using multiple primers that bind to different locations within the *Trp63* locus, and a luciferase activity assay, that the TRP63 protein was not only present in the *Brdm2* mutant but also contained the DNA binding and oligomerization domains although lacking the carboxy-terminal SAM (sterile α-motif) and post-SAM domains. Wolff and co-workers (2009) detected specifically the γ isoform of two variants of *Trp63* - TA-P63 and ΔN-P63 - from the mutated allele. My immuno-blot experiments probed lysates from the entire MdP using a different antibody targeting the α, β and γ isoforms belonging only to the ΔN-P63 variant. Nonetheless, like Wolff and colleagues' report (2009), I saw a strong presence of ΔN-P63 protein in homozygote mandibular lysates. Taken together with what was revealed by (Wolff et al., 2009), my results strongly suggest that the transcription and translation of at least the ΔN-p63 γ isoform occurs in embryos despite that both *Trp63* alleles have been mutated.

How then are the various phenotypes – limbless, toothless, under-developed skin – present in the homozygote despite the expression of ΔN-p63γ? To understand this, we need to closely examine the actual *Trp63* locus and the physical location of the insertion mutation:

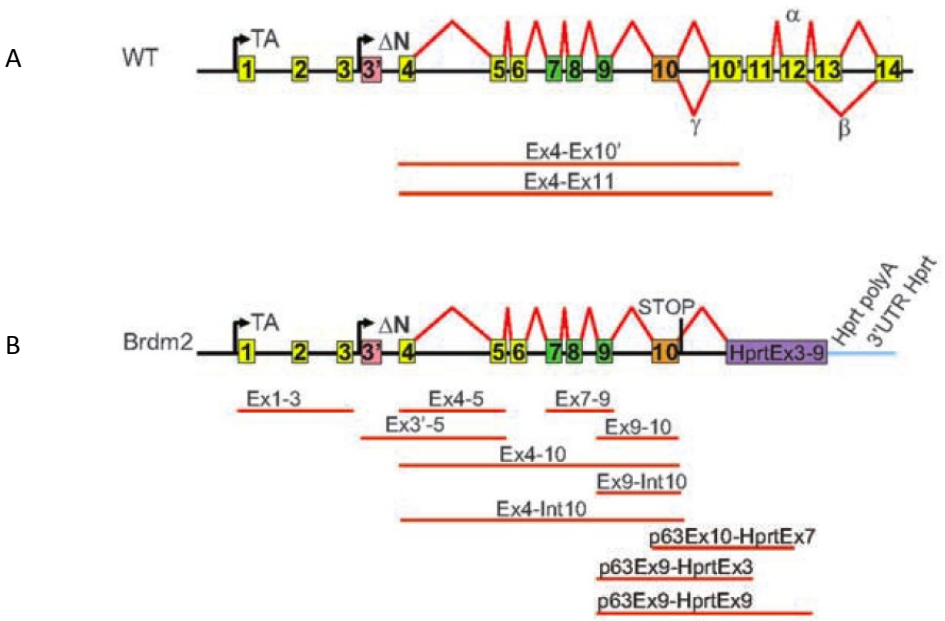

Figure 2 (Introduction 1.2) A, illustrates a normal *Trp63* allele found in wild type mice and the resulting sequence in the mutated mice in Figure 2B. Transcription and translation of a wild type allele would yield all α, β and γ isoforms for TA-P63 and ΔN-P63 variants. However, in the mutant allele the *TA-p63* and *ΔN-p63* variants are still transcribed and translated up to exon 10. This excludes the α and β isoforms but, according to (Wolff et al., 2009), not the γ isoform. Thus, in the homozygote, truncated ΔN-P63 proteins are produced lacking the α and β isoforms, thus rendering these proteins incapable of properly participating in the development of epithelial-derived structures such as limbs, teeth, hair follicles and skin.

Here, it is important to emphasize that the presence of TAp63 variant and its various isoforms are not seen in the MdP of wild type mice (Laurikkala et al., 2006). Rather, Laurikkala et al (2006) showed that the ΔN-P63 variant is strongly expressed in the wild type MdP, particularly in the tooth organ. My data reaffirm the conclusions made by (Wolff et al., 2009), that the normal expression of the ΔN-p63γ isoform is insufficient to properly develop teeth, hair follicles and limbs within the *Brdm2* mutant mice. In contrast, the absence of the other two ΔN-P63 isoforms, α

and β, likely explains the toothless (yet normal mandible) phenotype seen in homozygotes. Laurikkala et al (2006) reported a similar finding from immunoblots performed on extracted skin tissue (presumably non-MdP albeit not clearly stated as such) from E13 and E14 wild type and homozygote mice: the predominant isoform in wild type skin lysates was ΔN-p63α. Interestingly, amongst the mutants, skin samples showed no isoforms of ΔN-P63 protein (Laurikkala et al., 2006). My results, however, do not speak to specific isoforms of the ΔN-P63 but confirm that ΔN-P63 protein products of some type are present in the homozygote MdP. Also, the difference between my results and those of Laurikkala and colleagues (2006) might be explained by the different sources of antibodies used to detect the ΔN-P63: my antibodies were from Santa Cruz Biotechnology (Dallas, U.S.A.) and Laurikkala's study used antibodies from Neomarker (Fremont, U.S.A.). Second, different samples were used to test the presence of ΔN-P63: my study used the entire MdP while (Laurikkala et al., 2006) used skin. Moreover, the Laurikkala et al. (2006) article unfortunately contains a few gaps, particularly due to the omission of immunohistochemistry for ΔN-P63 isoforms in *Brdm2* mutant embryos as negative controls. A useful future project would be to show the presence of the various isoforms of ΔN-P63 in the wild type mouse and how this expression is altered in the homozygote.

Although the following detail does little to help clarify the debate about protein production in the *Brdm2* mutant, it is worth mentioning that Birkaya and colleagues (2007) demonstrated that the three isoforms of ΔN-P63 collectively control the transcription of 62 downstream genes in keratinocytes. The protein products from these 62 genes are involved in wide range of biochemical functions from notch signaling to iron metabolism. I believe my work has added 3 more candidate targets that are regulated at least at the transcript level by ΔN-P63. It is therefore important in the future to test, using chromatin immuno-precipitation, which isoforms of the ΔN-P63 variant regulate the expression of the four candidate

genes (*Fermt1*, *Pltp*, *Krt2-8* and *Cbln1*) identified in my study and, using *in situ*, to investigate the distribution of α, β and γ isoforms in the MdP.

2.4.6 Future directions and conclusions

Clearly, much more work is required to understand the complex roles that the five studied genes – *Trp63*, *Fermt1*, *Cbln1*, *Pltp* and *Krt2-8* – and their protein products may play during odontogenesis. Localization studies need to be conducted to determine and compare the precise location of mRNAs and proteins for *Fermt1*, *Pltp* and *Cbln1* in the (dental) epithelium of the putative mandibles of homozygote, heterozygote and wild type mice. I suspect that FERMT1 will be expressed at the epithelial-mesenchymal interface as FERMT1 binds to integrins for their normal cell signalling (Patel et al., 2013). Also, specifically in the homozygote embryo, since communication between single-layered epithelia and the underlying mesenchyme is disrupted (Yang et al., 1999), I would propose that FERMT1 expression would be disrupted in the homozygote MdP *except* that western blot data showed relatively normal levels of FERMT1 in the homozygote compared to the wild type. Thus, while general expression levels are near normal, FERMT1 protein localization in the homozygote might be altered, contributing to the extreme phenotype. Therefore, I predict that the homozygote would lack FERMT1 specifically in the oral epithelium that is committed to tooth formation.

Another possibility is that FERMT1 is present at normal levels in epithelial and mesenchyme cells but is not anchored to the cell membranes (Lai-Cheong et al., 2008) and thus cannot interact with integrins to perform its function. It would be interesting to experimentally test if an epithelial transplant from a wild type MdP to a *Brdm2* mutant MdP stripped of its epithelium would re-establish communication between the epithelium and mesenchyme in the homozygote. Such transplant experiments have been performed with Msx1 mutants (Bei et al., 2000). I predict that if a successful epithelial transplant is done well before the early stages of

odontogenesis then it would be possible to rescue the toothless phenotype. Furthermore, to determine a protein's function one could also mutate or, better yet, *delete* the allele, thus rendering the protein incapable of carrying out its function or of simply being made at all. This can be performed for the genes studied as well the isoforms of ΔN-P63, particularly the α and β. This work would then provide more direct insights into how odontogenesis copes with a loss of function or a deletion of my three studied genes. With proper protocols, trained personnel, and access to necessary laboratory equipment, generating a knockout or mutant mice can be accomplished within a few months, at a cost of $7,000-12,000. Alternatively, mutant or knockout mouse generation can be outsourced to well-established laboratories such as Jackson or genOway Laboratories.

A nearer-future goal would be to characterize how the TRP63 protein interacts with FERMT1, KRT2-8 and CBLN1 through the various stages of tooth development beginning at E10. Protein-protein or protein-DNA interaction studies would give a more precise and complete understanding of molecular interactions among these genes. Such tests can be accomplished relatively quickly with co-immuno-precipitation, and affinity purification coupled with mass spectrophotometry. However, from my RNA work alone, it is evident that upon mutation of TRP63, *Cbln1* and *Krt2-8* are up-regulated while *Fermt1* is down-regulated. Post-translation, the protein expression levels are a bit complicated, and this is where the above-mentioned methods are essential to test if TRP63 is in physical contact with these three proteins. If TRP63 binds to any one of the protein products of the genes studied, and the proteins are expressed in odonto-specific regions within the jaws, then can we conclude that TRP63 works with the protein products of the genes to directly promote odontogenesis, and that these genes act in the *Trp63* signaling network.

It is also important to determine if the *Brdm2* mutant phenotype is due to lack of communication between the epithelia and mesenchyme and/or

compromised structural integrity of the incompetent epithelium. In other words, is the epithelium structurally sound but genetically incapable of effectively communicating with the mesenchyme; or are the cells atrophying, dying, or failing to proliferate as needed? Epithelial layer viability can be tested via excision of the layer and subsequent cell culture to test if the epithelial cells grow. Subsequently, the bromodeoxyuridine (BrdU) cell proliferation assay can be performed to label and thus detect any proliferating epithelial cells (i.e., in S-phase). It is clear that the various skin layers fail to develop in newborn mice (Mills et al., 1999). As such, I think that it is likely that in the *Brdm2* mutant both the health of the epithelial cell layer and the epithelia-mesenchymal connection are compromised, and that these two problems accelerate the formation of the various phenotypes present in the *Brdm2* mutant.

As mentioned above, for all the studies done and published, the individual roles that the three ΔN-P63 isoforms play during tooth development are still unclear. Hence, another future goal could be to generate isoform-specific knockouts for *ΔN-p63* variant of *Trp63*. It is already known from (Wolff et al., 2009) that the γ isoform is transcribed and present within the mutant, and that, taken with my own results, its presence is not enough for odontogenesis to proceed. Laurikkala and co-workers (2006) revealed with immunohistochemistry and *in-situ* hybridization assays that *ΔN-p63* is strongly expressed in the invaginating epithelium at cap stage, as well as in the outer enamel epithelium during bell stage of odontogenesis; however and unfortunately, these researchers did not clarify which of the specific isoforms they probed for.

Despite the strengths of experiments performed it is important to acknowledge a few limitations in the present study. Firstly, for the RT-qPCR assay, probing for *Trp63* transcripts was done through specific primers targeting exon 14. Unfortunately, these primers were the only ones used for identifying levels of Trp63 in all three genotypes at all four embryonic stages. Considering that there is

contention about the mRNA and protein products of the mutated *Trp63* allele, generation of multiple primers targeting specific exons is necessary to accurately determine the true make-up of the transcript products of the mutated *Trp63* alleles. Furthermore, the TRP63 antibodies used in this study were specific for the α, β and γ isoforms belonging to the ΔN-P63 variant. Specific isoforms levels, however; were not determined, as that would require reference bands generated by isoform-transfected cell lysates. Also, this study utilized digested MdP comprising of epithelial, mesenchymal, neural, muscular, and other tissue types, therefore any subtle genetic changes in the relatively small developing tooth organ would be masked by the presence of non-tooth tissues.

In summary, mutation of both wild type *Trp63* alleles arrests the development of all epithelial-derived structures such as teeth, hair and limbs. The *Brdm2* mutant mouse, which develops normal lower mandible and no teeth, is thus an appropriate and useful model for researchers interested in identifying the distinct set of genes that work in odonto-specific molecular networks. The caveat is that the study of the entire macerated MdP, including dental and non-dental tissues, inevitably conflates the functions and expression domains of genes-of-interest. Thus future work would do well to probe either isolated tissue types or assess the entire MdP without mixing structures using immunohistochemistry and *in situ* hybridization. Nonetheless, microarray molecular analyses spanning E10-13 of the presumptive mandible in *Brdm2* mutant mice revealed significant differences in levels of mRNA expression of many genes including *Krt1-14, Krt2-8, Krt1-18, Krt-15, Cbln1* and *Fermt1*. The goal of this study was to test the veracity of microarray results revealing differences in mRNA expression, using RT-qPCR, and to quantify post-translation products (i.e., proteins) of a subset of genes. Gene-specific RT-qPCR analysis corroborated the differences flagged by microarray assays between the homozygote mice relative to same-aged heterozygote littermates. Expression of *Cbln1* and *Krt2-8* was significantly increased while the opposite was seen for *Fermt1* amongst E10-13 mandibular tissues. These changes however, were restricted to

mRNA, not protein. Western blot analysis of the mandibular prominence aged E12-13 revealed minute upregulation and/or downregulation for CBLN1 and FERMT1 in homozygotes relative to wild type and heterozygote samples. Hence, it is clear than that two copies of a dysfunctional *Trp63* allele do not affect the expression of CBLN1 and FERMT1 proteins even if they do perturb the activity of the transcripts of these same genes.

On a broader scale, the work presented here aimed to begin to unravel the molecular requirements of normal tooth morphogenesis to the exclusion of lower jaw morphogenesis. My work focused on a subset of genes that may function in the development of normal teeth. The activity of this subset of genes appears to be disturbed at the stage of mRNA expression due to a mutation in ΔN-P63 specifically. The fact that, within the *Brdm2* mutant, mandible formation proceeds normally and yet tooth development is arrested would suggest that there exists an unknown molecular pathway involved only in odontogenesis. According to the Venn diagram (Figure 19), such a pathway would be restricted to the green region. However, caution must be maintained in directly associating these studied genes to odontogenesis, as that would require more experimentation, as mentioned above. My study has validated differences in the expression of some novel genes, whose mRNA and but not protein levels are altered by the mutation of ΔN-P63. Whether these targets directly promote, or participate, in the normal development of teeth to the exclusion of jaws remains a mystery. The work presented in this thesis does hint towards a ΔN-P63-dependent tooth specific pathway that is unassociated with the development of jaws.

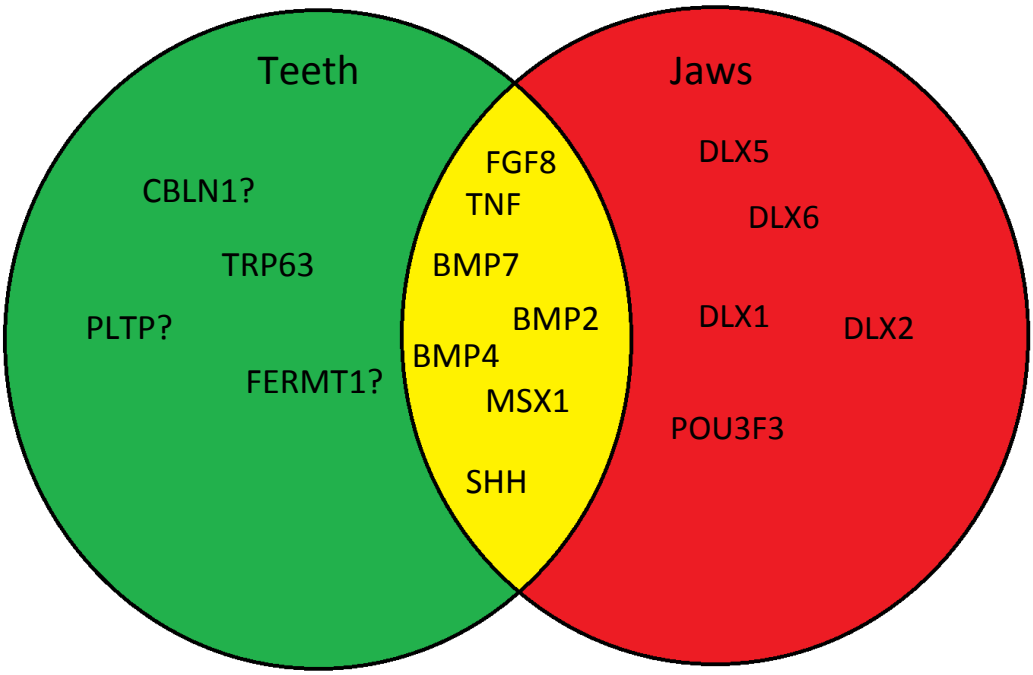

Figure 19. Venn diagram revisited, with inclusion of possible gene candidates involved in odonto-specific molecular mechanisms in the green region.

In closing, the data presented here does not negate the hypothesis that teeth and jaws develop via separate and distinct signaling pathways, rather it emphasizes that more experimentation is required to determine the roles of these genes and their protein product in odontogenesis. The mandible and teeth tissues arise from CNC derived cells that migrate anteriorly, early in development. Selective gene expression ultimately dictates certain CNC cells to give rise to teeth tissue and others to form mandible. I believe the genes highlighted in this study are candidates that participate in *probable* tooth-only genetic mechanisms. Secondly, my results suggest that TRP63 targets *Cbln1, Krt2-8, Fermt1* and *Pltp* within the MdP. While I am unable to preclude that these genes also normally function in mandible morphogenesis, if they do then their roles would appear to be non-essential.

Exploring the genetics behind tooth morphogenesis is absolutely crucial to understanding this process relative to the upper jaw skeleton/mandible tissues that

first encapsulate and, later, form adjacent to the dentition as it mineralizes and erupts. The presented molecular work helps address the current need to unravel the distinct demands for the development of the two tissues, but to more completely characterize how odonto-mandibular formation successfully occurs, it is important to understand how the genes ultimately work to drive morphology and structure. A complementary approach and a solution to this challenge is to visualize and measure the morphology, structure and positions of the teeth relative to the surrounding jaw tissues. In the next chapter I present and discuss the new 3D imaging technique, using a silver-based contrast agent, that I helped pioneer to see and study the physical relationships between tooth and jaw tissues throughout embryogenesis in mouse.

3 Development of a method to visualize tooth and jaw formation in 3D using synchrotron light

The following chapter is a summary of a published research article (Raj et al., 2014).

3.1 Introduction

This chapter highlights our studies of tooth and jaw morphology in 3D in mice aged E10 and older using X-ray based synchrotron and desktop μ-CT scanning. Micro-CT scanning generally uses absorption properties of hard mineralized tissue imaged from a series of successfully different angles to form 3D-reconstructed images of the specimen. In this chapter I present a new, easy-to-follow, simple and relatively inexpensive technique to stain soft tissue for μ-CT scanning.

The first goal of this study was to test the effectiveness of Protargol (a tissue staining agent containing silver) to penetrate whole embryos aged E10-14, 16, 18 and P0-P1 (neonatal mice). Related to this first goal, I also compared and contrasted the overall staining effectiveness and subsequent μ-CT image quality of embryos stained with Protargol against embryos stained with phosphotungstic acid (PTA) and not stained at all, as control specimens. Second, and the crux of this work, I compared and contrasted synchrotron μ-CT with conventional desktop μ-CT using Protargol-stained whole embryos to test if one or both of these imaging modalities visualized in high-resolution and histological detail the earliest development of teeth in 3D.

I hypothesized that visualizing tooth organogenesis in 3D in whole embryos would be successful via Protargol absorption into whole, uncut embryos and subsequent detection of silver by near K-edge high-resolution μ-CT imaging at the synchrotron. Staining embryos aged E16 and older might prove less effective due to

bone mineralization and advanced development of skin, which of course acts like a natural barrier to external substances. I expected that both Protargol and PTA would have superior soft tissue penetration capabilities compared to unstained specimens (control) in terms of visualizing internal and, especially, soft-tissue structures. Furthermore, as synchrotron μ-CT scanning can be optimized for: 1) Protargol stained specimens (i.e. by tuning the beam's photon energy just above the K-edge of silver for maximum contrast while maintaining higher flux than desktop μ-CT systems); and 2) smaller E10-14 embryos via easily inter-changeable camera systems that provide extremely high resolutions, I predicted, that synchrotron scanning would clearly visualize the onset of tooth organogenesis in whole, Protargol-stained mouse embryos.

3.2 Materials and Methods

3.2.1 Staining embryonic tissue for synchrotron and desktop µ-CT scanning

Mouse embryos aged E10-14, 16, 18 and P0-P1 (neonates) were collected in cold L-15 (Life Technologies, Carlsbad, U.S.A.) from pregnant *Trp63*$^{+/-}$ mothers. Heads of embryos were excised from the body and fixed overnight in a solution of 4% paraformaldehyde (PFA) (Thermo Fisher, Waltham, U.S.A.)/5% gluteraldehyde (Thermo Fisher, Waltham, U.S.A.) in 1x PBS. The following day, the heads were dehydrated with a graded ethanol (EtOH) series of 25% and 50% in 1x PBS, and then 75% and 95% ethanol in distilled water, with a final wash of 100% EtOH. Specimens were then stained with a 1% Protargol-S (Poly-sciences, Warrington, U.S.A.) solution at 37°C for 12-48 hr at 37°C, Phosphotungstic acid (PTA, Thermo Fisher, Waltham, U.S.A.) at 3(1%(wt/vol PTA)):7 (100% EtOH) overnight at 4°C. Protargol-S is also called silver-proteinate or simply silver stain in this thesis. Some embryos were also left unstained as controls. Subsequently, specimens were µ- -CT scanned using a desktop system or synchrotron technology. It should be noted that both synchrotron and desktop scanning used metal filters, in attempts to refine the beams for optimized imaging. See Table 10 below for details of the samples imaged and analyzed in this thesis:

Table 10. Detail summary of number of embryonic heads scanned, the staining agent used, and scanning modality (desktop μ-CT, underline, and synchrotron μ-CT no underline).

Age	Unstained	PTA-stained	Protargol/ silver-stained	Desktop μCT scanned	Synchrotron μCT scanned
E10	1	1	1, 1	3	1
E11	–	7	5, 1	12	1
E12	3	2	2, 1	7	1
E13	1	1, 1	1, 1	2	3
E14	–	3	1, 1	4	1
E16	1	1	1, 2	3	2
E18	1	2	4	7	–
P0-1	–	–	3, 1	3	1

Scanning parameters (Table 11 below) were optimized for each specific specimen.

Table 11. Summary of scanning parameters for desktop and synchrotron μ-CT

	Desktop μ-CT	**Synchrotron μ-CT**
Source	Hamamatsu 100/250 source.	Biomedical Imaging and Therapy-Bending Magnet beam-line (BMIT-BM) 05B1-1
Voltage	40-kVp voltage and 250 μA source current.	25.5-28 KeV*
Camera	SkyScan 11 mega-pixel camera.	E10–13 - AA40 beam monitor (Hamamatsu) + C9300-124 camera system (Hamamatsu) E16, 18, neonatal - AA60 beam monitor (Hamamatsu) + C9300-124
Filter	Aluminum (0.5mm)	Tin (0.5 mm) and Aluminum (5 mm)

Note, asterisk (*) indicates photon energy slightly above the K-edge of silver. K-edge is the minimum photon energy required to remove the electron closest to the nucleus of a particular atom. Imaging above K-edge absorbs the photon, thus creating absorption based-contrast.

Raw synchrotron data were corrected for x-ray beam decay with Athabasca Recon (U of Calgary https://bonelab.ucalgary.ca/node/501). Both synchrotron and desktop μ-CT data were than reconstructed using NRecon (Bruker, Belgium). Reconstruction parameters such as ring artifact, smoothing, and scan alignment

correction were applied appropriately to each scan. 3D renderings and virtual sectional images of each scan were generated via Amira (FEI, Hillsboro, U.S.A.).

3.3 Results

Firstly, I present and compare tissue contrast and detail visualized using unstained and PTA-stained to Protargol-stained specimens scanned using conventional desktop µ-CT. Next, I compare unstained, PTA-stained, and Protargol stained specimens scanned using synchrotron µ-CT. Lastly, I qualitatively compare desktop and synchrotron µ-CT image renderings for the absence/presence and clarity of oral-dental structures that each imaging modality is capable of showing.

3.3.1 Silver-stained specimens provided better soft tissue contrast compared to PTA-stained or unstained specimens

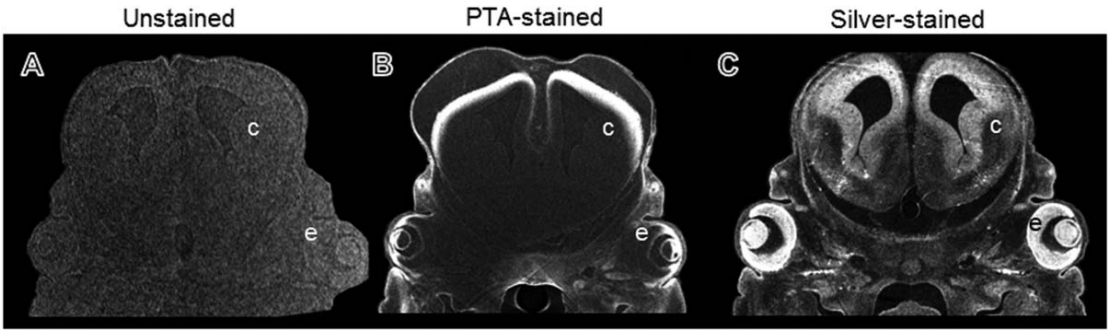

Figure 20. Synchrotron µ-CT scans of E13 mouse embryos that were unstained (A), PTA-stained (B), or silver-stained (C), revealing that, under these scanning parameters, soft tissue contrast is optimal in the silver-soaked embryo. Legend: c, cerebral hemisphere; e, eye.

Coronal view comparing silver-stained, PTA-stained and unstained E13 specimens scanned with synchrotron µ-CT revealed a clear difference among the various staining agents (Figure 20). Silver-soaked embryos (Figure 20C) provided excellent contrast both externally and internally. PTA-stained specimens (Figure

20B) showed good soft tissue contrast limited to external structures while unstained specimens (Figure 20A) were impossible to see in any clear detail due to minimal contrast.

3.3.2 Desktop μ-CT scanning

3.3.2.1 Scans of unstained specimens show high contrast only for mineralized tissues

Micro-CT performed on an unstained E12 specimen (Figure 21A) using the desktop scanner revealed little soft tissue contrast. There was no visual contrast for structures such as eyes, whisker primordia, vessels, and connective tissue. Scans of more mature E16-P1 unstained specimens did however show detailed contrast for mineralized bone in the head, face and rib cage (Figure 21B). Nonetheless, the relatively limited resolution of the desktop scanner combined with poor soft tissue contrast in unstained specimens made it impossible to visualize the developing dentition.

3.3.2.2 PTA stain creates extensive soft tissue contrast in specimens aged E10-E14, but not E16-P1.

Soft tissues such as the heart, somites, neural tube, and MdP were clearly visible in PTA-stained E10-14 specimens scanned using desktop μ-CT (Figure 21C). However, 3D rendering of the MdP did not show tooth organs. Nonetheless, external or more superficial structures such as eyes and whisker primordia (Figure 21D) were better highlighted in PTA-stained specimens. Micro-CT scans of the older, more mature PTA-stained E16, 18, P0-1 specimens revealed the limitations of this specific staining agent. 3D renderings of PTA-stained E16, 18, P0-1 embryos reveal a uniform deposit of the stain on the outermost layer of the skin (Figure 21E, F). For improved penetration of PTA, E16 specimens were decapitated below the neck prior

to staining. As expected, this effected soft and hard tissue contrast within E16 decapitated heads (Figure 21E) versus E18 intact specimens (Figure 21F). Strangely, contrast was more pronounced and penetration was more thorough in the intact E18 embryo compared to the decapitated head of an E16 embryo. Specifically, bone was not visible in whole heads (E16) but was clearly highlighted in the older (E18) whole embryos.

3.3.2.3 E10-14 specimens stained with Protargol show great soft tissue detail.

Protargol staining of E10-14 embryos and subsequent desktop μ-CT yielded better soft tissue contrast than PTA-stained or unstained specimens scanned with the same modality. Internal tissues such as somites were brighter and more easily distinguishable in Protargol-stained (Figure 21G, H) compared to PTA-stained embryos (Figure 21C, D). Furthermore, the silver-based stain provided excellent tissue contrast for the neural tube, (Figure 21G, H) and eyes (Figure 21G). Due to resolution limitations of the desktop μ-CT system, dental tissues were not visible in any great detail in the Protargol stained embryos.

Older E16-P1 decapitated specimens stained with Protargol or unstained were similar in internal mineralized tissue contrast (not shown). Surface renderings of Protargol stained E18 specimen showed only skin morphology and external ear structures. Eyes at E18 were not visible because the eyelids were closed as of E16 (Theiler, 1989; Findlater et al., 1993) and, like skin, these lids acted as a physical barrier for the stain. However, in intact E16-18 embryos, Protargol appeared to collect evenly on the outermost layer of skin, particularly around the whisker primordia, represented by intense bright dots on surface renderings of desktop μ-CT scans.

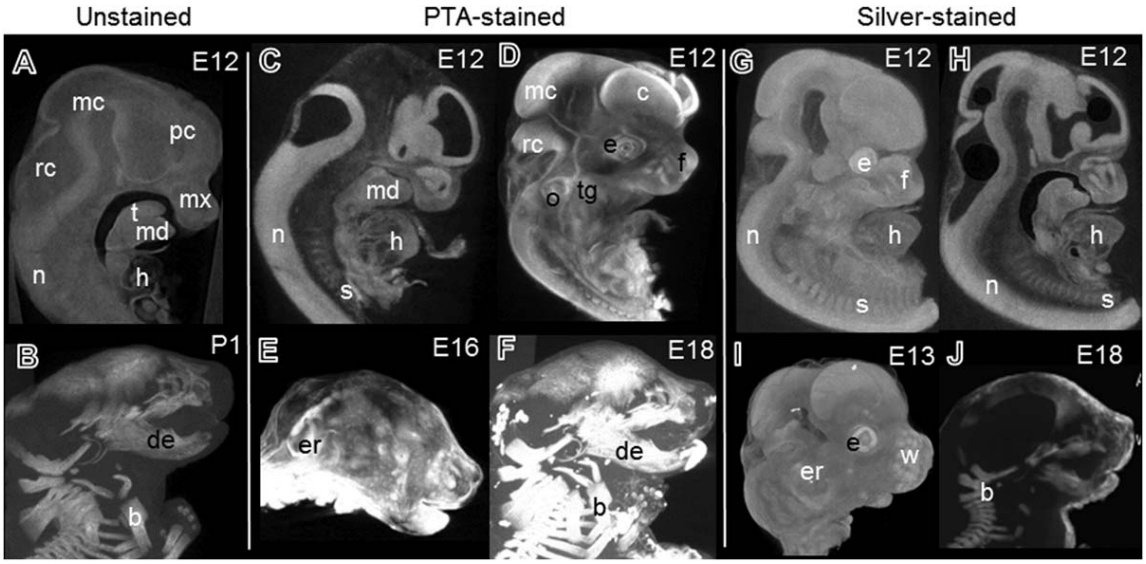

Figure 21. Desktop μ -CT scans of mouse embryos unstained (A, B), stained with PTA (C-F), or Protargol (G-J). A) Unstained E12 embryo representative of E10-14 specimens showing soft tissue as a grey mass with low contrast. B) Older unstained E16 embryo showing contrast for only mineralized structures such as bone. C) Software generated sagittal section of PTA-stained E12 embryo, (D) surface rendering of the same embryo revealing external features. Older PTA-soaked specimens: E16 (E), and E18 (F), stained with PTA revealing the limits of stain penetration. Surface volume rendering of Protargol-stained E12 (G), and a cross-sectional sagittal view (H) from the same scan, as well as surface rendering of E13, showing excellent stain penetration resulting in clear visualization of developing soft tissue. Like PTA, Protargol did not penetrate older specimens (J) hence internal structures were poorly stained and tissue contrast was minimal to none. Legend: b, bone; c, cerebral hemisphere; de, dentary; e, eye; er, ear; f, facial process; h, heart; hb, hindbrain; heart; mc, mesencephalon; md, mandibular process; mt, metencephalon; n, neural tube; o, otic placode; pc, prosencephalon; rc, rhombencephalon; s, somite; t, tongue; tg, trigeminal ganglion; w, whisker primordia.

3.3.3 Synchrotron µ-CT Scanning

3.3.3.1 Synchrotron µ-CT of silver-stained embryos detected structures in histological detail not visible using desktop µ-CT.

Amongst the synchrotron scans, Protargol-soaked specimens were imaged more clearly and comprehensively than PTA or unstained specimens. For E10-13, desktop and synchrotron µ-CT scans revealed exceptional detail of trigeminal ganglion, otic and brain vesicles (E10–11, Figure 22, E12–13, Figure 23), the lens and the surrounding retinal tissue (Figure 23 D, H), as well as the developing brain, mandible and upper jaw structures (E13, Figure 23 G, H). Due to Protargol's ability to penetrate various structures at these early embryonic stages (E10-13), contrast was enhanced in other tissues such as: skeletal muscles (Figure 22 G, H), bones, and cartilages (Figure 23. A–H) in both desktop and synchrotron µ-CT, albeit superior in the latter. Synchrotron scans were better than desktop scans for visualizing certain tissue types such as the eye and its surrounding muscles, tongue and the trigeminal ganglion. Virtual transverse sections of a synchrotron µ-CT scan (Figure 23. F, H) of an E13 specimen soaked in Protargol revealed anatomical features not visible in the desktop µ-CT scan (Figure 23 E, G). Protargol however, did accumulate within cavities and blood vessels, creating intense spots of absorption leading to artifacts and making it difficult to visualize surrounding tissues, in both synchrotron and desktop µ-CT scan. In general, synchrotron µ-CT generated finer, more detailed images of developing soft tissue structures both externally and internally for a whole mouse embryo.

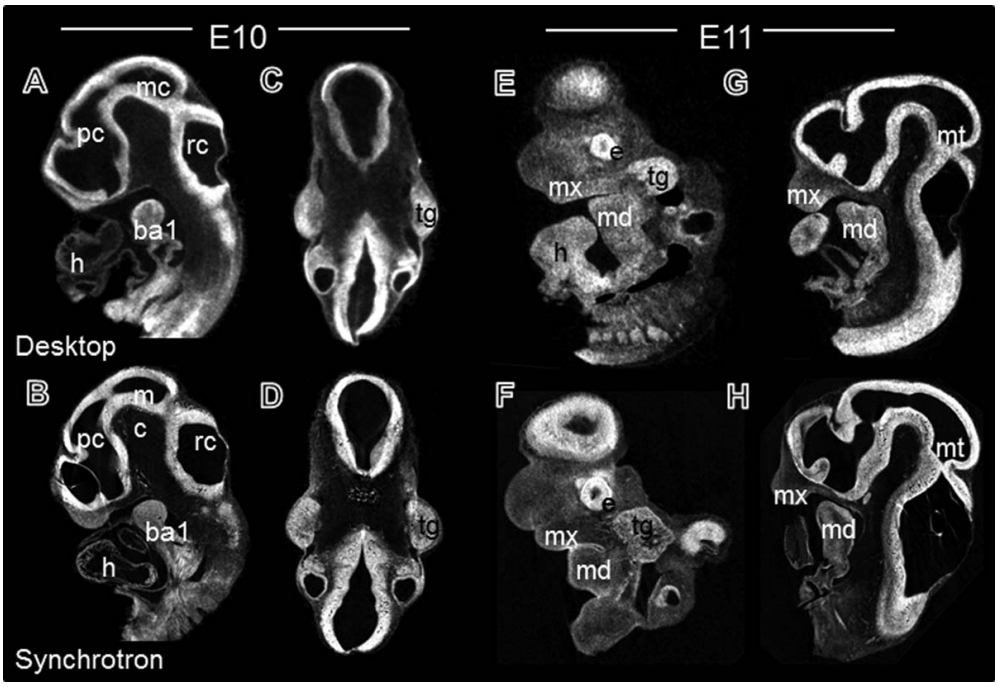

Figure 22. Internal anatomy of soft tissue in Protargol stained mouse embryo E10, 11 using desktop and synchrotron μ-CT. Scans from the synchrotron, with its greater flux, better camera system, and a peak beam energy of 28.1 KeV, just above the K-edge of silver, produced images with greater resolution relative to desktop scans. Embryonic tissue from E10 (A-D), and E11 (E-H) scanned using desktop μ-CT (A, C, E, G) and synchrotron μ-CT (B, D, F, H) enabling the visualization of neural tissues (e.g., trigeminal ganglion brain, and somites), organs (e.g., heart and eye), and craniofacial structures (e.g., first branchial arch; mandibular and maxillary processes) in detail. Legend: b, bone; e, eye; h, heart; mb, midbrain; mc, mesencephalon; md, mandibular process; mx, maxillary process; n, neural tube; pc, prosencephalon; rc, rhombencephalon; s, somite; tg, trigeminal ganglion.

Specimens aged E10 (Figure 22 A–D) and E11 (Figure 22E–H) scanned using the desktop system (Figure 22 A, C, E, G) and at the synchrotron beam line (Figure 22 B, D, F, H) showing neural tissues (e.g., trigeminal ganglion).

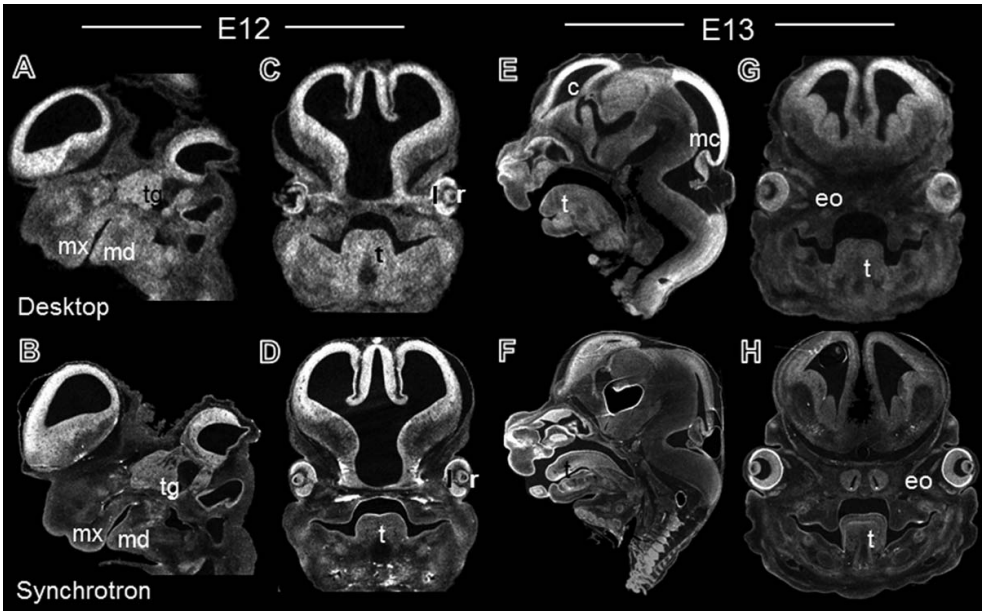

Figure 23. Protargol-stained embryos from E12 (A-D) and E 13 (E-H) scanned using desktop (A, C, E, G) and synchrotron (B, D, F, H) μ-CT in sagittal (A, B, E, F) and coronal (C, D, G, H) planes. In comparison to desktop μ-CT, synchrotron μ-CT showed much finer, histology-like detail. Specifically, tooth germs appeared in desktop μ-CT (C, G) as a dense mass, however finer detail of the actual tooth germ anatomy is visible only in synchrotron μ-CT scans (D, H). In addition, Protargol was absorbed by several other tissue types: muscles, cartilages, non-mineralized bone, nerves, and the eye lens. Legend: b, bone; c, cerebral hemisphere; eo, extrinsic ocular muscles; h, heart; l, lens; m, muscle; mb, midbrain; mc, mesencephalon; n, neural tube; r, retina, s, somite; t, tongue; tg, trigeminal ganglion.

3.3.3.2 Histology-like detail of dental tissue is possible with synchrotron µ-CT of silver-stained embryo

After comparing desktop and synchrotron µ-CT scans of silver-stained specimens, it is evident that synchrotron imaging shows in extremely fine detail the earliest stages of tooth development. Synchrotron scans (Figure 24 A, C, D) revealed the various tissues of developing first molar and incisor, while desktop (Figure 24 B) scans show the onset of first molar and incisor as simply a grey mass (Figure 24B below and Figure 23E). Various other tissue types such as the premature upper and lower jaw skeletons and their associated muscles (Figure 23B, D) were also visible in desktop µ-CT with increased resolution in the synchrotron scans. The superior resolution of synchrotron µ-CT scans combined with Protargol's excellent absorption abilities, enabled the direct study of the 3D structure of the developing tooth germ (Figure 24). A close-up coronal view of the tooth-germ indicated spherically shaped structure (Figure 24D. i) inside hashed-line square) however, rotating the view 90 degrees through the orange line (Figure 24D. i, iii), the shape of the molar now looks like an "elongated tube", spanning the length of the MxP (Figure 24D. iii) inside hashed-line rectangle). Such a detailed view of the developing bud was only possible in silver-stained and not in PTA-stained or unstained embryos. Despite the advantages of Protargol over other stains, limitations of this staining agent were seen in E15 specimens whereby contrast was restricted to external morphology with very minimal internal tissue contrast (Not shown).

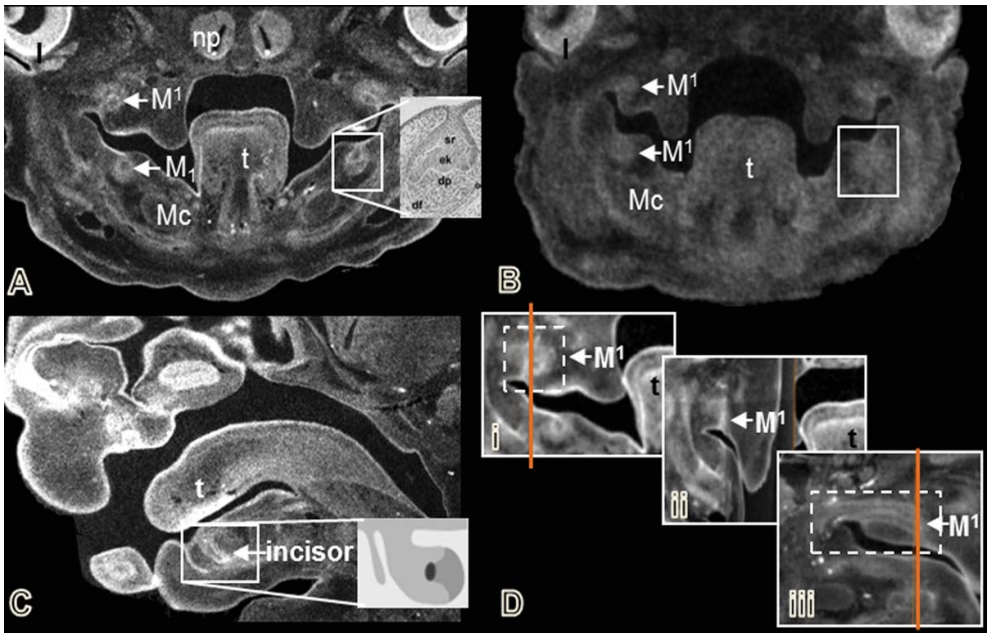

Figure 24. Synchrotron (A, C, D) as well as desktop (B) µ-CT scans of Protargol-stained E13 embryo, revealing details of early tooth morphogenesis in clear histological detail in synchrotron scans (solid boxes encompassing incisor and molar tooth germs). First molars (M1: A, B, D) and incisor (C) have started to form at E13. (D) First molar germ at bud stage, frontal (i) view, perpendicular to it (orange line, ii) and a sagittal view (iii) showing the spherical bud (i, broken square) and tubular (iii, broken rectangle), two different shapes exposed by different viewing angles. Legend: l, eye lens; Mc, Meckel's cartilage; M1, first molar; np, nasal pit; t, tongue. Inset picture of molar cap stage tissue section (Thesleff, 2009); inset incisor cartoon (Jheon et al., 2013).

Therefore, in summary, desktop and synchrotron µ-CT revealed that Protargol-stained embryos staged E10-15 were superior to PTA-stained or un-stained specimens in enhancing soft tissue contrast. Also, between synchrotron and desktop µ-CT, the former exceeded in producing µ -CT scans with the finest details of developing embryonic tissue. Lastly, the silver-based Protargol stain proves to be a valuable tool in better understanding the processes by which teeth develop.

3.4 Discussion

3.4.1 New use of Protargol as a contrast-creating agent in whole mouse embryo µ-CT scanning. A non-destructive yet histology-like approach to studying morphology in 3D.

Synchrotron µ-CT scanning of intact, whole embryo heads stained with Protargol showed the greatest detail of internal organs and structures, including tooth primordia, and different tissue types. Desktop µ-CT scans also visualized in 3D the internal anatomy of the developing tooth organs in Protargol-stained embryos. However, unsurprisingly, the resolution, clarity and detail seen in the images of Protargol-stained synchrotron µ -CT scanned embryos were notably superior to desktop µ -CT images. To my knowledge this is the first time that Protargol has been used to stain whole embryonic tissue and, specifically, to visualize tooth organogenesis.

Protargol consists mainly of silver, which has an achievable K-edge energy, particularly at the Canadian Light Source (CLS) Synchrotron. Taking advantage of the specific K-edge of silver, we used the synchrotron BMIT beam-line to enhance the detection of silver-impregnated tissues. Scanning with this specific silver K-edge beam energy translates to better X-ray absorption for Protargol (Mizutani and Suzuki, 2012), which creates the greater density differences that are necessary to see and distinguish among soft tissues. The absorption and contrast-creating abilities of Protargol and PTA stained samples were thus compared in this study. As assessed by overall µ-CT image quality (i.e., clarity and detail visible), images taken by synchrotron-scanning PTA-stained samples were generally inferior to those of silver-stained samples. Nonetheless, PTA did exhibit good stain penetration and provided adequate contrast to visualize large soft tissues, such as eyes and the surrounding muscles, Meckel's cartilage and external features such as hair follicles, in younger E10-14 mice.

The staining power of both PTA and Protargol was limited because both were insufficiently absorbed in older specimens aged E16-P1. The reason for this with respect to the PTA stain was that its penetration was limited by the greater molecular weight of the PTA molecule (Metscher, 2009a), which was further exacerbated by the maturation of the skin acting like a natural barrier to the stain. Although Protargol is relatively much smaller in weight compared to PTA, it too was unable to penetrate the skin of E16-P1 specimens. To overcome this barrier problem, a longer incubation period with PTA solution was tested, as recommended by (Metscher, 2009a). However, my results indicated that a prolonged incubation time would not improve the penetration of Protargol stain because, within 24 hours, younger specimens were saturated externally with Protargol. Also, with a 24 hour incubation in Protargol and after desktop μ-CT imaging of E18-P1 mice, these specimens still showed poor contrast among soft internal structures. Therefore, doubling the incubation time with Protargol did not improve visualization of soft internal tissue structures and I would propose that a longer incubation time with PTA would yield a similar result. In the future, it would be worth experimenting with different concentrations of staining solution to address penetration issues in older embryos. However, it is important to note that increasing the staining solution concentration may present a similar problem; an increase in the deposition of the stain on the outer surfaces of the embryo (Uchihara, 2007), which in turn would further obscure visibility.

As another solution, recently our lab experimented with cutting E16-P1 head specimens into two halves, in sagittal as well as peri-coronal planes, prior to staining and scanning in order to improve Protargol stain penetration. Analysis of the scanned data is ongoing yet preview scans do show better stain penetration in the cut vs. uncut (control) specimens. Cutting the specimens into two-equal halves, is however sub-optimal if one aims to study form and structure, as the specimen is physically altered. Furthermore, at E16-P1 the specimen heads have a good amount

of soft delicate tissue and, while cutting with even a new razor blade, the specimen is briefly deformed which can create damage and thus artifacts in the scan data.

3.4.2 Protargol is simple, economical and time-saving relative to other silver-based stains.

From the results above I conclude that a 1% Protargol solution is ideal to visualize soft embryonic tissue at stages earlier than E15 using X-ray based μ-CT. Firstly, staining with Protargol requires no special equipment and can be performed by anyone who possesses basic laboratory skills. Secondly, Protargol poses minimal health risk compared to other contrast agents such PTA, or osmium tetroxide. PTA or osmium tetroxide handling requires some precaution, such as a fume hood, and appropriate respiratory mask whereas Protargol powder does not. Thirdly, Protargol is available through Sigma at a relatively reasonable cost. Thus while the expense of accessing a μ-CT scanning system, particularly a synchrotron, may be substantial, the expense of buying the Protargol compound and executing the staining protocol is nominal.

Importantly, the Protargol staining protocol outlined in this study is more efficient than previously described synchrotron μ-CT studies using silver nitrate. For instance, the Bodian silver staining method requires the presence of metallic copper in a 1% silver stain solution (Bodian, 1936). The need for copper for this method to work can potentially inhibit optimum uptake of silver by the tissues. Another commonly used method, the Golgi impregnation method (Mizutani et al., 2008), used to stain human brain for light microscopy involves a complex protocol, over a week in length, compared to the method presented here that takes 24 hours. Even more striking is that these previously established methods are dependent on thin, sectioned slice of tissue. This is acceptable if one intends to study simple 2D tissue anatomy, but is certainly not ideal to study the 3D relationship among tissues that develop in close proximity to one-another. Also, the methods mentioned above have been primarily used to stain nerve tissue and their efficacy for staining other types

of tissues is not known. Apart from staining nerves in histological sections, Protargol's ability in highlighting all other tissue types in uncut, and intact whole embryonic tissues was largely unknown. In this study, Protargol highlighted not only nervous tissue, but also epithelial and muscular tissues, among other tissues types. A comparative μ-CT study of whole embryos stained using Golgi impregnation method and with Protargol would be needed to assess the effectiveness of each stain in creating soft tissue contrast for μ-CT scanning, but it is unlikely that this study is warranted since it is clear that Protargol performs very well and is such a relatively fast and simple staining procedure.

Another staining protocol (Watz et al., 2005) used silver nitrate to stain human lung specimens. This protocol is more time consuming and labor intensive compared to our Protargol staining protocol. The Watz method involved staining the lung specimens for 72 hours in a vacuum water aspirator, preventing the formation of bubbles and allowing even distribution of silver nitrate throughout the specimen. Using a vacuum water aspirator can be tested in future μ-CT scans as a number of our scans showed trapped air bubbles in the cavities of the embryo. Lastly, a third approach (Butzloff, 2011) used a 30% silver nitrate solution to stain honeybee specimens at 22C for 12 hr. Afterwards, the specimen was exposed to 470 nm dental curing lamp thereby converting the silver particles to a metallic state (Uchihara, 2007). In contrast, my Protargol method did not involve developing the silver embedded within embryos and yet provided excellent soft tissue contrast for both desktop and synchrotron μ-CT.

From the collection of μ-CT scan data some technical limitations are recognized, primarily with desktop images. Firstly, the desktop scanner's flux is much smaller than any synchrotron. This coupled with the fact that desktop scanners have a limited choice of camera systems translates to scans that fail to clearly visualize tiny embryonic tissues. Secondly, the desktop μ-CT system uses a polychromatic cone beam, composed of an array of photon energies. In theory, the

beam can be filtered to a monochromatic beam; however that would lead to a further decrease in flux and result in much longer scan times. Thus, desktop vs. synchrotron μ-CT scan comparisons reveal that the former is limited in generating optimum contrast and resolution for visualizing the various structures of teeth and jaws in the developing embryo. These limitations were overcome by the use of high-resolution synchrotron μ-CT allowing us to see, in detail, dental development as it actually occurs in close proximity to mandibular development.

3.4.3 Protargol staining combined with synchrotron μ-CT scanning gives insight into the early stages of tooth development.

The original goal of this project was to visualize tooth morphogenesis using PTA staining agent combined with desktop μ-CT scanning. In mice, tooth development initiates at about E11 by the thickening of the dental lamina (Jernvall and Thesleff, 2000). Thereafter, bud formation begins to appear around E13 followed by cap stage at E13-15 (Jernvall and Thesleff, 2000). Ideally, desktop μ-CT scanning systems would at least show in coarser-grain the 3D morphology of the developing tooth organ. However, based on our results, while desktop μ-CT scans of PTA-stained embryos did show the developing tooth, the resolution was below that required to visualize the various, specific parts of the tooth organ (dental papilla, enamel knot, and stellate reticulum). This lack of detail persisted for scans of even Protargol-stained specimens, underscoring the need for a high-resolution μ-CT imaging system. As expected, synchrotron imaging revealed much greater detail and contrast of the various structures within the tooth organ. Detail imaging of the landscape of the jaw and teeth was possible with the synchrotron due to its high-intensity, collimated beam of photons tuned to just above the K-edge of silver to enhance contrast for soft tissues soaked in Protargol. Synchrotron scans were further enhanced with a custom camera setup more powerful and better suited for small tissue imaging.

Interestingly, PTA-stained specimens scanned at the synchrotron did not reveal great internal tissue contrast. This could be explained by the fact that imaging of PTA-soaked embryos was performed with the same photon energy as Protargol-soaked embryos. Ideally, PTA-stained embryos imaging would be best if performed at or just above the K-edge of Tungsten (80 keV), the main metal in PTA, to maximize contrast. However this is currently not feasible, at least at the Canadian Light Source, as the flux at that high energy would be very low and detector efficiency would drastically drop, resulting in very low contrast in the stained specimens.

3.4.4 Protargol as a novel tool with which to study developmental morphology of different tissue types.

I have presented in this study the use of a silver-based Protargol stain as a contrast agent in μ-CT imaging. In the past this contrast agent has been extensively used for histological staining of sectioned neural tissue (Bodian, 1936). In this chapter, I demonstrate the staining capabilities of Protargol in whole embryos. Protargol's ability to easily penetrate the various tissues in the embryo is not dependent on the use of harsh digestion reagents or any other destructive process, thus making it an ideal staining reagent for accurate morphological studies. In the past, conventional histology has been used to acquire 3D images of molar tissues (Chlastakova et al., 2011; Lungova et al., 2011). Lungova and colleagues (2011) used 7 μm thick histological sections that were virtually stitched together with special software. This produced great images of the molar within the lower jaw albeit with some technically difficulties. For instance, generating 3D reconstructions from 2D histological images is extremely time consuming, and error-prone. Each section must be precisely aligned to generate the most accurate, reliable 3D rendering. Furthermore, the method used by Lungova and colleagues (2011) is problematic if quantitative analysis is to be performed because as the sample is cut, soft tissue can be deformed, and subsequent stitching of the images can introduce further artifacts.

Similarly, Chalastakova and colleagues (2011) studied third molar development using methods practiced by Lungova et al. (2011).

Unfortunately, both studies also necessitated treating samples with Ethylenediaminetetraacetic acid (EDTA), a harsh decalcifying agent essential to dissolve bone for efficient tissue-sectioning. Both studies also use mice aged between P0 to 14 days after birth. At this stage of development, bone is in the process of mineralizing and teeth have deposits of dentin (i.e., mineralized tissue), hence there would be less or no requirement to stain the specimens for μ-CT scanning (Theiler, 1989) or physically section the mineralizing tissue. Moreover, the jaws and teeth at these later stages are much bigger; hence, desktop μ-CT could likely be adequate in generating clear and detailed images of the teeth and surrounding upper jaw skeleton/mandible organs. I believe, the use of destructive chemicals and physical sectioning used by Lungova and colleagues (2011) and Chalastakova and colleagues (2011) are sub-optimum methods to study development and morphology of molars within P0-14 day mice. The work presented in this chapter reveals an alternative method that involves little manipulation and no damage to the sample that results in efficient 3D imaging best for both descriptive and empirical studies.

The synchrotron data suggests that the molar tooth develops not like a spherical organ, but rather like a tubular shaped structure spanning the length of the MdP. This raises a few important questions. Firstly, how does this elongated structure give rise to three distinct and separate molars? Does the tube-like structure subdivide into three individual molars or does the mandible produce three structures each giving rise to an individual molar? From the work performed by Lungova and colleagues (2011), these questions do not have a clear and distinct answer. I believe it is 3D μ-CT imaging than can help us in resolving these inquiries, ultimately improving our understanding of how teeth and jaws form, interact, and evolve through their development. Micro-CT conducted using synchrotron light also

enabled the visualization of specific parts of the tooth organ, eyes, muscles, and cartilages. Perhaps in the future, desktop μ-CT systems may improve to provide synchrotron-like μ-CT image clarity, however at this time my research suggests that synchrotron μ-CT is the optimal scanning modality enabling the accurate study of tooth development through time.

3.5 Future directions and Conclusions

In conclusion, the new Protargol-staining protocol developed in this study is effective in providing excellent embryonic soft tissue contrast for desktop and synchrotron μ-CT imaging. Protargol easily penetrated specimens staged E10-13, staining various tissue types such as cartilage, bone, epithelia, tooth germ, facial features, nerves, and muscles. Older larger specimens E16, E18, and newborns were challenging to stain as the now well-developed skin prohibited Protargol from penetrating into deeper tissues. Furthermore, Protargol-treated embryos that were synchrotron scanned with a tuned near K-edge imaging energy provided an advantage over desktop scans by exploiting K-edge absorption properties of silver. Protargol staining and subsequent synchrotron imaging enabled characterization of the 3D shape, size, and organization of miniscule tissues such as teeth.

Future work using synchrotron-based μ-CT will focus on silver labeling of proteins in whole mouse embryos. This novel technique called Enzyme Metallography developed by Nanoprobes (Yaphank, U.S.A.), utilizes HRP enzymes on secondary antibodies for deposition of silver particles at the target of the primary antibody. If successful, the sample can then be scanned at the synchrotron above the K-edge of silver, to detect the presence of the silver and by extension the presence of the protein. Such a study has been performed with chick embryo labeled for alpha-tubulin, and type II collagen and subsequent desktop μ-CT (Metscher and Muller, 2011). Metscher and Muller's study however did not use the K-edge properties of silver, hence it is difficult to determine if the contrast is truly as a

result of silver or is background contrast by the specimen itself. In the future, our lab plans to use this antibody specific labeling method with high-resolution synchrotron μ-CT, enabling us to visualize the localization of the mentioned proteins within the craniofacial prominence. Such a technique will further enhance our understanding of how protein expression of the studied genes is patterned across the various developmental stages particularly with respect to tooth morphogenesis.

Currently, our collected synchrotron and desktop μ-CT data is being used to quantify the tooth organ and its organization within the jaw prominence and relative to ossifying bones of the jaw skeleton. In future it would be useful to focus on determining the physical area required for three molars to grow, and how this area may be altered within the toothless *Brdm2* mutant that develops normal mandible. Undoubtedly, teeth have specific spatial needs, particularly beyond the cap stage at E15 when teeth occupy a large space within the mandibular and MxP. Exactly what the minimum space requirements are, and how this may affect the timing and positioning of tooth development, remain unclear. Understanding the genetics that coordinate upper jaw skeleton/mandible and tooth development as well as how a tooth-specific GRN work to print in 3D the morphology of teeth, will enable us to better model how these dentitions and jaws form and vary in their shapes and sizes.

4 Conclusion

This study has taken a first step to identify participants of a gene regulatory network for tooth morphogenesis exclusive of jaw skeletal morphogenesis. Using the "toothless" *Brdm2* mutant, I isolated a collection of genes previously not associated with tooth (or in some cases, jaw) morphogenesis. In the present study, transcript levels of *Cbln1,* and *Krt2-8* were up-regulated, while *Fermt1* was down-regulated and *Pltp* levels were unaltered in homozygotes compared to phenotypically normal mice. Recall, that at these developmental stages, tooth development is normally initiated by cross-signaling between the dental epithelium and underlying mesenchyme within the jaw primordium.

Interestingly, the differences in transcript levels detected in the mutants did not correspond entirely to alterations at the protein level. The Discussion of this thesis addressed this conundrum, with a consensus that in the homozygote, protein expression of these genes were likely being rescued by TRP63-independent pathways. Of course, caution must be exercised here in either completely negating the role of these proteins in odontogenesis, or firmly asserting that they are involved in tooth formation. My view is that there *may* exist some mechanism with which these proteins participate in the normal formation of teeth, the precise details of which are simply unknown at the moment.

In conclusion, one of my hypotheses was that, in the homozygote the mRNA *and* protein levels would mirror each other for the genes-of-interest. Based on my results, an alternative hypothesis - that in homozygote MdP, expression changes will be seen only for transcripts and not for fully-folded protein products - was supported. As also mentioned in the Discussion, much more experimentation is needed to unequivocally determine how the studied proteins may work together to dictate the formation of teeth in mice.

Another aim of this study was to pilot a method to visualize the 3D morphology and structure of the developing teeth within the jaws of whole (i.e., un-sectioned) embryonic mice. Synchrotron μ-CT powerfully captured in histological detail the structures of minutely-sized tissues including the tooth organ and its various internal layers. This study also validated a new, unconventional and effective way to incorporate Protargol, a silver-based stain, into whole embryonic tissues as a contrast agent for subsequent μ-CT imaging to directly and quickly capture a "3-dimensional view" of the earliest signs of teeth developing in the embryonic mice that is much more effective than conventional 3D reconstructions using 2D sections through the tooth organ/jaw primordium. This simple method can be readily adopted by any researcher who wishes to see and even measure the developmental morphology of soft tissues - not just dental or jaw structures - without physically destroying a specimen as is requisite for classic histology and microscopy work.

This study has shown the exceptional ability and superiority of Protargol relative to PTA, to be detected within embryonic tissue using available synchrotron technology tuned to optimal beam energy. There appeared to be clear differences in the penetration of the two staining agents amongst the specimens, with Protargol being superior to PTA in integrating into internal soft tissues. Interestingly, PTA stain was unable to penetrate deeper tissues within the brain and neck regions as μ-CT imaging showed contrast restricted to outer/external embryo surfaces. In addition, I hypothesized that visualizing tooth organogenesis would have been possible if Protargol was effectively absorbed by the specimen and synchrotron μ-CT, configured to near the K-edge of silver was used. This hypothesis was supported by μ-CT scanning data from synchrotron, showing penetration into deep tissues, proving the great ability of Protargol to create contrast at those early embryonic stages.

In conclusion, the work presented here, driven by the hypothesis that jaw skeleton and teeth form via separate signaling pathways if not GRNs, has validated a suite of genes that are *probable* candidates that help control tooth morphogenesis independently of jaw skeletal morphogenesis. I hope that future work will characterize in detail the roles of this suite of genes and their products in the multi-step process of odontogenesis.

5 References

Ahlberg PE, Systematics Association. 2001. Major events in early vertebrate evolution : palaeontology, phylogeny, genetics, and development. London ; New York: Taylor & Francis. xiv, 418 p. pp.

Alappat S, Zhang ZY, Chen YP. 2003. Msx homeobox gene family and craniofacial development. Cell Res 13:429-442.

Albers JJ, Wolfbauer G, Cheung MC, Day JR, Ching AF, Lok S, Tu AY. 1995. Functional expression of human and mouse plasma phospholipid transfer protein: effect of recombinant and plasma PLTP on HDL subspecies. Biochim Biophys Acta 1258:27-34.

Alberts B. 2002. Molecular biology of the cell. New York: Garland Science. xxxiv, 1548 p. pp.

Barbosa AC, Funato N, Chapman S, McKee MD, Richardson JA, Olson EN, Yanagisawa H. 2007. Hand transcription factors cooperatively regulate development of the distal midline mesenchyme. Dev Biol 310:154-168.

Bei M, Kratochwil K, Maas RL. 2000. BMP4 rescues a non-cell-autonomous function of Msx1 in tooth development. Development 127:4711-4718.

Benazet JD, Zeller R. 2009. Vertebrate limb development: moving from classical morphogen gradients to an integrated 4-dimensional patterning system. Cold Spring Harb Perspect Biol 1:a001339.

Bensoussan-Trigano V, Lallemand Y, Saint Cloment C, Robert B. 2011. Msx1 and Msx2 in limb mesenchyme modulate digit number and identity. Dev Dyn 240:1190-1202.

Beverdam A, Merlo GR, Paleari L, Mantero S, Genova F, Barbieri O, Janvier P, Levi G. 2002. Jaw transformation with gain of symmetry after Dlx5/Dlx6 inactivation: mirror of the past? Genesis 34:221-227.

Birkaya B, Ortt K, Sinha S. 2007. Novel in vivo targets of DeltaNp63 in keratinocytes identified by a modified chromatin immunoprecipitation approach. BMC Mol Biol 8:43.

Blais SA, MacKenzie LA, Wilson MVH. 2011. Tooth-like scales in Early Devonian eugnathostomes and the 'outside-in' hypothesis for the origins of teeth in vertebrates. Journal of Vertebrate Paleontology 31:1189-1199.

Bodian D. 1936. A new method for staining nerve fibers and nerve endings in mounted paraffin sections. Anatomical Record 65:89-97.

Bonilla-Claudio M, Wang J, Bai Y, Klysik E, Selever J, Martin JF. 2012. Bmp signaling regulates a dose-dependent transcriptional program to control facial skeletal development. Development 139:709-719.

Britanova O, Depew MJ, Schwark M, Thomas BL, Miletich I, Sharpe P, Tarabykin V. 2006. Satb2 haploinsufficiency phenocopies 2q32-q33 deletions, whereas loss suggests a fundamental role in the coordination of jaw development. Am J Hum Genet 79:668-678.

Britz HM, Jokihaara J, Leppanen OV, Jarvinen T, Cooper DM. 2010. 3D visualization and quantification of rat cortical bone porosity using a desktop micro-CT system: a case study in the tibia. J Microsc 240:32-37.
Brunskill EW, Potter AS, Distasio A, Dexheimer P, Plassard A, Aronow BJ, Potter SS. 2014. A gene expression atlas of early craniofacial development. Dev Biol 391:133-146.
Butzloff PR. 2011. Micro-CT imaging of denatured chitin by silver to explore honey bee and insect pathologies. PLoS One 6:e27448.
Calderwood DA, Campbell ID, Critchley DR. 2013. Talins and kindlins: partners in integrin-mediated adhesion. Nat Rev Mol Cell Biol 14:503-517.
Caton J, Tucker AS. 2009. Current knowledge of tooth development: patterning and mineralization of the murine dentition. J Anat 214:502-515.
Celli J, Duijf P, Hamel BC, Bamshad M, Kramer B, Smits AP, Newbury-Ecob R, Hennekam RC, Van Buggenhout G, van Haeringen A, Woods CG, van Essen AJ, de Waal R, Vriend G, Haber DA, Yang A, McKeon F, Brunner HG, van Bokhoven H. 1999. Heterozygous germline mutations in the p53 homolog p63 are the cause of EEC syndrome. Cell 99:143-153.
Chai Y, Bringas P, Jr., Shuler C, Devaney E, Grosschedl R, Slavkin HC. 1998. A mouse mandibular culture model permits the study of neural crest cell migration and tooth development. Int J Dev Biol 42:87-94.
Chai Y, Jiang X, Ito Y, Bringas P, Jr., Han J, Rowitch DH, Soriano P, McMahon AP, Sucov HM. 2000. Fate of the mammalian cranial neural crest during tooth and mandibular morphogenesis. Development 127:1671-1679.
Chai Y, Mah A, Crohin C, Groff S, Bringas P, Jr., Le T, Santos V, Slavkin HC. 1994. Specific transforming growth factor-beta subtypes regulate embryonic mouse Meckel's cartilage and tooth development. Dev Biol 162:85-103.
Chen Y, Bei M, Woo I, Satokata I, Maas R. 1996. Msx1 controls inductive signaling in mammalian tooth morphogenesis. Development 122:3035-3044.
Chen YH, Ishii M, Sucov HM, Maxson RE, Jr. 2008. Msx1 and Msx2 are required for endothelial-mesenchymal transformation of the atrioventricular cushions and patterning of the atrioventricular myocardium. BMC Dev Biol 8:75.
Chlastakova I, Lungova V, Wells K, Tucker AS, Radlanski RJ, Misek I, Matalova E. 2011. Morphogenesis and bone integration of the mouse mandibular third molar. Eur J Oral Sci 119:265-274.
Choi YS, Zhang Y, Xu M, Yang Y, Ito M, Peng T, Cui Z, Nagy A, Hadjantonakis AK, Lang RA, Cotsarelis G, Andl T, Morrisey EE, Millar SE. 2013. Distinct functions for Wnt/beta-catenin in hair follicle stem cell proliferation and survival and interfollicular epidermal homeostasis. Cell Stem Cell 13:720-733.
Couly GF, Coltey PM, Le Douarin NM. 1993. The triple origin of skull in higher vertebrates: a study in quail-chick chimeras. Development 117:409-429.
Davenport HA, McArthur J, Bruesch SR. 1939. Staining paraffin sections with protargol 3 The optimum pH for reduction 4 A two hour staining method. Stain Technology 14:21-26.

de Crespigny A, Bou-Reslan H, Nishimura MC, Phillips H, Carano RA, D'Arceuil HE. 2008. 3D micro-CT imaging of the postmortem brain. J Neurosci Methods 171:207-213.
Depew MJ, Lufkin T, Rubenstein JL. 2002. Specification of jaw subdivisions by Dlx genes. Science 298:381-385.
Depew MJ, Simpson CA, Morasso M, Rubenstein JL. 2005. Reassessing the Dlx code: the genetic regulation of branchial arch skeletal pattern and development. J Anat 207:501-561.
Desrumaux C, Deckert V, Athias A, Masson D, Lizard G, Palleau V, Gambert P, Lagrost L. 1999. Plasma phospholipid transfer protein prevents vascular endothelium dysfunction by delivering alpha-tocopherol to endothelial cells. FASEB J 13:883-892.
Donoghue PC, Rucklin M. 2014. The ins and outs of the evolutionary origin of teeth. Evol Dev.
Duijf PH, Vanmolkot KR, Propping P, Friedl W, Krieger E, McKeon F, Dotsch V, Brunner HG, van Bokhoven H. 2002. Gain-of-function mutation in ADULT syndrome reveals the presence of a second transactivation domain in p63. Hum Mol Genet 11:799-804.
Elliott JC, Dover SD. 1982. X-ray microtomography. J Microsc 126:211-213.
Findlater GS, McDougall RD, Kaufman MH. 1993. Eyelid development, fusion and subsequent reopening in the mouse. J Anat 183 (Pt 1):121-129.
Foley JO. 1943. A protargol method for staining nerve fibers in frozen or celloidin sections. Stain Technology 18:27-33.
Foster FS, Mehi J, Lukacs M, Hirson D, White C, Chaggares C, Needles A. 2009. A new 15-50 MHz array-based micro-ultrasound scanner for preclinical imaging. Ultrasound Med Biol 35:1700-1708.
Foster FS, Pavlin CJ, Harasiewicz KA, Christopher DA, Turnbull DH. 2000. Advances in ultrasound biomicroscopy. Ultrasound Med Biol 26:1-27.
Franco E, Galloway KE. 2015. Feedback loops in biological networks. Methods Mol Biol 1244:193-214.
Fraser GJ, Hulsey CD, Bloomquist RF, Uyesugi K, Manley NR, Streelman JT. 2009. An ancient gene network is co-opted for teeth on old and new jaws. PLoS Biol 7:e31.
Fried K, Hildebrand C. 1982. Qualitative structural development of the feline inferior alveolar nerve. J Anat 134:517-531.
Fujimori S, Novak H, Weissenbock M, Jussila M, Goncalves A, Zeller R, Galloway J, Thesleff I, Hartmann C. 2010. Wnt/beta-catenin signaling in the dental mesenchyme regulates incisor development by regulating Bmp4. Dev Biol 348:97-106.
Glanemann C, Loos A, Gorret N, Willis LB, O'Brien XM, Lessard PA, Sinskey AJ. 2003. Disparity between changes in mRNA abundance and enzyme activity in Corynebacterium glutamicum: implications for DNA microarray analysis. Appl Microbiol Biotechnol 61:61-68.

Harada H, Toyono T, Toyoshima K, Yamasaki M, Itoh N, Kato S, Sekine K, Ohuchi H. 2002. FGF10 maintains stem cell compartment in developing mouse incisors. Development 129:1533-1541.
Hardcastle Z, Mo R, Hui CC, Sharpe PT. 1998. The Shh signalling pathway in tooth development: defects in Gli2 and Gli3 mutants. Development 125:2803-2811.
Has C, Castiglia D, del Rio M, Diez MG, Piccinni E, Kiritsi D, Kohlhase J, Itin P, Martin L, Fischer J, Zambruno G, Bruckner-Tuderman L. 2011. Kindler syndrome: extension of FERMT1 mutational spectrum and natural history. Hum Mutat 32:1204-1212.
Hernandez-Acosta NC, Cabrera-Socorro A, Morlans MP, Delgado FJ, Suarez-Sola ML, Sottocornola R, Lu X, Gonzalez-Gomez M, Meyer G. 2011. Dynamic expression of the p53 family members p63 and p73 in the mouse and human telencephalon during development and in adulthood. Brain Res 1372:29-40.
Herz C, Aumailley M, Schulte C, Schlotzer-Schrehardt U, Bruckner-Tuderman L, Has C. 2006. Kindlin-1 is a phosphoprotein involved in regulation of polarity, proliferation, and motility of epidermal keratinocytes. J Biol Chem 281:36082-36090.
Hirai H, Pang Z, Bao D, Miyazaki T, Li L, Miura E, Parris J, Rong Y, Watanabe M, Yuzaki M, Morgan JI. 2005. Cbln1 is essential for synaptic integrity and plasticity in the cerebellum. Nat Neurosci 8:1534-1541.
Holembowski L, Schulz R, Talos F, Scheel A, Wolff S, Dobbelstein M, Moll U. 2011. While p73 is essential, p63 is completely dispensable for the development of the central nervous system. Cell Cycle 10:680-689.
Huelsken J, Vogel R, Erdmann B, Cotsarelis G, Birchmeier W. 2001. beta-Catenin controls hair follicle morphogenesis and stem cell differentiation in the skin. Cell 105:533-545.
Huuskonen J, Jauhiainen M, Ehnholm C, Olkkonen VM. 1998. Biosynthesis and secretion of human plasma phospholipid transfer protein. J Lipid Res 39:2021-2030.
Huuskonen J, Olkkonen VM, Jauhiainen M, Metso J, Somerharju P, Ehnholm C. 1996. Acyl chain and headgroup specificity of human plasma phospholipid transfer protein. Biochim Biophys Acta 1303:207-214.
Huysseune A, Sire JY, Witten PE. 2009. Evolutionary and developmental origins of the vertebrate dentition. J Anat 214:465-476.
Ingale Y, Shankar AA, Routray S, Agrawal M, Kadam A, Patil T. 2013. Ectopic teeth in ovarian teratoma: a rare appearance. Case Rep Dent 2013:970464.
Ito-Ishida A, Kakegawa W, Kohda K, Miura E, Okabe S, Yuzaki M. 2014. Cbln1 downregulates the formation and function of inhibitory synapses in mouse cerebellar Purkinje cells. Eur J Neurosci 39:1268-1280.
Jang C, Obeyesekere VR, Dilley RJ, Alford FP, Inder WJ. 2006. 11Beta hydroxysteroid dehydrogenase type 1 is expressed and is biologically active in human skeletal muscle. Clin Endocrinol (Oxf) 65:800-805.

Jeong J, Li X, McEvilly RJ, Rosenfeld MG, Lufkin T, Rubenstein JL. 2008. Dlx genes pattern mammalian jaw primordium by regulating both lower jaw-specific and upper jaw-specific genetic programs. Development 135:2905-2916.
Jernvall J, Thesleff I. 2000. Reiterative signaling and patterning during mammalian tooth morphogenesis. Mech Dev 92:19-29.
Jheon AH, Seidel K, Biehs B, Klein OD. 2013. From molecules to mastication: the development and evolution of teeth. Wiley Interdiscip Rev Dev Biol 2:165-182.
Jiang XC, Bruce C. 1995. Regulation of murine plasma phospholipid transfer protein activity and mRNA levels by lipopolysaccharide and high cholesterol diet. J Biol Chem 270:17133-17138.
Jiang XC, Bruce C, Mar J, Lin M, Ji Y, Francone OL, Tall AR. 1999. Targeted mutation of plasma phospholipid transfer protein gene markedly reduces high-density lipoprotein levels. J Clin Invest 103:907-914.
Jiang XC, D'Armiento J, Mallampalli RK, Mar J, Yan SF, Lin M. 1998. Expression of plasma phospholipid transfer protein mRNA in normal and emphysematous lungs and regulation by hypoxia. J Biol Chem 273:15714-15718.
Johnson JT, Hansen MS, Wu I, Healy LJ, Johnson CR, Jones GM, Capecchi MR, Keller C. 2006. Virtual histology of transgenic mouse embryos for high-throughput phenotyping. PLoS Genet 2:e61.
Kantaputra PN, Hamada T, Kumchai T, McGrath JA. 2003. Heterozygous mutation in the SAM domain of p63 underlies Rapp-Hodgkin ectodermal dysplasia. J Dent Res 82:433-437.
Kassai Y, Munne P, Hotta Y, Penttila E, Kavanagh K, Ohbayashi N, Takada S, Thesleff I, Jernvall J, Itoh N. 2005. Regulation of mammalian tooth cusp patterning by ectodin. Science 309:2067-2070.
Kavety B, Jenkins NA, Fletcher CF, Copeland NG, Morgan JI. 1994. Genomic structure and mapping of precerebellin and a precerebellin-related gene. Brain Res Mol Brain Res 27:152-156.
Klein OD, Minowada G, Peterkova R, Kangas A, Yu BD, Lesot H, Peterka M, Jernvall J, Martin GR. 2006. Sprouty genes control diastema tooth development via bidirectional antagonism of epithelial-mesenchymal FGF signaling. Dev Cell 11:181-190.
Konig A, Bruckner-Tuderman L. 1991. Epithelial-mesenchymal interactions enhance expression of collagen VII in vitro. J Invest Dermatol 96:803-808.
Kontges G, Lumsden A. 1996. Rhombencephalic neural crest segmentation is preserved throughout craniofacial ontogeny. Development 122:3229-3242.
Koster MI, Dai D, Marinari B, Sano Y, Costanzo A, Karin M, Roop DR. 2007. p63 induces key target genes required for epidermal morphogenesis. Proc Natl Acad Sci U S A 104:3255-3260.
Kostner GM, Oettl K, Jauhiainen M, Ehnholm C, Esterbauer H, Dieplinger H. 1995. Human plasma phospholipid transfer protein accelerates exchange/transfer of alpha-tocopherol between lipoproteins and cells. Biochem J 305 (Pt 2):659-667.

Lai-Cheong JE, Parsons M, McGrath JA. 2010. The role of kindlins in cell biology and relevance to human disease. Int J Biochem Cell Biol 42:595-603.
Lai-Cheong JE, Ussar S, Arita K, Hart IR, McGrath JA. 2008. Colocalization of kindlin-1, kindlin-2, and migfilin at keratinocyte focal adhesion and relevance to the pathophysiology of Kindler syndrome. J Invest Dermatol 128:2156-2165.
Laurikkala J, Mikkola ML, James M, Tummers M, Mills AA, Thesleff I. 2006. p63 regulates multiple signalling pathways required for ectodermal organogenesis and differentiation. Development 133:1553-1563.
Lewis R. 1997. Medical applications of synchrotron radiation x-rays. Phys Med Biol 42:1213-1243.
Liem KF, Walker WF. 2001. Functional anatomy of the vertebrates : an evolutionary perspective. Fort Worth: Harcourt College Publishers. xvii, 703 p. pp.
Liu C, Gu S, Sun C, Ye W, Song Z, Zhang Y, Chen Y. 2013. FGF signaling sustains the odontogenic fate of dental mesenchyme by suppressing beta-catenin signaling. Development 140:4375-4385.
Lopardo T, Lo Iacono N, Marinari B, Giustizieri ML, Cyr DG, Merlo G, Crosti F, Costanzo A, Guerrini L. 2008. Claudin-1 is a p63 target gene with a crucial role in epithelial development. PLoS One 3:e2715.
Lu CH, Rincon-Limas DE, Botas J. 2000. Conserved overlapping and reciprocal expression of msh/Msx1 and apterous/Lhx2 in Drosophila and mice. Mech Dev 99:177-181.
Lungova V, Radlanski RJ, Tucker AS, Renz H, Misek I, Matalova E. 2011. Tooth-bone morphogenesis during postnatal stages of mouse first molar development. J Anat 218:699-716.
Lusa S, Jauhiainen M, Metso J, Somerharju P, Ehnholm C. 1996. The mechanism of human plasma phospholipid transfer protein-induced enlargement of high-density lipoprotein particles: evidence for particle fusion. Biochem J 313 (Pt 1):275-282.
Massey JB, Hickson D, She HS, Sparrow JT, Via DP, Gotto AM, Jr., Pownall HJ. 1984. Measurement and prediction of the rates of spontaneous transfer of phospholipids between plasma lipoproteins. Biochim Biophys Acta 794:274-280.
Matsuda K, Miura E, Miyazaki T, Kakegawa W, Emi K, Narumi S, Fukazawa Y, Ito-Ishida A, Kondo T, Shigemoto R, Watanabe M, Yuzaki M. 2010. Cbln1 is a ligand for an orphan glutamate receptor delta2, a bidirectional synapse organizer. Science 328:363-368.
McGrath JA, Duijf PH, Doetsch V, Irvine AD, de Waal R, Vanmolkot KR, Wessagowit V, Kelly A, Atherton DJ, Griffiths WA, Orlow SJ, van Haeringen A, Ausems MG, Yang A, McKeon F, Bamshad MA, Brunner HG, Hamel BC, van Bokhoven H. 2001. Hay-Wells syndrome is caused by heterozygous missense mutations in the SAM domain of p63. Hum Mol Genet 10:221-229.
Metscher BD. 2009a. MicroCT for comparative morphology: simple staining methods allow high-contrast 3D imaging of diverse non-mineralized animal tissues. BMC Physiol 9:11.

Metscher BD. 2009b. MicroCT for developmental biology: a versatile tool for high-contrast 3D imaging at histological resolutions. Dev Dyn 238:632-640.
Metscher BD, Muller GB. 2011. MicroCT for molecular imaging: quantitative visualization of complete three-dimensional distributions of gene products in embryonic limbs. Dev Dyn 240:2301-2308.
Mills AA, Zheng B, Wang XJ, Vogel H, Roop DR, Bradley A. 1999. p63 is a p53 homologue required for limb and epidermal morphogenesis. Nature 398:708-713.
Mitsiadis TA, Drouin J. 2008. Deletion of the Pitx1 genomic locus affects mandibular tooth morphogenesis and expression of the Barx1 and Tbx1 genes. Dev Biol 313:887-896.
Miura E, Iijima T, Yuzaki M, Watanabe M. 2006. Distinct expression of Cbln family mRNAs in developing and adult mouse brains. Eur J Neurosci 24:750-760.
Mizutani R, Suzuki Y. 2012. X-ray microtomography in biology. Micron 43:104-115.
Mizutani R, Takeuchi A, Uesugi K, Ohyama M, Takekoshi S, Osamura RY, Suzuki Y. 2008. Three-dimensional microtomographic imaging of human brain cortex. Brain Res 1199:53-61.
Mohamed SS, Atkinson ME. 1983. A histological study of the innervation of developing mouse teeth. J Anat 136:735-749.
Murdock DJ, Dong XP, Repetski JE, Marone F, Stampanoni M, Donoghue PC. 2013. The origin of conodonts and of vertebrate mineralized skeletons. Nature 502:546-549.
Nassif A, Senussi I, Meary F, Loiodice S, Hotton D, Robert B, Bensidhoum M, Berdal A, Babajko S. 2014. Msx1 role in craniofacial bone morphogenesis. Bone 66:96-104.
Noden DM. 1978. The control of avian cephalic neural crest cytodifferentiation. II. Neural tissues. Dev Biol 67:313-329.
Ohazama A, Sharpe PT. 2004. TNF signalling in tooth development. Curr Opin Genet Dev 14:513-519.
Oka K, Oka S, Sasaki T, Ito Y, Bringas P, Jr., Nonaka K, Chai Y. 2007. The role of TGF-beta signaling in regulating chondrogenesis and osteogenesis during mandibular development. Dev Biol 303:391-404.
Oshima RG. 2002. Apoptosis and keratin intermediate filaments. Cell Death Differ 9:486-492.
Osumi-Yamashita N, Ninomiya Y, Doi H, Eto K. 1994. The contribution of both forebrain and midbrain crest cells to the mesenchyme in the frontonasal mass of mouse embryos. Dev Biol 164:409-419.
Pan D, Caruthers SD, Senpan A, Schmieder AH, Wickline SA, Lanza GM. 2011. Revisiting an old friend: manganese-based MRI contrast agents. Wiley Interdiscip Rev Nanomed Nanobiotechnol 3:162-173.
Pan PY, Chen RS, Ting CL, Chen WL, Dong CY, Chen MH. 2014. Multiphoton microscopy imaging of developing tooth germs. J Formos Med Assoc 113:42-49.

Panganiban G, Rubenstein JL. 2002. Developmental functions of the Distal-less/Dlx homeobox genes. Development 129:4371-4386.
Paradis MR, Raj MT, Boughner JC. 2013. Jaw growth in the absence of teeth: the developmental morphology of edentulous mandibles using the p63 mouse mutant. Evol Dev 15:268-279.
Patel H, Zich J, Serrels B, Rickman C, Hardwick KG, Frame MC, Brunton VG. 2013. Kindlin-1 regulates mitotic spindle formation by interacting with integrins and Plk-1. Nat Commun 4:2056.
Peterkova R, Lesot H, Viriot L, Peterka M. 2005. The supernumerary cheek tooth in tabby/EDA mice-a reminiscence of the premolar in mouse ancestors. Arch Oral Biol 50:219-225.
Peters H, Neubuser A, Kratochwil K, Balling R. 1998. Pax9-deficient mice lack pharyngeal pouch derivatives and teeth and exhibit craniofacial and limb abnormalities. Genes Dev 12:2735-2747.
Pfaffl MW, Horgan GW, Dempfle L. 2002. Relative expression software tool (REST) for group-wise comparison and statistical analysis of relative expression results in real-time PCR. Nucleic Acids Res 30:e36.
Pozniak CD, Radinovic S, Yang A, McKeon F, Kaplan DR, Miller FD. 2000. An anti-apoptotic role for the p53 family member, p73, during developmental neuron death. Science 289:304-306.
Pozzi S, Zambelli F, Merico D, Pavesi G, Robert A, Maltere P, Gidrol X, Mantovani R, Vigano MA. 2009. Transcriptional network of p63 in human keratinocytes. PLoS One 4:e5008.
Radlanski R, Renz H, Klarkowski M. 2003. Prenatal development of the human mandible. Anatomy and Embryology 207:221-232.
Raj MT, Prusinkiewicz M, Cooper DM, George B, Webb MA, Boughner JC. 2014. Technique: imaging earliest tooth development in 3D using a silver-based tissue contrast agent. Anat Rec (Hoboken) 297:222-233.
Rao R, Albers JJ, Wolfbauer G, Pownall HJ. 1997. Molecular and macromolecular specificity of human plasma phospholipid transfer protein. Biochemistry 36:3645-3653.
Restelli M, Lopardo T, Lo Iacono N, Garaffo G, Conte D, Rustighi A, Napoli M, Del Sal G, Perez-Morga D, Costanzo A, Merlo GR, Guerrini L. 2014. DLX5, FGF8 and the Pin1 isomerase control DeltaNp63alpha protein stability during limb development: a regulatory loop at the basis of the SHFM and EEC congenital malformations. Hum Mol Genet 23:3830-3842.
Ribi W, Senden TJ, Sakellariou A, Limaye A, Zhang S. 2008. Imaging honey bee brain anatomy with micro-X-ray-computed tomography. J Neurosci Methods 171:93-97.
Rissanen TT, Korpisalo P, Karvinen H, Liimatainen T, Laidinen S, Grohn OH, Yla-Herttuala S. 2008. High-resolution ultrasound perfusion imaging of therapeutic angiogenesis. JACC Cardiovasc Imaging 1:83-91.

Romano RA, Smalley K, Liu S, Sinha S. 2010. Abnormal hair follicle development and altered cell fate of follicular keratinocytes in transgenic mice expressing DeltaNp63alpha. Development 137:1431-1439.
Rucinski M, Ziolkowska A, Szyszka M, Malendowicz LK. 2009. Precerebellin-related genes and precerebellin 1 peptide in the adrenal gland of the rat: expression pattern, localization, developmental regulation and effects on corticosteroidogenesis. Int J Mol Med 23:363-371.
Rucklin M, Giles S, Janvier P, Donoghue PC. 2011. Teeth before jaws? Comparative analysis of the structure and development of the external and internal scales in the extinct jawless vertebrate Loganellia scotica. Evol Dev 13:523-532.
Rufini A, Barlattani A, Docimo R, Velletri T, Niklison-Chirou MV, Agostini M, Melino G. 2011. p63 in tooth development. Biochem Pharmacol 82:1256-1261.
Sarkar L, Cobourne M, Naylor S, Smalley M, Dale T, Sharpe PT. 2000. Wnt/Shh interactions regulate ectodermal boundary formation during mammalian tooth development. Proc Natl Acad Sci U S A 97:4520-4524.
Satokata I, Maas R. 1994. Msx1 deficient mice exhibit cleft palate and abnormalities of craniofacial and tooth development. Nat Genet 6:348-356.
Scacheri PC, Rozenblatt-Rosen O, Caplen NJ, Wolfsberg TG, Umayam L, Lee JC, Hughes CM, Shanmugam KS, Bhattacharjee A, Meyerson M, Collins FS. 2004. Short interfering RNAs can induce unexpected and divergent changes in the levels of untargeted proteins in mammalian cells. Proc Natl Acad Sci U S A 101:1892-1897.
Schroder M, Kaufman RJ. 2005. ER stress and the unfolded protein response. Mutat Res 569:29-63.
Shebl FM, Pinto LA, Garcia-Pineres A, Lempicki R, Williams M, Harro C, Hildesheim A. 2010. Comparison of mRNA and protein measures of cytokines following vaccination with human papillomavirus-16 L1 virus-like particles. Cancer Epidemiol Biomarkers Prev 19:978-981.
Sire JY. 2001. Teeth outside the mouth in teleost fishes: how to benefit from a developmental accident. Evol Dev 3:104-108.
Sire JY, Akimenko MA. 2004. Scale development in fish: a review, with description of sonic hedgehog (shh) expression in the zebrafish (Danio rerio). Int J Dev Biol 48:233-247.
Sire JY, Allizard F, Babiar O, Bourguignon J, Quilhac A. 1997. Scale development in zebrafish (Danio rerio). J Anat 190 (Pt 4):545-561.
Smith MM. 2003. Vertebrate dentitions at the origin of jaws: when and how pattern evolved. Evol Dev 5:394-413.
Smith MM, Coates MI. 1998. Evolutionary origins of the vertebrate dentition: phylogenetic patterns and developmental evolution. Eur J Oral Sci 106 Suppl 1:482-500.
Talos F, Wolff S, Beyer U, Dobbelstein M, Moll UM. 2010. Brdm2 - an aberrant hypomorphic p63 allele. Cell Death Differ 17:184-186.
Tam PP, Loebel DA. 2007. Gene function in mouse embryogenesis: get set for gastrulation. Nat Rev Genet 8:368-381.

Tasli PN, Aydin S, Yalvac ME, Sahin F. 2014. Bmp 2 and bmp 7 induce odonto- and osteogenesis of human tooth germ stem cells. Appl Biochem Biotechnol 172:3016-3025.
Teaford MF, Smith MM, Ferguson MWJ. 2000. Development, function, and evolution of teeth. New York: Cambridge University Press. ix, 314 p. pp.
ten Berge D, Brugmann SA, Helms JA, Nusse R. 2008. Wnt and FGF signals interact to coordinate growth with cell fate specification during limb development. Development 135:3247-3257.
Theiler K. 1989. The house mouse : atlas of embryonic development. New York: Springer-Verlag. 178 p. p.
Thesleff I. 2006. The genetic basis of tooth development and dental defects. Am J Med Genet A 140:2530-2535.
Thesleff IaT, M. 2009. Tooth organogenesis and regeneration (January 31, 2009), StemBook, ed. The Stem Cell Research Community, StemBook, doi/10.3824/stembook.1.37.1.
Thomas BL, Tucker AS, Qui M, Ferguson CA, Hardcastle Z, Rubenstein JL, Sharpe PT. 1997. Role of Dlx-1 and Dlx-2 genes in patterning of the murine dentition. Development 124:4811-4818.
Thomason HA, Dixon MJ, Dixon J. 2008. Facial clefting in Tp63 deficient mice results from altered Bmp4, Fgf8 and Shh signaling. Dev Biol 321:273-282.
Thomason HA, Zhou H, Kouwenhoven EN, Dotto GP, Restivo G, Nguyen BC, Little H, Dixon MJ, van Bokhoven H, Dixon J. 2010. Cooperation between the transcription factors p63 and IRF6 is essential to prevent cleft palate in mice. J Clin Invest 120:1561-1569.
Tian Q, Stepaniants SB, Mao M, Weng L, Feetham MC, Doyle MJ, Yi EC, Dai H, Thorsson V, Eng J, Goodlett D, Berger JP, Gunter B, Linseley PS, Stoughton RB, Aebersold R, Collins SJ, Hanlon WA, Hood LE. 2004. Integrated genomic and proteomic analyses of gene expression in Mammalian cells. Mol Cell Proteomics 3:960-969.
Truong AB, Kretz M, Ridky TW, Kimmel R, Khavari PA. 2006. p63 regulates proliferation and differentiation of developmentally mature keratinocytes. Genes Dev 20:3185-3197.
Tucker A, Sharpe P. 2004. The cutting-edge of mammalian development; how the embryo makes teeth. Nat Rev Genet 5:499-508.
Tucker AS, Al Khamis A, Sharpe PT. 1998a. Interactions between Bmp-4 and Msx-1 act to restrict gene expression to odontogenic mesenchyme. Dev Dyn 212:533-539.
Tucker AS, Matthews KL, Sharpe PT. 1998b. Transformation of tooth type induced by inhibition of BMP signaling. Science 282:1136-1138.
Turnbull DH, Mori S. 2007. MRI in mouse developmental biology. NMR Biomed 20:265-274.
Uchihara T. 2007. Silver diagnosis in neuropathology: principles, practice and revised interpretation. Acta Neuropathol 113:483-499.

Ussar S, Moser M, Widmaier M, Rognoni E, Harrer C, Genzel-Boroviczeny O, Fassler R. 2008. Loss of Kindlin-1 causes skin atrophy and lethal neonatal intestinal epithelial dysfunction. PLoS Genet 4:e1000289.

Ussar S, Wang HV, Linder S, Fassler R, Moser M. 2006. The Kindlins: subcellular localization and expression during murine development. Exp Cell Res 312:3142-3151.

van Bokhoven H, Hamel BC, Bamshad M, Sangiorgi E, Gurrieri F, Duijf PH, Vanmolkot KR, van Beusekom E, van Beersum SE, Celli J, Merkx GF, Tenconi R, Fryns JP, Verloes A, Newbury-Ecob RA, Raas-Rotschild A, Majewski F, Beemer FA, Janecke A, Chitayat D, Crisponi G, Kayserili H, Yates JR, Neri G, Brunner HG. 2001. p63 Gene mutations in eec syndrome, limb-mammary syndrome, and isolated split hand-split foot malformation suggest a genotype-phenotype correlation. Am J Hum Genet 69:481-492.

Vanbokhoven H, Melino G, Candi E, Declercq W. 2011. p63, a story of mice and men. J Invest Dermatol 131:1196-1207.

Vogel C, Marcotte EM. 2012. Insights into the regulation of protein abundance from proteomic and transcriptomic analyses. Nat Rev Genet 13:227-232.

Vuletic S, Jin LW, Marcovina SM, Peskind ER, Moller T, Albers JJ. 2003. Widespread distribution of PLTP in human CNS: evidence for PLTP synthesis by glia and neurons, and increased levels in Alzheimer's disease. J Lipid Res 44:1113-1123.

Wada A, Tsutamoto T, Ohnishi M, Sawaki M, Fukai D, Maeda Y, Kinoshita M. 1999. Effects of a specific endothelin-converting enzyme inhibitor on cardiac, renal, and neurohumoral functions in congestive heart failure: comparison of effects with those of endothelin A receptor antagonism. Circulation 99:570-577.

Watz H, Breithecker A, Rau WS, Kriete A. 2005. Micro-CT of the human lung: imaging of alveoli and virtual endoscopy of an alveolar duct in a normal lung and in a lung with centrilobular emphysema--initial observations. Radiology 236:1053-1058.

Wolff S, Talos F, Palacios G, Beyer U, Dobbelstein M, Moll UM. 2009. The alpha/beta carboxy-terminal domains of p63 are required for skin and limb development. New insights from the Brdm2 mouse which is not a complete p63 knockout but expresses p63 gamma-like proteins. Cell Death Differ 16:1108-1117.

Yanagisawa H, Hammer RE, Richardson JA, Emoto N, Williams SC, Takeda S, Clouthier DE, Yanagisawa M. 2000. Disruption of ECE-1 and ECE-2 reveals a role for endothelin-converting enzyme-2 in murine cardiac development. J Clin Invest 105:1373-1382.

Yanagisawa H, Yanagisawa M, Kapur RP, Richardson JA, Williams SC, Clouthier DE, de Wit D, Emoto N, Hammer RE. 1998. Dual genetic pathways of endothelin-mediated intercellular signaling revealed by targeted disruption of endothelin converting enzyme-1 gene. Development 125:825-836.

Yang A, Kaghad M, Wang Y, Gillett E, Fleming MD, Dotsch V, Andrews NC, Caput D, McKeon F. 1998. p63, a p53 homolog at 3q27-29, encodes multiple products with transactivating, death-inducing, and dominant-negative activities. Mol Cell 2:305-316.

Yang A, Schweitzer R, Sun D, Kaghad M, Walker N, Bronson RT, Tabin C, Sharpe A, Caput D, Crum C, McKeon F. 1999. p63 is essential for regenerative proliferation in limb, craniofacial and epithelial development. Nature 398:714-718.

Yang A, Walker N, Bronson R, Kaghad M, Oosterwegel M, Bonnin J, Vagner C, Bonnet H, Dikkes P, Sharpe A, McKeon F, Caput D. 2000. p73-deficient mice have neurological, pheromonal and inflammatory defects but lack spontaneous tumours. Nature 404:99-103.

You L, Yin J. 2000. Patterns of regulation from mRNA and protein time series. Metab Eng 2:210-217.

Yuasa T, Kataoka H, Kinto N, Iwamoto M, Enomoto-Iwamoto M, Iemura S, Ueno N, Shibata Y, Kurosawa H, Yamaguchi A. 2002. Sonic hedgehog is involved in osteoblast differentiation by cooperating with BMP-2. J Cell Physiol 193:225-232.

Zeller R. 2010. The temporal dynamics of vertebrate limb development, teratogenesis and evolution. Curr Opin Genet Dev 20:384-390.

Zeller R, Lopez-Rios J, Zuniga A. 2009. Vertebrate limb bud development: moving towards integrative analysis of organogenesis. Nat Rev Genet 10:845-858.

Zhang YD, Chen Z, Song YQ, Liu C, Chen YP. 2005. Making a tooth: growth factors, transcription factors, and stem cells. Cell Res 15:301-316.

Zhao B, Grimes SN, Li S, Hu X, Ivashkiv LB. 2012. TNF-induced osteoclastogenesis and inflammatory bone resorption are inhibited by transcription factor RBP-J. J Exp Med 209:319-334.

Zhou Z, Lu ZR. 2013. Gadolinium-based contrast agents for magnetic resonance cancer imaging. Wiley Interdiscip Rev Nanomed Nanobiotechnol 5:1-18.